



UNIVERSITAT DE
BARCELONA

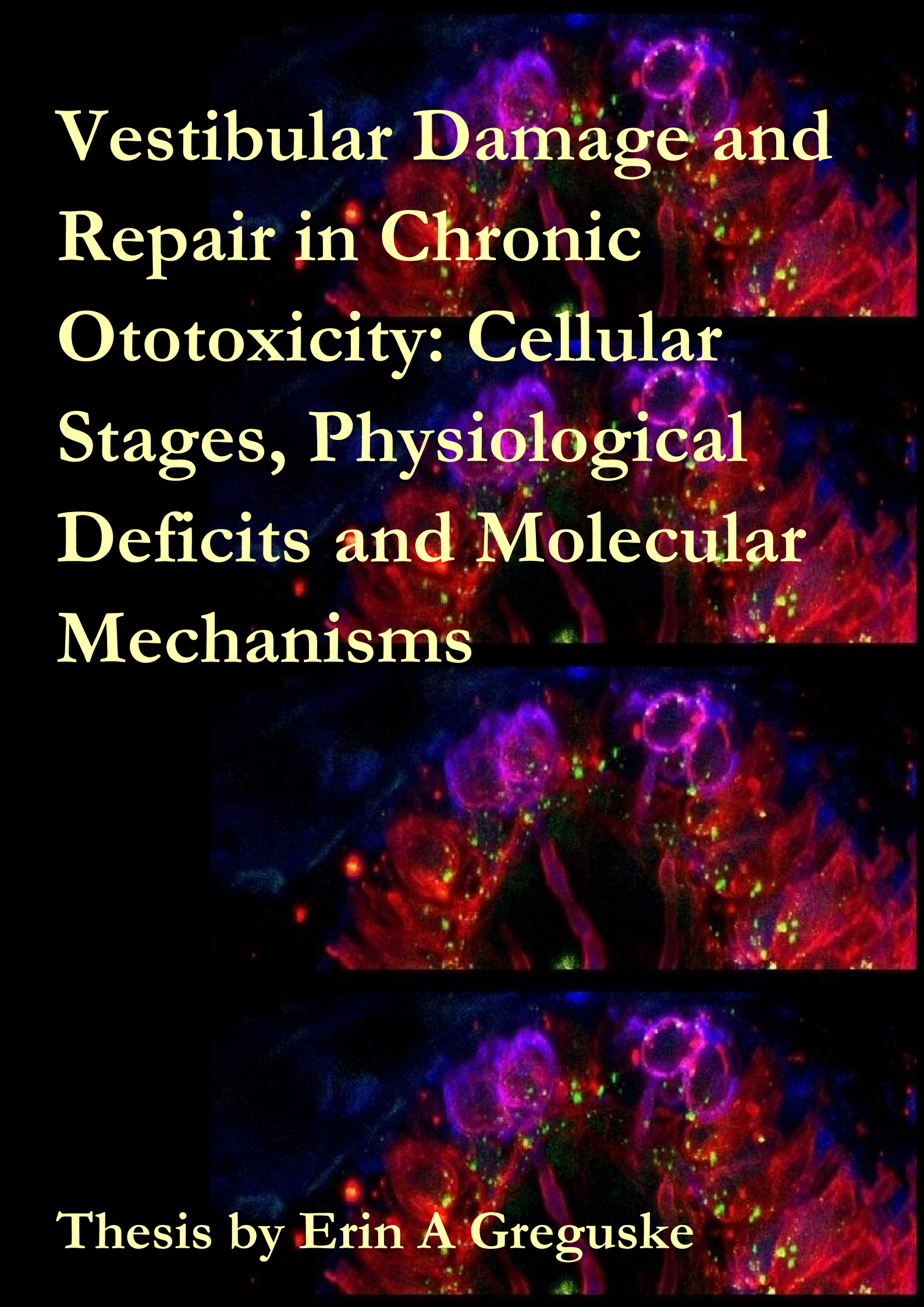
Vestibular Damage and Repair in Chronic Ototoxicity: Cellular Stages, Physiological Deficits and Molecular Mechanisms

Erin A. Greguske

ADVERTIMENT. La consulta d'aquesta tesi queda condicionada a l'acceptació de les següents condicions d'ús: La difusió d'aquesta tesi per mitjà del servei TDX (www.tdx.cat) i a través del Dipòsit Digital de la UB (diposit.ub.edu) ha estat autoritzada pels titulars dels drets de propietat intel·lectual únicament per a usos privats emmarcats en activitats d'investigació i docència. No s'autoritza la seva reproducció amb finalitats de lucre ni la seva difusió i posada a disposició des d'un lloc aliè al servei TDX ni al Dipòsit Digital de la UB. No s'autoritza la presentació del seu contingut en una finestra o marc aliè a TDX o al Dipòsit Digital de la UB (framing). Aquesta reserva de drets afecta tant al resum de presentació de la tesi com als seus continguts. En la utilització o cita de parts de la tesi és obligat indicar el nom de la persona autora.

ADVERTENCIA. La consulta de esta tesis queda condicionada a la aceptación de las siguientes condiciones de uso: La difusión de esta tesis por medio del servicio TDR (www.tdx.cat) y a través del Repositorio Digital de la UB (diposit.ub.edu) ha sido autorizada por los titulares de los derechos de propiedad intelectual únicamente para usos privados enmarcados en actividades de investigación y docencia. No se autoriza su reproducción con finalidades de lucro ni su difusión y puesta a disposición desde un sitio ajeno al servicio TDR o al Repositorio Digital de la UB. No se autoriza la presentación de su contenido en una ventana o marco ajeno a TDR o al Repositorio Digital de la UB (framing). Esta reserva de derechos afecta tanto al resumen de presentación de la tesis como a sus contenidos. En la utilización o cita de partes de la tesis es obligado indicar el nombre de la persona autora.

WARNING. On having consulted this thesis you're accepting the following use conditions: Spreading this thesis by the TDX (www.tdx.cat) service and by the UB Digital Repository (diposit.ub.edu) has been authorized by the titular of the intellectual property rights only for private uses placed in investigation and teaching activities. Reproduction with lucrative aims is not authorized nor its spreading and availability from a site foreign to the TDX service or to the UB Digital Repository. Introducing its content in a window or frame foreign to the TDX service or to the UB Digital Repository is not authorized (framing). Those rights affect to the presentation summary of the thesis as well as to its contents. In the using or citation of parts of the thesis it's obliged to indicate the name of the author.

The background of the entire page is a fluorescence microscopy image showing a dense population of cells. The cells are stained with multiple dyes, resulting in a complex pattern of colors. Red staining is prominent, outlining cell membranes and some internal structures. Green and blue staining are also visible, with blue likely representing nuclei stained with DAPI. The overall appearance is that of a tissue section or a cell culture monolayer under high-magnification light microscopy.

**Vestibular Damage and
Repair in Chronic
Ototoxicity: Cellular
Stages, Physiological
Deficits and Molecular
Mechanisms**

Thesis by Erin A Greguske



UNIVERSITAT DE
BARCELONA

Vestibular Damage and Repair in Chronic Ototoxicity: Cellular Stages, Physiological Deficits and Molecular Mechanisms

Doctoral Thesis presented by

Erin A Greguske

L'Hospitalet de Llobregat, 2019



UNIVERSITAT DE
BARCELONA

Doctoral Program in Biomedicine

Vestibular Damage and Repair in Chronic Ototoxicity: Cellular Stages, Physiological Deficits and Molecular Mechanisms

Department of Physiological Sciences

Faculty of Medicine and Health Sciences, Campus Bellvitge

Universitat de Barcelona

Doctoral Candidate

Erin A Greguske

Thesis Director

Dr. Jordi Llorens Baucells

The work of this Thesis was financed by:

- **Grant FI-DGR 2015** (9015-355847/2014) “Damage and Repair in the Vestibular Sensory Epithelia during Chronic Ototoxicity and Recovery”, from the Agency for Management of University and Research Grants (AGAUR), Generalitat de Catalunya
- **Grant FPU14-05426** “Vestibular Damage and Repair in Chronic Ototoxicity: Cellular Stages, Physiological Deficits and Molecular Mechanisms”, from the Ministry of Education, Culture and Sport of Spain
- **Project BFU2012-31164** “Vestibular Damage and Repair in Chronic Ototoxicity: Cellular Stages, Physiological Deficits and Molecular Mechanisms”, from the Ministry of Economy and Competitiveness of Spain
- **Project BFU2015-66109-R** “Damage and Repair of the Vestibular Synapses during Chronic Ototoxicity”, from the Ministry of Economy and Competitiveness of Spain
- **Minor Grant** “Synaptic Damage in the Vestibular Epithelium in a Chronic Ototoxicity Model”, from the Ménière’s Society in the United Kingdom

Acknowledgements

Keeping it sweet and simple:

Thank you to all my family and loved ones for believing in me every step of the way on this long academic journey. Your support and love were everything in helping me cultivate the passion I have for science and to always finish strong.

Thank you to my friends, old and new, for the endless words of encouragement and hype, which kept me happy and sane.

Thank you to my colleagues for your teachings that helped me persevere throughout my pursuit of knowledge and a special thanks to Benja and Josep of the CCiTUB and Klaas of the UMIC for all of your help.

And thank you Jordi for your endless patience and guidance throughout the years; for believing in my academic strength and helping me achieve this goal.

Index

1. Abbreviations	1
2. Abstract	7
3. Introduction	11
3.1. The Inner Ear.....	13
3.2. The Vertebrate Ear.....	14
3.3. The Vestibular System.....	14
3.4. The Vestibular Sensory Hair Cells.....	16
3.5. The Vestibular Sensory Afferents.....	17
3.6. Vestibular Sensory Hair Cell Signal Transmission.....	19
3.7. Vestibular Signaling Pathway to the CNS.....	21
3.8. The Auditory System.....	22
3.9. The Organ of Corti, the Sensory Epithelium of the Cochlea.....	23
3.10. The Cochlear Sensory Hair Cells.....	23
3.11. The Cochlear Sensory Afferents.....	25
3.12. The Auditory Efferent Pathway.....	25
3.13. Cochlear Sensory Hair Cell Signal Transmission.....	25
3.14. Auditory Signaling Pathway to the CNS.....	26
3.15. Ototoxicity and Aminoglycoside Antibiotics.....	27
3.16. Animal Studies of Ototoxicity.....	28
3.17. The Introduction of Nitriles for Progressive Ototoxic Studies.....	29
4. Objectives	33
5. Methodology	37
5.1. Animals.....	39
5.2. Ototoxic IDPN Exposure.....	39
5.3. Vestibular Dysfunction Ratings (VDRs).....	41
5.4. Auditory Brainstem Response (ABR) Measurements.....	41
5.5. Tissue Dissection and Epithelia/Ganglia Extraction.....	42
5.6. Immunofluorescent Studies.....	42
5.6.1. First Protocol/Study.....	43
5.6.2. Second Protocol/Study.....	43
5.6.3. Third Protocol/Study.....	44
5.6.4. Fourth Protocol/Study.....	44
5.6.5. Fifth Protocol/Study.....	44
5.7. Cochlear Place-Frequency Maps.....	47

5.8. Confocal Microscopy and Image Analysis.....	47
5.9. Scanning Electron Microscopy (SEM) Ultrastructural Studies.....	49
5.10. Transmission Electron Microscopy (TEM) Ultrastructural Studies.....	50
5.11. qRT-PCR Studies.....	50
5.12. RNA-sequencing (RNAseq).....	52
5.13. Data Analysis-SPSS.....	52
6. Results.....	55
6.1. Preliminary Total RNA Isolation Study.....	57
6.1.1. Testing various protocols.....	57
6.1.2. Qiagen proves to be the most consistent, efficient, and effective protocol.....	58
6.2. Characterizing Vestibular Damage.....	59
6.2.1. Effects of sub-chronic IDPN on 129S1 body weight.....	59
6.2.2. Effects of sub-chronic IDPN on 129S1 vestibular function.....	60
6.2.3. SEM analysis of stereociliary damage and HC loss following sub- chronic IDPN exposure.....	61
6.2.4. Light Microscopy and TEM analysis of calyceal junction loss, stereociliary fusion, and HC extrusion following sub-chronic IDPN exposure.....	64
6.2.5. Molecular analysis of calyceal junction dismantlement following sub- chronic IDPN exposure.....	66
6.2.6. mRNA expression of tenascin-c in the vestibular sensory epithelia is altered following sub-chronic IDPN exposure.....	68
6.2.7. Molecular analysis of synaptic uncoupling and post-synaptic density protein alterations following sub-chronic IDPN exposure.....	69
6.2.8. mRNA expression of various synaptic, scaffolding, and signaling proteins in the vestibular sensory epithelia and ganglia are altered following sub-chronic IDPN exposure.....	75
6.2.9. Preliminary RNAseq data of the vestibular ganglia and vestibular sensory epithelia demonstrate a depression in signal transmission in the afferent and cell-cell adhesion in the epithelia following sub- chronic IDPN exposure.....	76
6.2.10. Corroborating RNAseq results with qRT-PCR analyses of selected neurotrophic factors, synaptic, receptor, and kinase proteins and proteins associated with molecule transport.....	81
6.3. Characterizing Auditory Damage.....	82
6.3.1. Effects of sub-chronic IDPN on 129S2 body weight.....	82

6.3.2.	Effects of sub-chronic IDPN on 129S2 vestibular function.....	83
6.3.3.	IDPN exposure strongly affects the hearing of treated mice.....	83
6.3.4.	IDPN exposure causes a robust loss of OHCs, but IHCs remain intact.....	86
6.3.5.	IDPN exposure causes a loss of Caspr1 in vestibular sensory epithelia, but not in the organ of Corti.....	88
6.3.6.	IDPN exposure causes a decrease in active synapses in both cochlear and vestibular sensory epithelia.....	91
7.	Discussion.....	97
7.1.	Sub-Chronic IDPN Intoxication.....	99
7.2.	The Vestibular Model.....	99
7.2.1.	Establishing the sub-chronic IDPN mouse exposure model.....	99
7.2.2.	Sub-chronic IDPN effects on the morphology of the vestibular sensory epithelia and ganglia.....	100
7.2.3.	Sub-chronic IDPN effects on proteins involved with the calyceal junction in type I vestibular hair cells and their afferents.....	101
7.2.4.	Sub-chronic IDPN effects on active synapses of vestibular hair cells.....	102
7.2.5.	Sub-chronic IDPN effects on scaffolding proteins of the post-synaptic vestibular afferent.....	104
7.2.6.	Possible mechanisms affected within vestibular sensory epithelia and ganglia by sub-chronic IDPN exposure.....	106
7.3.	The Auditory Model.....	108
7.3.1.	Sub-chronic IDPN effects on a second sub-strain of mouse.....	108
7.3.2.	Sub-chronic IDPN effects on mouse hearing.....	108
7.3.3.	Sub-chronic IDPN effects on inner and outer hair cell morphology.....	110
7.3.4.	Sub-chronic IDPN does not directly affect Caspr1.....	111
7.3.5.	Sub-chronic IDPN effects on the active synapses of cochlear inner hair cells.....	111
7.4.	Sub-Chronic IDPN Effect Similarities and Differences between the Vestibular and Auditory Systems.....	112
8.	Conclusions.....	117
9.	Bibliography.....	121

1. Abbreviations

129S1: 129S1/SvImJ Mouse Strain	LVN: Lateral Vestibular Nucleus
129S2: 129S2/SvPasCrl Mouse Strain	MAGUK: Membrane-Associated Guanylate Kinase
ABR: Auditory Brainstem Response	MLF: Medial Longitudinal Fasciculus
AMPA(R): α -amino-3-hydroxy-5-methyl-4-isoxazolepropionic acid receptor	MSO: Medial Superior Olivary Complex
ATD: Amino-Terminal Domain	MVN: Medial Vestibular Nucleus
AVCN: Anteroventral Cochlear Nucleus	NaKAa3: Na ⁺ /K ⁺ -ATPase α 3 Subunit
Caspr1: Contactin Associated Protein 1	NMDA: N-methyl-D-aspartate Receptor
CNS: Central Nervous System	OHC: Outer Hair Cell
CtBP2/ribeye: C-Terminal Binding Protein 2/ribeye	PBS: Phosphate Buffered Saline
DAS: Dorsal Acoustic Stria	PBT: PBS with 0.6% Triton-X 100
dB SPL: Decibel Sound Pressure Level	PFA: Paraformaldehyde
DCN: Dorsal Cochlear Nucleus	PSD: Post-Synaptic Density
DE: Differentially Expressed	PSD95: Post-Synaptic Density Protein 95
ER: Endoplasmic Reticulum	PVCN: Posteroventral Cochlear Nucleus
GluA/R: Glutamate AMPA Receptor	RIN: RNA Integrity Number
HC: Hair Cell	SE: Standard Error
HCI: Type I Hair Cell	SEM: Scanning Electron Microscopy
HCII: Type II Hair Cell	Shank: SH3 and Multiple Ankyrin Repeat Domains Protein
Homer1: Homer Protein Homolog 1	SOC: Superior Olivary Complex
I/O: Input/Output (Function Slope)	SVN: Superior Vestibular Nucleus
IAS: Intermediate Acoustic Stria	TEM: Transmission Electron Microscopy
IDPN: 3,3'-iminodipropionitrile	TMD: Transmembrane Domain
IHC: Inner Hair Cell	TRPC: Transient Receptor Potential Cation Channel
IP₃: Inositol Trisphosphate	VAS: Ventral Acoustic Stria
IVN: Inferior Vestibular Nucleus	VCN: Ventral Cochlear Nucleus
LBD: Ligand Binding Domain	VDR: Vestibular Dysfunction Rating
LSO: Lateral Superior Olive	WO: WashOut (mice)

Figures

- **b**: Bouton (fig. 4,23,24)
- **c**: Calyx Afferent (fig. 4,23,24,42)
- **C**: Cuticular Plate Region (fig. 16)
- **cc**: Complex Calyx (fig. 4,24)
- **HCI**: Type I Hair Cell (fig. 4,23,24,42)
- **HCII**: Type II Hair Cell (fig. 4,23,24)
- **I**: Type I Hair Cell (fig. 16)
- **II**: Type II Hair Cell (fig. 16)
- **nc**: Calyx Afferent Nerve Terminal (fig. 16)
- **sc** or **SC**: Supporting Cell (fig. 4,16,23,24,42)

Genes

- **Actb**: Actin Beta
- **AGAP3**: ArfGAP with GTPase Domain, Ankyrin Repeat and PH Domain 3
- **AP2A1**: Adaptor Related Protein Complex 2 Subunit Alpha 1
- **AP2B1**: Adaptor Related Protein Complex 2 Subunit Beta 1
- **ARF3**: ADP Ribosylation Factor 3
- **ARPC1B**: Actin Related Protein 2/3 Complex Subunit 1B
- **ASAP2**: ArfGAP with SH3 Domain, Ankyrin Repeat and PH Domain 2
- **ATP6V0A1**: ATPase H⁺ Transporting V0 Subunit A1
- **ATP6V1A**: ATPase H⁺ Transporting V1 Subunit A
- **ATP6V1B2**: ATPase H⁺ Transporting V1 Subunit B2
- **BDNF**: Brain Derived Neurotrophic Factor
- **Camk1G**: Calcium/Calmodulin Dependent Protein Kinase IG
- **Chrna6**: Cholinergic Receptor Nicotinic Alpha 6 Subunit
- **CLTC**: Clathrin Heavy Chain
- **Cntnap1**: Contactin Associated Protein 1 (Caspr1)
- **DLG4**: Post-Synaptic Density Protein 95 (PSD95)
- **DLGAP1**: DLG Associated Protein 1 (GKAP1)
- **DNAJC6**: DnaJ Heat Shock Protein Family (Hsp40) Member C6
- **EHD2**: EH Domain Containing 2
- **EPS15**: Epidermal Growth Factor Receptor Pathway Substrate 15
- **F2R**: Coagulation Factor II Thrombin Receptor
- **FGFR2**: Fibroblast Growth Factor Receptor 2
- **GAPDH**: Glyceraldehyde-3-Phosphate Dehydrogenase
- **Gria2**: Glutamate Ionotropic Receptor AMPA Type Subunit 2 (GluA2)
- **GRK2**: G Protein-Coupled Receptor Kinase 2
- **H2-D1**: H-2 Class I Histocompatibility Antigen, D-B Alpha Chain
- **H2-K1**: H-2 Class I Histocompatibility Antigen, K-B Alpha Chain
- **KCNQ5**: Potassium Voltage-Gated Channel Subfamily Q Member 5
- **KIF5A**: Kinesin Family Member 5A
- **LDLRAP1**: Low Density Lipoprotein Receptor Adaptor Protein 1
- **NGFR**: Nerve Growth Factor Receptor
- **Nptx2**: Neuronal Pentraxin 2
- **PDCD6IP**: Programmed Cell Death 6 Interacting Protein
- **PRKCI**: Protein Kinase C Iota
- **RAB11FIP2**: RAB11 Family Interacting Protein 2

- **RAB5A:** RAB5A, Member RAS Oncogene Family
- **REST:** RE1 Silencing Transcription Factor
- **SH3GL2:** SH3 Domain Containing GRB2 Like 2, Endophilin A1
- **SLC17A6:** Solute Carrier Family 17 Member 6 (VGLUT2)
- **SLC2A4:** Solute Carrier Family 2 Member 4 (GLUT4)
- **STX1B:** Syntaxin 1B
- **STXBP1:** Syntaxin Binding Protein 1
- **SYT1:** Synaptotagmin 1
- **TFRC:** Transferrin Receptor
- **Tnc:** Tenascin-c
- **UNC13A:** Unc-13 Homolog A
- **UNC13B:** Unc-13 Homolog B
- **VAMP2:** Vesicle Associated Membrane Protein 2

Total RNA Isolation Study

- **½Gang:** Vestibular Ganglia from one ear of a single mouse (1 ganglia) for the total RNA isolation study
- **½IVE:** Vestibular Epithelia from one ear of a single mouse (3 cristae, 1 utricle) for the total RNA isolation study
- **GE:** GE illustra RNAspin Mini Kit and its protocol from the manufacturer
- **GEx2:** GE illustra RNAspin Mini Kit and its protocol from the manufacturer with a double DNase I digestion step
- **I Gang:** Vestibular Ganglia from both ears of a single mouse (2 ganglia) for the total RNA isolation study
- **IVE:** Vestibular Epithelia from both ears of a single mouse (6 cristae, 2 utricles) for the total RNA isolation study
- **PGang(2):** Vestibular Ganglia pooled from two animals (4 ganglia) for the total RNA isolation study
- **PGang(4):** Vestibular Ganglia pooled from four animals (8 ganglia) for the total RNA isolation study
- **PVE(2):** Vestibular Epithelia pooled from two animals (12 cristae, 4 utricles) for the total RNA isolation study
- **PVE(4):** Vestibular Epithelia pooled from four animals (24 cristae, 8 utricles) for the total RNA isolation study
- **Q:** Qiagen RNeasy Mini Kit and its protocol from the manufacturer with the carrier RNA step
- **T:** Laboratory-established TRIZOL protocol
- **TRIZOL:** Guanidinium Thiocyanate-Phenol-Chloroform Extraction

2. Abstract

Progressive ototoxicity of the inner ear is prevalent in patients administered aminoglycoside antibiotics with little understanding of how this damage occurs and to what extent it can be recovered. Numerous *in vitro* and *in vivo* studies using acute methods have been completed to demonstrate various types of damage in vestibular and auditory tissue, including hair cell damage that results in apoptosis or necrosis, excitotoxic damage, and/or degeneration of their afferents. However, progressive damage has only just recently been studied utilizing a sub-chronic exposure rat model; this model takes into account the progressive exposure mirrored in aminoglycoside administration that is not implied in acute experimentation. With this in mind, the sub-chronic exposure model was adapted for a new mouse model to characterize the progressive damage taking place in vestibular sensory epithelia and ganglia, along with a preliminary characterization in cochlear sensory epithelia. Mice were exposed to 30 mM IDPN (3,3'-iminodipropionitrile) in regular drinking water for 8 weeks, and monitored for vestibular deficits using an established test battery; auditory deficits were recorded using auditory brainstem response (ABR) measurements. Various techniques for identifying functional, histological (scanning/transmission electron microscopy; immunoconfocal), and molecular (mRNA; protein) data were utilized to study alterations in the vestibular and auditory tissues after sub-chronic intoxication. In the vestibular tissue, SEM/TEM imaging demonstrated progressive damage with the loss of calyceal junctions between type I hair cells and their calyx afferents, the fragmentation and retraction of the afferents, stereociliary bundle coalescence, and the unique mechanism of hair cell extrusion, where the cell is ejected from the epithelia into the endolymphatic cavity. Immunoconfocal and qRT-PCR data demonstrated a loss of caspr1 and tenascin-c in the calyceal junctions of type I hair cells and their afferents. A loss of active synapses between hair cells and their afferents was also noted, where active synapses were defined by the pre-synaptic ribeye of the hair cells and the post-synaptic GluA2 receptor of the afferents. Synaptic scaffolding protein expression was upregulated (PSD95, Homer1), which translated into an increase in the protein level (PSD95), likely for hair cell-afferent synapse stabilization and compensation. Progressive damage was noted to be at least partially or completely recoverable up until stereocilia coalescence of the hair cells. Finally, the expression of numerous scaffolding and signaling proteins were shown to be downregulated (qRT-PCR; RNAseq) during the exposure in the vestibular epithelium and ganglion, leading to the hypothesis of a depression in cell-cell adhesion between hair cells and their afferents and a depression in afferent signaling, resulting in an overall depressed system. In the cochlea, profound hearing loss was observed in a tonotopic pattern during the exposure; higher frequencies were affected first with longer exposure times affecting lower frequencies. Outer hair cells were lost tonotopically due to prolonged exposure, followed by active synapse loss of the inner hair cells. Those intoxicated for the first two weeks demonstrated a capacity for recovery before any outer hair cell or active synapse losses were seen. A sub-chronic ototoxic IDPN model demonstrates the progressive damage of the inner ear, allowing for the study of this damage and its potential for recoverability, gaining a clearer understanding of the mechanisms affecting the tissues.

3. Introduction

3.1 The Inner Ear

A healthy, functional inner ear, comprised of the auditory and vestibular systems, never impedes daily life until someone unexpectedly experiences what it means for it to be dysfunctional. Hearing loss due to old age is a natural occurrence (presbycusis), and is the third most prevalent health condition in older adults (data from the Hearing Loss Association of America). However, approximately 15% of adults aged 18 and over in the United States report some trouble in hearing (Blackwell et al., 2014). Meanwhile, one in four people 65 and older will typically experience a fall each year (data from the National Council on Aging), but it is estimated that more than 35% of adults aged 40 or older in the United States have experienced some form of a vestibular disorder (Smith and Darlington, 2013). Despite the fact that every person will eventually experience a weakening in inner ear function, there are no absolute options that protect and maintain optimal inner ear function, or any post-traumatic solutions that completely restore one's auditory or vestibular functions.

A known inner ear aggressor is ototoxic compounds, compounds that specifically target the sensorial hair cells of the inner ear and cause their degeneration, with numerous medications falling into this category. The varying percentage of patients taking these medications that experience ototoxicity can be from 10-33% affected, but the chances of recoverability from ototoxic symptoms are not fully understood. Those exposed to a short-term dysfunction can experience varying degrees of hearing loss, dizziness, disorientation, and/or vertigo, which can be recovered in a few days. However, those with permanent damage or long-term dysfunctions may experience numerous symptoms with varying degrees of severity for dizziness, vertigo, imbalance, spatial disorientation, visual disturbances, hearing changes, cognitive alterations, or psychological changes. Vestibular dysfunctions are managed, not cured, and include treatment options like specific head, body, and eye exercises to retrain the brain to recognize and process signals from the vestibular system, coordinating them in new ways to compensate for the damage. Some other options are dietary adjustments, medications (mainly for short-term disruptions), and surgery (corrective or destructive). Those with hearing loss may receive hearing aids or cochlear implants to ameliorate the loss, but they do not restore the full range of hearing. A person diagnosed with a long-term dysfunction has to manage their symptoms over the rest of their life time, depending on when symptoms began. It can be highly disruptive to a person's life not just physically, but psychologically as well.

Likewise, the options available for protecting cochlear and vestibular sensorial hair cells are extremely limited, if nonexistent. Preemptive protection for cochlear hair cells involves protecting our ears from loud acoustic trauma; this is managed individually by moderating head phone volume and using protective noise-cancelling gear. There are no preemptive protections available, or known, for vestibular hair cells. If inner ear injury occurs, like the possibility of being exposed to a loud noise outside of our control or from exposure to ototoxic medications, there are no options currently available to protect or promote inner ear health. This has led to numerous molecular mechanisms being targeted for research purposes in order to understand their roles in hair cell damage and degeneration.

One of the largest focuses of study is the effects of ototoxic compounds on the inner ear. Patients experiencing symptoms of ototoxicity show diverse recoverability, including complete, partial, or no recovery. The mechanisms causing these symptoms have been under heavy research for decades, but the concept of either the auditory or vestibular systems being able to recover from noted damage remains mostly unexplored. Pinpointing the proteins and mechanisms implicated in reversible sensorial hair cell damage may be the key to unlocking new methods in protecting and/or promoting inner ear health before, during, and after the insult. In order to understand reversible damage within these two systems, an extensive understanding of the vertebrate inner ear needs to be taken into account.

3.2 The Vertebrate Ear

The vertebrate ear consists of three regions: the outer ear, the middle ear, and the inner ear (fig. 1). The outer ear is comprised of the pinna and the ear canal. The pinna is the fleshy exterior part of the ear, which funnels sound waves into it. The middle ear contains the tympanum, also referred to as the ear drum, the three ossicles, and the oval and round windows. The three ossicles are the middle ear bones and are referred to as the malleus, incus, and stapes. They transmit the sound waves from the outer ear to the middle ear, amplifying the pressure of the sound wave being transmitted through the air to match the pressure needed to transmit the sound wave in the fluid filled membrane system of the cochlea. The inner ear consists of the bony labyrinth and contains the three semicircular canals, the vestibule, and the cochlea.

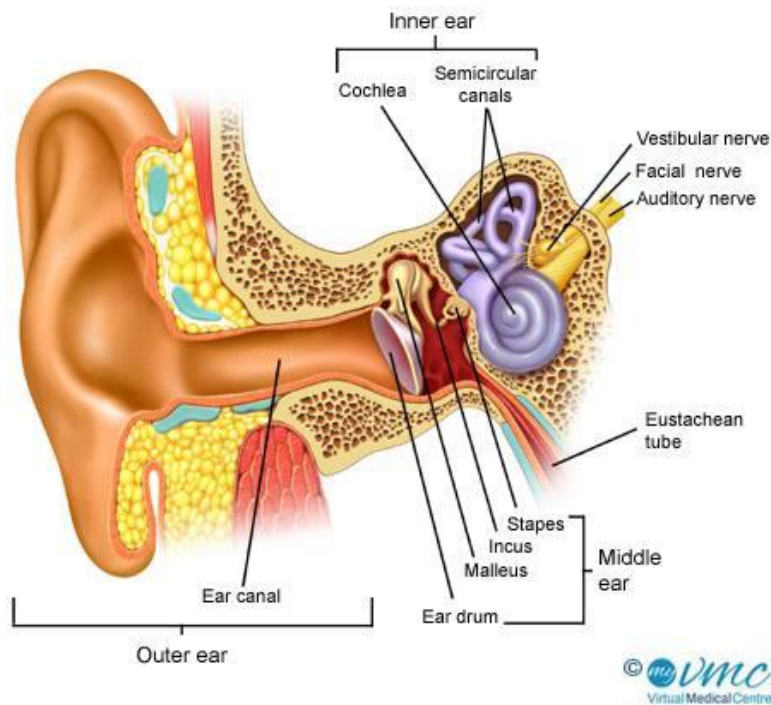


Figure 1: Diagram of the anatomy of a human ear. Image is adapted from <https://www.myvmc.com/anatomy/ear/>.

The vertebrate inner ear is a highly specialized and sophisticated system that coordinates an organism's sense of hearing, and the equilibrium and proprioception of the body. Comparative studies demonstrate frequent cases of complex gravity sensors in metazoans and so the detection of airborne sound is an evolutionarily new addition to the "vestibular" ear. The frequency of gravity related receptors in metazoans suggest that the vertebrate ear may have started off for gravitational function at first. The introduction of angular acceleration detection found in vertebrates and very few non-vertebrates indicates a parallel evolution with increased locomotor performance and maneuverability. Terrestrial hearing organs then evolved in tetrapod ancestors from vestibular precursors, which would eventually give way to current inner ear morphology and function (Fritzsche and Straka, 2014).

3.3 The Vestibular System

The vestibular system is located within the inner ear and includes the semicircular canals, a component of the bony labyrinth (fig. 2A). There are three semicircular canals that are interconnected at right angles to one another: horizontal, superior, posterior. Where each canal meets with the vestibule, the central region of the bony labyrinth, is a dilated cavity called the osseous ampulla and within each is a crista ampullaris (fig. 2B). The cristae ampullae are a part of the vestibular sensory epithelia and include a thick gelatinous cover referred to as a cupula, and numerous hair cells and supporting cells. Due to the orientation of the

canals, different canals can become stimulated depending on the movement of the head in specific planes, or more than one canal can become stimulated when a movement is not on one of those planes. The superior and posterior canals are positioned vertically at 90° angles from one another. The horizontal canal is oriented at a 30° incline from the horizontal plane, and is the shortest canal. The horizontal crista detects head rotations around a vertical axis (e.g. swiveling the head in a “no” gesture), or rotation in the transverse plane. The superior crista detects the rotation of the head around the lateral axis (e.g. nodding), or rotation on the sagittal plane. The posterior crista detects head rotation around the left-right (frontal) axis (e.g. move the head towards the shoulders), or rotation in the coronal plane.

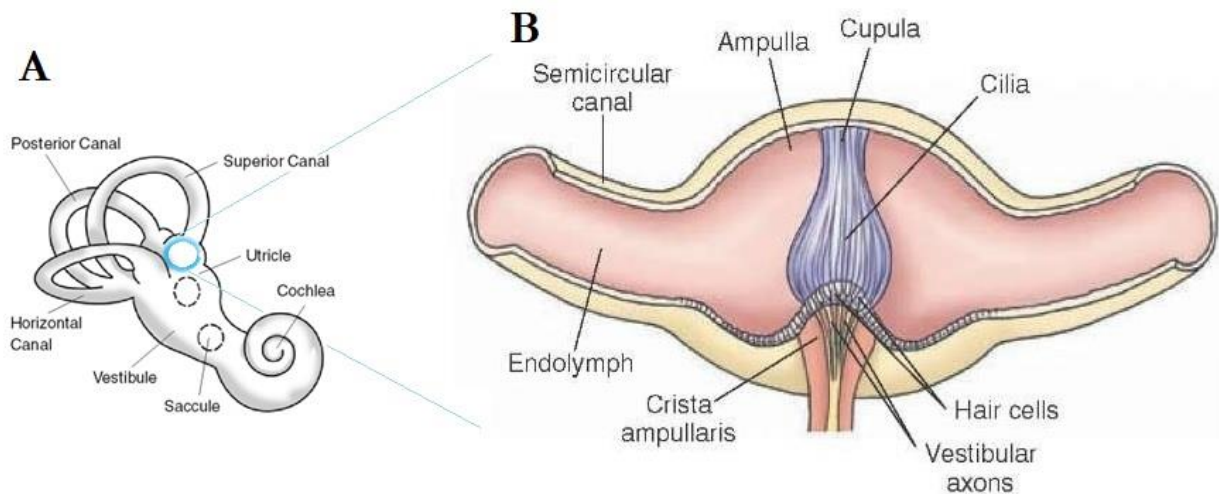
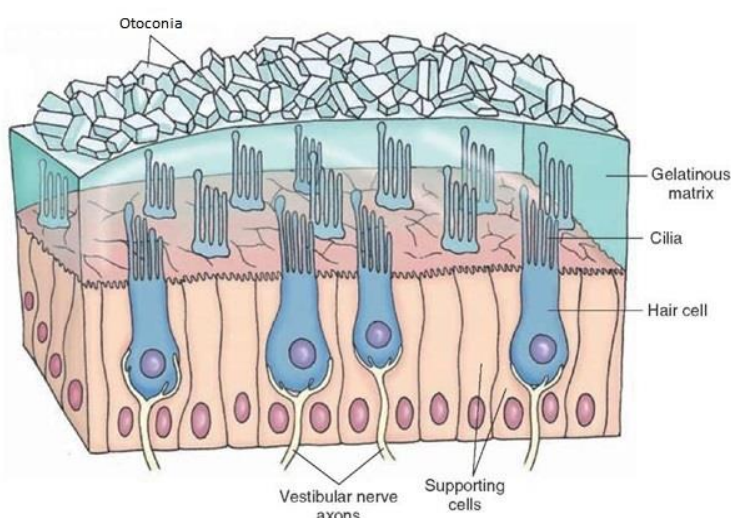


Figure 2: Diagram of the anatomy of the vestibular system. **A** Structure of the bony labyrinth that holds the vestibular system. **B** Enhanced diagram of a crista ampullaris. Images were adapted from http://www.nidcd.nih.gov/health/balance/balance_disorders.asp (A) and <http://what-when-how.com/neuroscience/auditory-and-vestibular-systems-sensory-system-part-2/> (B).

There are two otolith organs within the vestibule of the bony labyrinth, the utricle and the saccule (fig. 2A), which are also a part of the vestibular sensory epithelia. The utricle is circular in shape that is flattened transversely within the vestibule. The utricle is made up of hair cells and supporting cells, with a gelatinous layer embedded with otoconia over top of the cells (fig. 3). The otoconia are calcium carbonate crystals and give weight to the gelatinous matrix. The utricle detects linear accelerations and head-tilts in



the horizontal plane. The saccule is more oval in shape, and situated closer towards the cochlea. Like the utricle, it is made up of hair cells and supporting cells, with a gelatinous layer on top with the otoconia incorporated into the gelatinous matrix. The saccule detects linear accelerations and head tilts in the vertical plane; the saccule and utricle do not directly communicate with one another. The information sent from both organs help determine whether the head or the whole body is tilted, and to interpret the force of gravity on the organism.

Figure 3: Diagram of a section taken from an otolith organ with hair cells, supporting cells, the gelatinous matrix, and the otoconia. Image is from <http://what-when-how.com/neuroscience/auditory-and-vestibular-systems-sensory-system-part-2/>.

3.4 The Vestibular Sensory Hair Cells

Within the vestibular sensory epithelium, there are two types of sensory cells, referred to as type I hair cells (HCI) and type II hair cells (HCII) (fig. 4). HCII are cylindrical in shape, while HCI are amorphous-shaped. HCI are more concentrated within the central (striolar) regions of the sensory epithelium compared to HCII. Studies demonstrate that mice have 1413 ± 102 total hair cells in the cristae (Desai et al., 2005b), 3246 ± 58 total hair cells in the utricle, and 2477 ± 37 total hair cells in the saccule (Desai et al., 2005a). In the apical region there are stereocilia, the mechanosensing organelles of the cells, and they are between 10-50 mm in length and in bundles of 30-300 (Rzadzinska et al., 2004). They are specialized large microvellosities that resemble hair-like projections, hence the name “hair cells”, and are arranged in an ascending formation. The stereocilia of the hair cells of the cristae ampullae are all oriented in the same direction, whereas the stereocilia of utricular hair cells point towards the striolar region of the tissue and the stereocilia of saccular hair cells point away from the striolar region (Gray, 1997). At the core of the stereocilia, are rigid, cross-linked actin filaments; fine, filamentous structures, termed tip links, connect the tips of stereocilia in adjacent rows of the bundle. The tip links connect shorter stereocilia to its taller neighbors, stretching when the stereocilia are bent. The tip links act as springs, so when stretched, they open mechanically-gated cation selective receptors, allowing ions to flow into the hair cell (Tsuprun and Santi, 2002). Behind the tallest stereocilia is a cilium, referred to as the kinocilium, the only true cilium of the hair cell. The kinocilium has a microtubule-based cytoskeleton that acts as a scaffold for various proteins and supplies binding sites for molecular motor proteins. As the stereocilia bend towards the kinocilium, the mechanically-gated ion receptors open to allow for hair cell depolarization. However, bending away from the kinocilium causes the receptors to close, causing hyperpolarization, leading to inhibition of the cell.

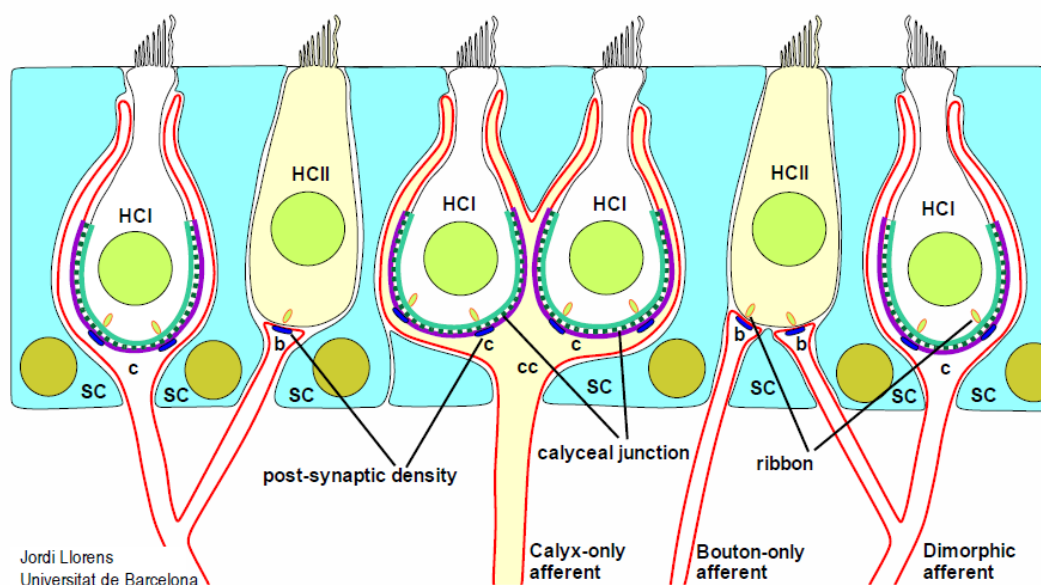


Figure 4: Diagram of the vestibular hair cells and their afferents in the different hair cell-afferent unit configurations. HCI: type I hair cell; HCII: type II hair cell; SC: supporting cell; c: calyx; b: bouton; cc: complex calyx. Image was created by Dr. Jordi Llorens of the Universitat de Barcelona.

In the basal region of the hair cells are ribbon synapses (fig. 5, yellow asterisks), characterized by the synaptic ribbon with the core protein of ribeye. The ribbons are synaptic structures found only in the retina and the inner ear. They are hypothesized to have a major role in organizing the synaptic vesicle dynamics that are necessary to sustain the high rates of neurotransmitter release that characterize these

sensory cells. Small vesicles tether to ribeye, up to 100 vesicles or more, and ribbon synapses are docked near the active zones of the plasma membrane where neurotransmitter release will occur (Parsons and Sterling, 2003). Voltage-gated calcium channels are located nanometers away from the ribbon synapses in order to facilitate signal transmission and cellular function. Ribbon synapses are heavily dependent on calcium (Ca^{2+}) and utilize the protein otoferlin as a calcium sensor, triggering vesicle and neurotransmitter release (Uthairah and Hudspeth, 2010). The ribbon synapse will release its entire vesicle pool when triggered, causing a large release of neurotransmitters, resulting in fast kinetics of neurotransmission.

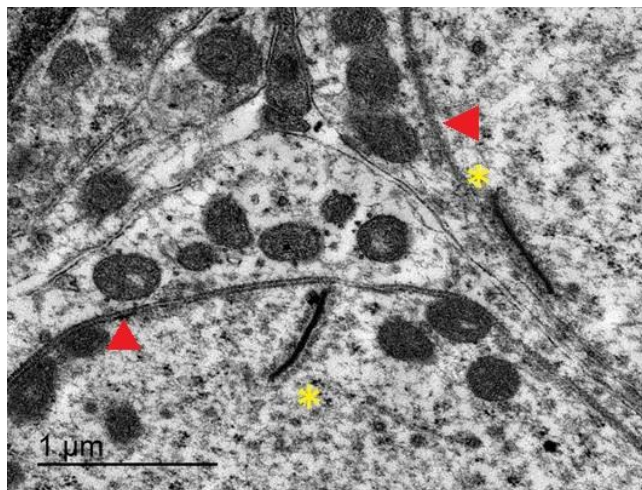


Figure 5: Transmission electron microscopy image demonstrating the ribbon synapses (yellow asterisks) with the small vesicles docked to it within HCIs. The HCIs have calyceal junctions that are electron dense (red solid arrows) that demarcate where the calyx afferent makes contact with them. Image is from unpublished data of the laboratory.

HCIIIs have simple bouton connections with their sensory afferent(s), while HCIs have a more unique connection. The afferents of HCIs form a calyx, which envelops the HCI from the basolateral surface up to the neck of the cell. Two-thirds of this contact forms the calyceal junction and has an electron dense membrane, identifiable in transmission electron microscopy (fig. 5, red arrows). A key junction protein found on the afferent side of the junction is *caspr1*, or contactin-associated protein 1 (Sousa et al., 2009). *Caspr1* is a part of the neurexin family and is mainly found in the paranodal sections of the axon in myelinated neurons; paranodal sections lie adjacent to the nodes of Ranvier, which are essential for saltatory conduction (rapid signal transmission) (Rios et al., 2000). The involvement of *caspr1* in nerve excitation and conduction, as well as maintaining stability of its connections (Zou et al., 2017), makes *caspr1* an important target for the calyceal junction structure. The calyx essentially seals off the HCI from other cells and signals and so it creates an intimate environment for signal transmission between them. Within the synaptic cleft of the calyceal junction is the extracellular matrix glycoprotein, tenascin-c. Tenascin-c is highly expressed during embryogenesis and is classified as an adhesion-modulating protein, inhibiting cellular adhesion to fibronectin (Chiquet-Ehrismann, 2004). Its regulation can be induced or repressed by numerous factors during remodeling, injury, or neoplasticity (Jones and Jones, 2000), making it another important target for calyceal junction structure. In total, the sensory afferents can create three different hair cell (HC)-afferent units with the HCIIIs and HCIs. There are calyx-only afferents (calretinin-positive afferents) that consist only of HCIs, HCII bouton afferent units that consist of HCIIIs only, and the dimorphic units, which make contact with HCIIIs and HCIs (calretinin-negative afferents) (fig. 4).

3.5 The Vestibular Sensory Afferents

The vestibular ganglia afferents are post-synaptic to the pre-synaptic hair cells of the vestibular sensory epithelia. Multiple afferents can make several bouton connections with numerous, different HCIIIs (fig. 6h), while a single afferent can form an individual calyx contacting one or more HCIs (fig. 6a,b). Likewise, a single dimorphic afferent can innervate multiple HCIIIs and HCIs as well (Holt et al., 2010, including fig. 6c-g). The morphology of the afferents consist of a single peripheral process (bouton, calyx-only, or dimorphic), a sensory neuron cell body, which are grouped in the vestibular sensory ganglion, an axon

that projects towards the central nervous system (CNS), and the axon terminal, which innervates with one of four vestibular nuclei or the cerebellum directly.

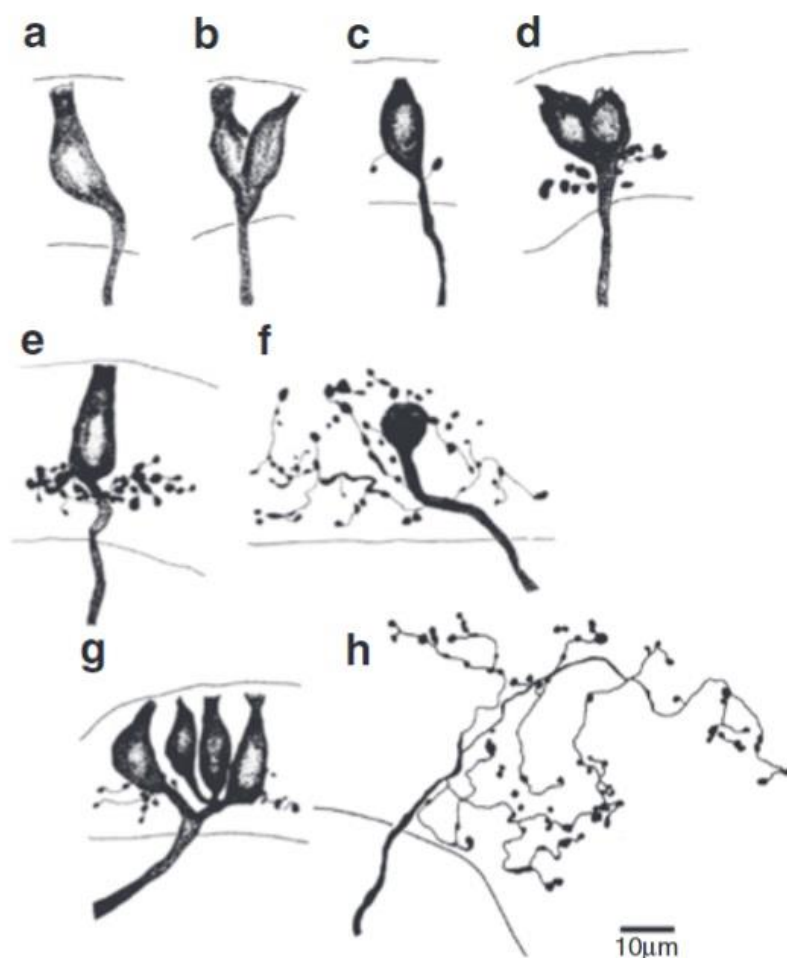


Figure 6: The different hair cell-afferent units in the vestibular crista visualized by extracellular deposit of horseradish peroxidase in the chinchilla vestibular nerve. The hair cell-afferent units are categorized as calyx-only (a,b), dimorphic (c-g), and bouton (h). Image is adapted from Holt et al., 2010.

On the peripheral processes are numerous receptors that neurotransmitters from the pre-synaptic hair cell interact with. The main neurotransmitter of the system is glutamate, and the majority of ligand-gated ion receptors on the afferent are ionotropic AMPA receptors, specifically with the subunits of GluA2, GluA3, and GluA4 (Niedzielski and Wenthold, 1995). Ionotropic AMPA receptors mediate fast synaptic transmission and are heterotetrameric, mainly assembled of symmetric “dimer of dimers” consisting of the subunit GluA2 and either GluA1, GluA3, or GluA4 (Mayer, 2005). The subunit GluA2 is the most abundant subunit within the central nervous system and plays an important role in AMPA receptor calcium impermeability, a function thought to be essential for proper brain function (fig. 7). The ionotropic AMPA receptors have been observed to be localized adjacent or superimposed to ribbon synapses in pre-synaptic hair cells; however, this is not necessarily always the case. In HCIs, ribbon synapses and AMPA receptors do not always colocalize, and they do not demonstrate a 1:1 ratio (Sadeghi et al., 2014). This has led to the hypothesis of glutamate spillover occurring during neurotransmitter release at HCIs into the synaptic cleft; the glutamate released from ribbon synapse active sites need to travel to AMPA receptor sites and can linger in the synaptic cleft. Glutamate spillover has demonstrated to be a prominent role in signal transmission for HCI-calyx synapses that results in slower excitation kinetics and may play a role in modifying afferent response sensitivity (Sadeghi et al., 2014).

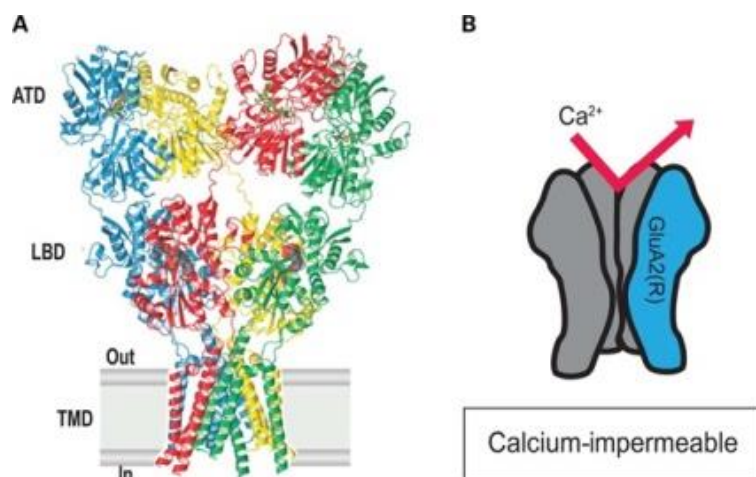


Figure 7: Structure of an ionotropic AMPA receptor. **A** The different GluA subunits (1-4) with an extracellular amino-terminal domain (ATD), the ligand binding domain (LBD), and a transmembrane domain (TMD). **B** Diagram demonstrating the more abundant GluA2 subunit with the “R” configuration, making the receptor impermeable to calcium. Image adapted from Wright and Vissel, 2012.

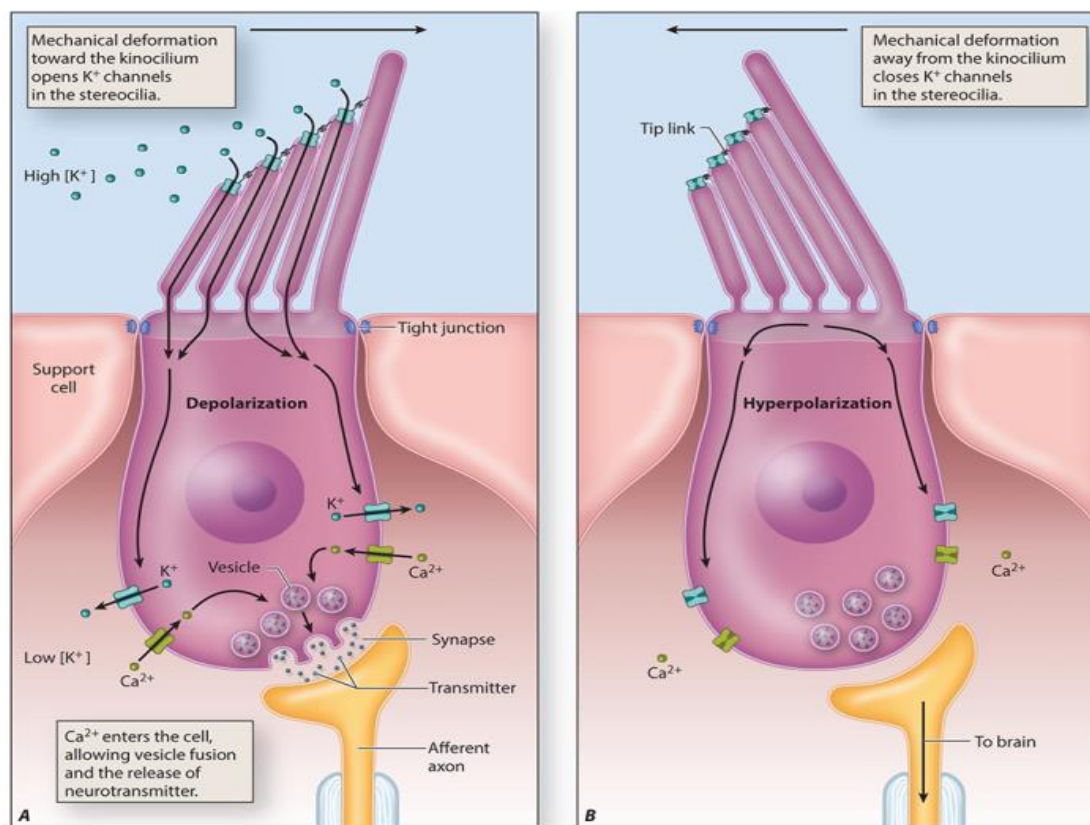
Ionotropic AMPA receptors are located in the peripheral processes of the afferent, and this is referred to as the post-synaptic density (PSD). The PSD is protein dense and is in close proximity to pre-synaptic active zones to ensure that receptors are located near neurotransmitter release sites. The PSD contains several hundred proteins, ranging from scaffolding and signaling proteins to numerous types of receptors (NMDA, AMPA); the role of the PSD is proposed to be where neurotransmitter receptors are concentrated and organized for the synaptic cleft, and as a major signaling hub. One of the most abundant scaffolding proteins, which are found almost explicitly in neurons in the CNS, is the post-synaptic density protein 95 (PSD95). It is a member of the membrane-associated guanylate kinase (MAGUK) family and one of its roles as a scaffolding protein is to cluster, support, and anchor ion channels in the PSD (Sheng and Sala, 2001). PSD95 also gives support to numerous other proteins like neuroligin, NMDA receptors, and potassium channels. An important and notable role of PSD95 is its stabilization of the PSD during synaptic plasticity (Meyer et al., 2014) and its ability to manage synaptic change, which makes it a highly desirable target for study.

Another major player of the PSD is the homer protein homolog 1, or Homer1. It is found abundantly in the PSDs of neurons in the CNS, although it can be found in other peripheral tissue. Homer1 has a tetrameric structure and is thought to cross link various proteins in the PSD, including metabotropic glutamate receptors, IP₃ receptors, Shank, TRPC family receptors, and more (Xiao et al., 1998). In combination with Shank, it is suggested that this complex makes up the core of the PSD, as well as a binding platform for other proteins, including PSD95 (Hayashi et al., 2009). Another notable role of Homer1 is for homeostatic plasticity, dampening neuronal response if input activity is too high and for synaptic plasticity and stabilization of the PSD, similar to PSD95 (Meyer et al., 2014). For this reason, Homer1 is also a highly regarded target in its ability to stabilize the PSD during synaptic changes and signal transmission.

3.6 Vestibular Sensory Hair Cell Signal Transmission

Hair cells use mechano-electro transduction in order to transmit signals acquired from external stimuli to the brain, and in the case of the vestibular system, to the brainstem. The different movements and rotations, accelerations and decelerations of the head, and the force of gravity, all cause the displacement of a specialized extracellular fluid, referred to as the endolymph, located within the semicircular canals and membranous labyrinth. The displacement of the endolymph moves the cupula of the cristae ampullae, in which the stereocilia of the hair cells are embedded. Depending on what plane the movement is occurring decides which cristae are being stimulated. Likewise, the stereocilia of the utricle and saccule are incorporated within the gelatinous matrix and the otoconia that lie above them; the otoconia give weight to the gelatinous matrix and contributes towards stereociliar displacement. As the

stereocilia are displaced towards the kinocilium, the tip links open the mechanically-gated cation selective receptors (Purves et al., 2004a). The endolymph has a high concentration of potassium (K^+) in it and is the most abundant ion in the fluid. Hair cells have a lower concentration of potassium within them, so potassium will flow into the cell when the ion receptors are opened (Bosher and Warren, 1968) (fig. 8). Hair cells have a resting potential of approximately -65 mV and when potassium depolarizes it to -60 to -55 mV (Eckrich et al., 2012), voltage-gated calcium receptors on the plasma membrane open, causing calcium (Ca^{2+}) to flow into the hair cell. High concentrations of calcium cause the vesicles at the numerous ribbon synapses to detach from the synaptic ribbon and fuse with the plasma membrane in the active zones, rapidly releasing neurotransmitters (glutamate) into the synaptic cleft (Beutner et al., 2001). The glutamate molecules bind to various ligand-gated ionotropic AMPA receptors on the post-synaptic afferent(s), causing receptor conformational changes and effectively opening them. Ions pass through the receptors and flow into the afferent(s) causing the afferent(s) to depolarize. This depolarization opens voltage-gated calcium channels and the signal is perpetuated along the afferent(s) towards central processing areas.



Source: Tony Mosconi, Victoria Graham:
Neuroscience for Rehabilitation
 Copyright © McGraw-Hill Education. All rights reserved.

Figure 8: Diagram demonstrating hair cell depolarization via mechano-electro signal transmission. Image is adapted from Neiberg et al., 2018.

3.7 Vestibular Signaling Pathway to the CNS

The afferents typify the vestibular sensory ganglia and they become a part of the vestibulocochlear nerve, the VIII cranial nerve, as it projects to the CNS. The vestibulocochlear nerve innervates with the brainstem at the junction between the pons and the medulla. There are four nearby vestibular nuclei in the rostral medulla and caudal pons that the nerve can project to (fig. 9), or it bypasses them and innervates directly with the cerebellum through the inferior cerebellar peduncle. The four vestibular nuclei are the inferior vestibular nucleus (IVN), medial vestibular nucleus (MVN), lateral vestibular nucleus (LVN), and superior vestibular nucleus (SVN). These nuclei mainly project to the spinal cord, the three extraocular motor nuclei (abducens nucleus, trochlear nucleus, oculomotor nuclear complex), to the thalamus, and to the cerebellum. These projections give input for controlling head and body position, controlling eye movements, coordinating the conscious perception of movement and gravity, and coordinating postural adjustments, respectively (Gray, 1997). The projections that bypass straight to the cerebellum coordinate movement to maintain balance.

Meanwhile, the two main descending tracts are the lateral vestibulospinal tract, derived from the LVN, and the medial vestibulospinal tract, derived from the MVN. The lateral vestibulospinal tract descends the length of the spinal cord on the same side and helps us to walk upright. The medial vestibulospinal tract extends bilaterally through the mid-thoracic levels of the spinal cord and affects head movements and helps to integrate head and eye movements (Gray, 1997).

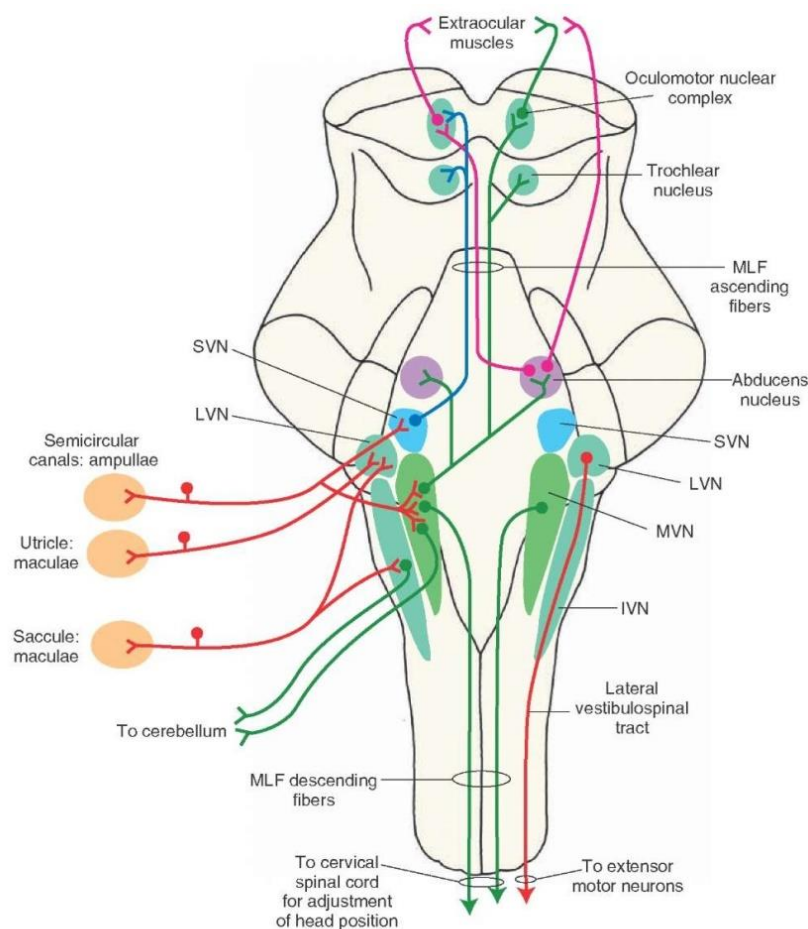


Figure 9: Diagram of the vestibular nerve pathway and its relays into the central nervous system for further processing.

SVN: superior vestibular nucleus;
 LVN: lateral vestibular nucleus;
 MVN: medial vestibular nucleus;
 IVN: inferior vestibular nucleus;
 MLF: medial longitudinal fasciculus.
 Image is adapted from
<https://wirindiagrampedia.com/>.

3.8 The Auditory System

The auditory system is also located in the inner ear, and consists of a snail-shaped structure as a part of the bony labyrinth, the cochlea. It consists of a spiral with two full turns and a three-quarter turn around its axis with three hollow chambers (fig. 10). The three chambers, or *scalae*, are the vestibular duct, the tympanic duct, and the cochlear duct. The vestibular duct, or *scala vestibuli*, contains perilymph, an extracellular fluid with high concentrations of sodium, and lies superior to the cochlear duct, touching the oval window. The tympanic duct, or *scala tympani*, contains perilymph and lies inferior to the cochlear duct and terminates at the round window. The cochlear duct, or *scala media*, contains endolymph and is the duct in-between the other two ducts. Reissner's membrane separates the vestibular duct from the cochlear duct, while the basilar membrane separates the tympanic duct from the cochlear duct.

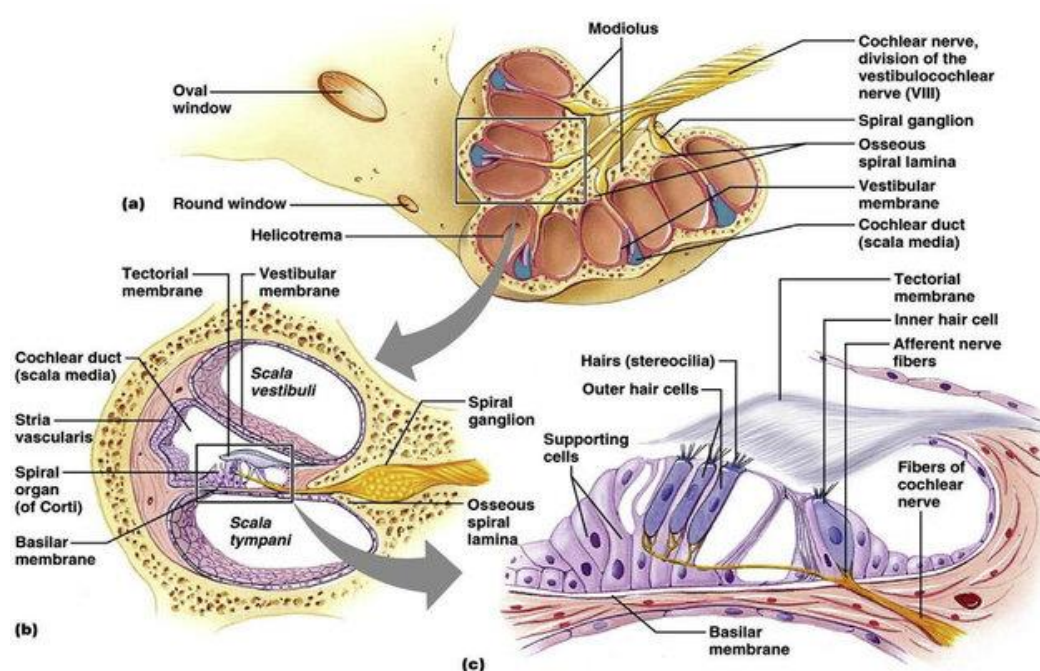


Figure 10: Diagram of cochlear anatomy. (a) Cross-section of the cochlea, looking into the $2\frac{3}{4}$ turns. (b) Enhanced view within the cochlea showing the three hollow ducts. The *scala vestibuli* (vestibular duct) is superior to the cochlear duct. The *scala tympani* (tympanic duct) is inferior to the cochlear duct. The *scala media* (cochlear duct) lies in-between the other two ducts and contains the organ of Corti. (c) Enhanced diagram of the organ of Corti. Image is adapted from Morrill and He, 2017.

Within the cochlear duct resides the organ of Corti, the sensory epithelium of the cochlea, the stria vascularis, and the tectorial membrane. The stria vascularis is the upper portion of the spiral ligament, a membrane that covers the outer surface of the bone, and has a variety of functions. It is a stratified epithelium and primarily contains marginal, intermediate, and basal cells, along with intraepithelial capillaries. These cells are involved in potassium ion transport, producing endolymph for the cochlear duct, and separating the stria vascularis from the spiral ligament. The tectorial membrane, a gel-like structure containing 97% water and its dry weight consisting mostly of collagen (Thalmann et al., 1986), runs parallel to the basilar membrane, but above the organ of Corti. The tectorial membrane consists of three zones: the limbal, middle, and marginal zones. The limbal zone is the thinnest with its inside edge attached to the spiral limbus, a thickened membrane covering the outer surface of the bone similar to the spiral ligament. The marginal zone is the thickest and is separated from the middle zone by Henson's stripe on the underside of the tectorial membrane. It lies over the sensory inner hair cells (IHCs) and outer hair cells (OHCs) of the organ of Corti and can stimulate the hair cells through fluid coupling (IHCs) or precisely via direct contact with the tallest stereocilia (OHCs).

3.9 The Organ of Corti, the Sensory Epithelium of the Cochlea

The organ of Corti lies on the basilar membrane and has a single row of inner hair cells and three rows of outer hair cells. The cells separating and supporting the IHCs and OHCs are called Deiters cells (Malgrange et al., 2002). The organ of Corti transduces auditory signals via the IHCs and OHCs and is organized tonotopically (fig. 11A); different frequencies of sound are localized to different locations on the epithelium, demonstrating a frequency gradient that spans the whole organ of Corti. The highest frequencies are perceived at the basal region of the organ of Corti, where the cochlea is more narrow and stiff and closest to the oval window (fig. 11B). The lower frequencies are perceived at the opposite end of the epithelium at the apical region, the interior spiral of the cochlea, and is wider and much more flexible (Fritzsch et al., 2011) (fig. 11D).

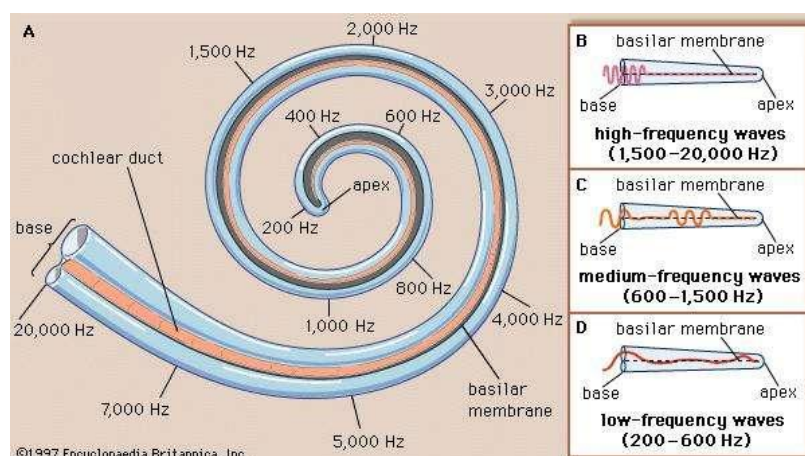


Figure 11: Diagram demonstrating the tonotopy of the human cochlea. **A** The basal region of the cochlea has the highest frequencies with a more narrow and rigid basilar membrane, while the apical region has the lowest frequencies with a wider and more flexible basilar membrane. **B-D** Example cochlea laid out showing where the different frequencies resonate on the basilar membrane. Image is adapted from <https://www.britannica.com/science/ear/Transmission-of-sound-within-the-inner-ear>.

Along the organ of Corti, the basilar membrane will vibrate at different sinusoidal frequencies due to the varying thickness, width, and rigidity of the membrane. At each cochlear region, the hair cells in those regions send a signal, which will be interpreted in the brain as the different frequencies. Thus, there is a tonotopic distribution of cochlear stimulation based on the physical properties of the basilar membrane. In addition, there are also differences in shape and molecular characteristics of the hair cells that vary along the cochlea. Although tonotopic differentiation is not fully understood, recent research suggests roles from Shh signaling (Bok et al., 2013), Smoothed transduced by Hh (Tateya et al., 2013), and/or BMP signaling (Mann et al., 2014) may contribute to tonotopic organization during development. Humans have a hearing range of 20 Hz to 20 kHz.

3.10 The Cochlear Sensory Hair Cells

The hair cells of the cochlea are cylindrical in shape and have bouton connections with their corresponding post-synaptic spiral ganglion afferents, similar to HCIIIs of the vestibular system. Mice have ~2250 OHCs and ~750 IHCs (Ehret and Frankenreiter, 1977) and it's estimated that the mouse has ~10000 hair cells per ear (auditory and vestibular combined) (Krey et al., 2017). On the apical surface of the cell, hair cells have stereocilia and are organized in a gradation of height, with the shortest being in the outer rows and the tallest in the center. Stereocilia anatomy and function are very similar to stereocilia anatomy and function as described for vestibular hair cells. The gradation of the stereocilia is thought to be of most importance within the cochlea for the tuning capability of the hair cells. The stereociliary bundles for both hair cell types are also organized in a "W" configuration with a step-like arrangement (fig. 12). In OHCs, this formation is sharply angled toward the apex, coinciding with the tectorial membrane, where the tallest row of stereocilia is coupled with the membrane. In IHCs, the formation is wider and arranged at a right angle to the organ of Corti; the stereociliary bundles are also free standing, meaning that they are not coupled with anything, like the OHCs are with the tectorial membrane (Lim,

1986). The movement of the tectorial membrane and the endolymph influence the hair cells in distinct ways to add a layer of complexity to auditory signal transduction.

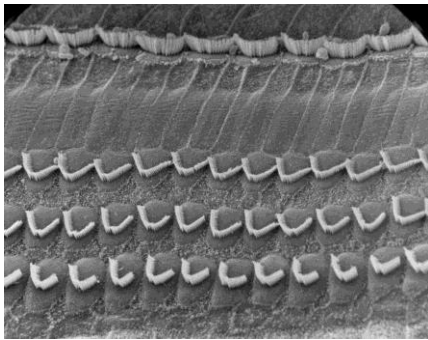


Figure 12: Scanning electron microscopy image of the three rows of OHCs and one row of IHCs of the organ of Corti. It is an exterior image, demonstrating the stereocilia bundles and their configurations. Image is adapted from <https://lab.research.sickkids.ca/harrison/background/hearing-loss/>.

In the basal region of the hair cells of the auditory system, they also have ribbon synapses, equivalent in function to the ribbon synapses found in vestibular hair cells. Unlike in the vestibular hair cells, ribbon synapses are at an almost 1:1 ratio to post-synaptic clusters of ionotropic AMPA receptors; in fact, ribbon synapses on the modiolar face and/or basal region of IHCs have larger synapses when compared to the pillar region of the IHCs (Liberman et al., 2011, including figure 13). The groupings of AMPA receptors demonstrated a reversed gradient in IHCs, where smaller groupings were associated with the larger ribbon synapses and larger groupings with smaller synapses. These observations link to cochlear nerve threshold and spontaneous discharge rate within the cochlea.

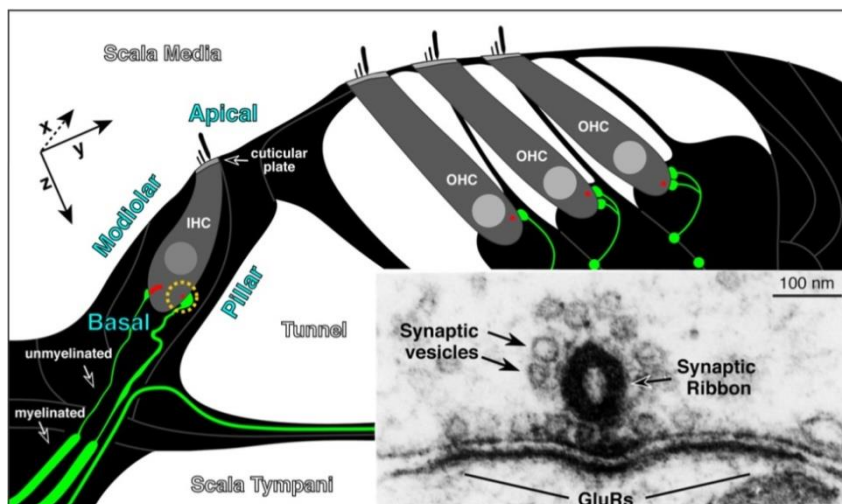


Figure 13: Diagram of the organ of Corti demonstrating where the modiolar and pillar regions of the IHC are. The larger ribbon synapses with the smaller groupings of AMPA receptors are in the basal/modiolar regions, and the smaller ribbon synapses with larger AMPA receptor groupings are in the pillar region. Smaller inset depicts a transmission electron microscopy image of a ribbon synapse with small vesicles docked to it, and the neighboring receptors of the post-synaptic afferent. Image is adapted from Liberman et al., 2011.

The IHCs detect and transform the sound vibrations that enter the ear into the electrical signals that are relayed by the cochlear nerve to the brain to be processed and interpreted as the different frequencies that can be perceived. IHCs are innervated by 95% of the afferents of the cochlear nerve that project toward the CNS (Purves et al., 2004b).

The OHCs amplify low-level sound and improve upon frequency selectivity (Ashmore, 2008). OHCs have demonstrated to have the ability to contract and elongate following changes of the intracellular potential, and this is referred to as electromotility. The specific motor protein prestin has been identified as the motor protein which aids OHCs in electromotility, leading to the function of sound amplification (Zheng et al., 2000). For the OHCs, only about 5% of afferents of the cochlear nerve that project toward the CNS innervate with them, while numerous efferent sensory neurons projecting from the brain innervate with the OHCs (Ashmore, 2008).

3.11 The Cochlear Sensory Afferents

The spiral ganglion is the group of cochlear afferents that carry receptor potentials of the hair cells of the cochlea to the brain. The afferents are bipolar: the peripheral processes make bouton connections with the hair cells, the cell bodies are grouped in the modiolus, the conical central axis of the cochlea that it spirals around, and the axons project to the CNS for further processing. There are two types of afferents: type I spiral ganglion afferents and type II spiral ganglion afferents. Type I afferents are myelinated and they make up about 95% of the afferent neuronal population. They exclusively contact IHCs and each receives input from a single active zone in a single IHC. They encode for sound intensity, timing, and frequency. Type II afferents differ from type I afferents in that they are unipolar, thin, not myelinated, and a single afferent can receive input from multiple OHCs (Weisz et al., 2014). The axons of the afferents that project to the CNS bundle together to become the cochlear nerve of the vestibulocochlear nerve, or the VIII cranial nerve. On the peripheral processes are the ionotropic AMPA receptors needed for glutamatergic transmission previously described for the vestibular system. These same receptors are present in the spiral ganglion afferents and carry the same level of importance.

3.12 The Auditory Efferent Pathway

The auditory efferent pathway of the mouse consists of the lateral efferent system, which originates from the lateral superior olive (LSO), and the medial efferent system, which originates from the periolivary region (medial, ventral, and anterior) near the medial superior olivary (MSO) complex and the trapezoid body (not present in humans). LSO efferents overlap significantly with type I spiral ganglion afferent input, mostly projecting ipsilaterally, and innervates with the dendrites of radial afferent fibers under IHCs. They are unmyelinated and it is a relatively small system when compared to other species. Medial efferents are myelinated, project near type II spiral ganglion afferents, project both contralaterally and ipsilaterally, and directly innervates with OHCs. The functions of these systems are for noise protection, improvement of signal to noise ratio, and supports adaptation and frequency selectivity via modification of the micromechanical properties of OHCs. The efferent system can be affected by different factors, like noise and ototoxic drugs (Ciuman, 2010).

3.13 Cochlear Sensory Hair Cell Signal Transmission

Auditory signal transmission begins with an external stimulus; sound travels in waves through the air and is funneled into the ear via the pinna. The waves travel down the ear canal until it reaches the tympanum. The sound waves vibrate the tympanum, and this vibration travels through to the bones of the middle ear (malleus, incus, stapes), magnifying the wave pressure as it travels through the three ossicles. The footplate of the stapes transmits the vibrations onto the oval window, causing pressure waves within the perilymph of the vestibular duct. The pressure waves perpetuate towards the helicotrema, the apex of the cochlea and where the vestibular duct and tympanic duct meet. The pressure waves travel through the helicotrema and into the tympanic duct, and finally dissipate when they arrive to the round window. The wave motion in the perilymph of the vestibular duct transmits to the endolymph fluid in the cochlear duct, and it displaces the basilar membrane at the corresponding soundwave frequency that it is resonating in. The movement of the basilar membrane also moves the organ of Corti, causing OHC stimulation. Depending on OHC depolarization or hyperpolarization, the OHCs change in length and move the organ of Corti more, amplifying the vibrations. The stereocilia of the IHCs are displaced (moved towards the kinocilium), and a similar cascade resulting in hair cell depolarization and signal transmission via the associated afferents occurs as previously described for the vestibular hair cells. The signal is transmitted through the spiral ganglion, which becomes the cochlear nerve, also known as the auditory nerve, of the vestibulocochlear nerve, the VIII cranial nerve, and projects to the CNS for further processing.

3.14 Auditory Signaling Pathway to the CNS

The primary auditory pathway is conveyed through four relays before it reaches the auditory cortex for final processing (fig. 14). The cochlear nerve afferents travel from the cochlea to terminate in the first relay, the cochlear nuclear complex, located ipsilaterally in the medulla of the brainstem. The cochlear nuclear complex has two major components: the dorsal cochlear nucleus (DCN) and the ventral cochlear nucleus (VCN). The VCN is subdivided into the anteroventral cochlear nucleus (AVCN) and the posteroventral cochlear nucleus (PVCN). The nuclei are tonotopically organized similarly to the cochlea. Afferents from the low-frequency region of the organ of Corti project to the lateral-ventral portion of the DCN and the ventrolateral parts of the VCN. Afferents from the high-frequency region of the organ of Corti project to the dorsal portion of the VCN and the dorsal-medial parts of the DCN. The intermediate frequencies project between the two nuclei to preserve tonotopic organization. The VCN receives all acoustic input from the cochlear nerve only, while the DCN receives input from the cochlear nerve and neurons from the VCN. The DCN and VCN have particular cells within them that sort and analyze the acoustic input being delivered to them. The VCN extracts information from the timing of the firing of the afferents and the pattern of activation of the cochlear nerve population in order to improve the precision of the timing of the acoustic input. Meanwhile, the DCN extracts information to determine the location of the head and ears for orienting sound and deciphering between expected sound and unexpected sound cues.

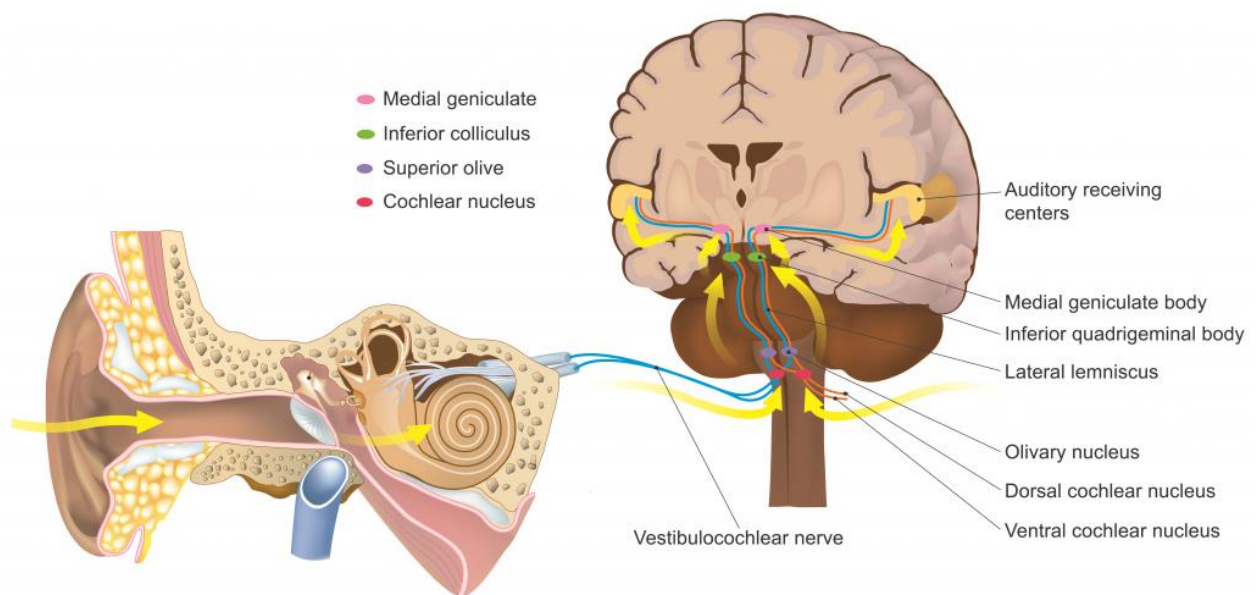


Figure 14: Diagram of the primary auditory pathway. The cochlear nerve projects to four relays (cochlear nuclear complex, superior olivary complex, inferior colliculus, medial geniculate) before it arrives to the auditory receiving cortical areas. Image is adapted from <https://teachmeanatomy.info/neuro/pathways/auditory-pathway/>.

The information extracted from the cochlear nuclear complex is transmitted via three major fiber bundles as parallel ascending pathways for further processing. The first fiber bundle, the ventral acoustic stria (VAS), projects through the medulla to the second relay, the superior olivary complex (SOC), with half of the fibers terminating on the contralateral side, while the other half terminates on the ipsilateral side. Efferent projections originate in the different regions of the SOC, the LSO and MSO, as described previously. The second fiber bundle, the dorsal acoustic stria (DAS), projects to the pons and terminates at the nuclei of the lateral lemniscus, a tract of axons within the brainstem that projects to various brainstem nuclei; the third fiber bundle, the intermediate acoustic stria (IAS), crisscrosses the medulla and also terminates at the lateral lemniscus. In turn, projections relayed to the SOC from the VAS will

ultimately come to terminate in the lateral lemniscus as well. The lateral lemniscus projects to the third relay, the inferior colliculus and primary midbrain nucleus of the auditory pathway, which integrates important functions like processing sound frequencies and integrating cues for localizing sound in space.

Two distinct pathways emerge from the inferior colliculus and innervate with the fourth relay, the ventral and dorsal medial geniculate nucleus of the thalamus. Neurons from the ventral area of the medial geniculate nucleus project to the primary auditory cortex, while neurons from the dorsal area of the medial geniculate nucleus project to the secondary auditory cortex, or the belt areas of the auditory cortex. The secondary auditory cortex is essential for sound detection and localization; it surrounds the primary auditory cortex and receives input from it. The primary auditory cortex identifies sound for perceptual processing. The different frequencies of sound are arranged similarly like in the cochlea, creating a tonotopic map on the cortex (fig. 15). The basal portion of the cochlea is represented in the medial portion of the cortex and the apical portion of the cochlea is located in the lateral portion of the cortex. Final processing of acoustic stimuli are completed in the auditory cortex leading to the identification and segregation of auditory cues, including pitch, volume, and mediating communication, and identifying the location of sound in space (Purves et al., 2004c).

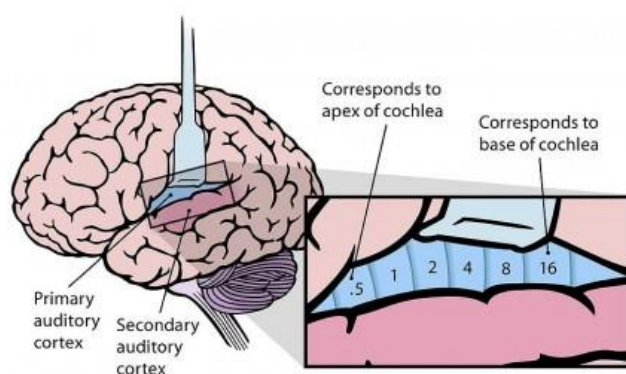


Figure 15: Diagram of the primary and secondary auditory cortices in the brain. The primary auditory cortex is organized with a tonotopic map, similar to the cochlea. The numbers represent frequencies in kHz. Image is adapted from Chittka and Brockmann, 2005.

3.15 Ototoxicity and Aminoglycoside Antibiotics

When sensorial hair cells of the vestibular and/or auditory systems are subjected to a specific kind of toxicity that causes their degeneration, it's referred to as ototoxicity. Exposure to ototoxic compounds causes impairment to the vestibular system leading to disequilibrium and vertigo, while impairment to the auditory system will cause varying degrees of hearing loss. Ototoxic examples for humans include pharmaceuticals like aminoglycoside antibiotics, anti-malarial drugs such as mefloquine, anti-neoplastic drugs like the chemotherapeutic agent cisplatin, and loop diuretics. The most common cases of ototoxicity in humans occur from the use of aminoglycoside antibiotics.

Aminoglycoside antibiotics are prescribed to combat gram negative bacterial infections, including *E. coli*, *Pseudomonas aeruginosa*, *Neisseria gonorrhoeae*, *Chlamydia trachomatis*, *Yersinia pestis*, and *Mycobacterium tuberculosis*. This medication inhibits protein synthesis by binding to the cytosolic, membrane-associated bacterial ribosome. The binding disrupts peptide elongation at the 30S ribosomal subunit, causing impairments of translational proofreading resulting in truncated proteins, premature termination, or altered amino acid composition. This leads to an inaccurately translated protein that will be incorporated into the bacterial cell membrane and cause changes in its permeability and further stimulate aminoglycoside transport into the bacteria (Mingeot-Leclercq et al., 1999). The first aminoglycoside antibiotic, streptomycin, was developed in 1944 and led to the successive introduction of numerous antibiotics like kanamycin, gentamicin, and tobramycin. However, the introduction of streptomycin brought to the forefront the debilitating consequences of ototoxicity of the inner ear. Ototoxicity can occur for any patient receiving

aminoglycoside treatment, although the likelihood and severity depends on which drug is being administered, the duration of the administration, and the dosage. The antibiotics are mostly administered intravenously and intramuscularly, although there are uses in some topical preparations for wounds, oral administration for gut decontamination, or in a nebulized form. Dosage and administration depend on the patient's weight and severity of the infection, and can be a single dose up to 80 days of administration. In general, 10% of patients taking aminoglycosides experience ototoxicity, but that can go up to as high as 33% in adult patients, and with a 3% chance of the damage being permanent (Virtual Medical Center, 2018). Symptoms of ototoxicity can present themselves as rapidly as following a single administration, or weeks later during or after the conclusion of a progressive administration. An ototoxic case series demonstrated a level of vestibulotoxicity in patients that occurred regardless of drug dosage or duration with diagnoses occurring from 4 days after treatment up to fifteen years after treatment (Ahmed et al., 2012). Damage may be permanent, semi-permanent, or completely recoverable, although the exact understanding of recoverability from aminoglycoside antibiotic ototoxicity is not fully known.

In many animal studies of vestibular dysfunction, the persistent use of a mild ototoxic substance over time causes a progressive deterioration, while more acute administrations can decimate the hair cell population. In the human population, it is more difficult to demarcate the onset of vestibulotoxicity, its progression, and its recoverability due to a lack of tests and tools to properly and accurately assess a patient's vestibular capacity (Llorens et al., 2018).

In the auditory system, cases of hearing impairment due to persistent ototoxic substance exposure can occur although less abundant when compared to noise-induced damage. Aminoglycosides in particular have demonstrated that up to 33% of patients administered experienced hearing loss, spreading from high to low frequencies depending on the duration of treatment and dose (Campo et al., 2015); OHCs have been shown to be particularly sensitive to antibiotics (Govaerts et al., 1990; Hashino et al., 1997; Forge and Schacht, 2000), while aminoglycosides can reside in the cochlea for several months after administration has ended (Tran Ba Huy et al., 1983; Dulon et al., 1993; Aran et al., 1999).

3.16 Animal Studies of Ototoxicity

Animal studies demonstrate that exposure to ototoxic substances may lead to permanent dysfunction due to the degeneration of the hair cells since these cells do not regenerate in the majority of mammalian species (Llorens et al., 1993). However, if a chronic aggressor is removed, symptoms may continue, or decrease up to either a complete or partial recovery of function. This variability does not follow the understood irreversibility of hair cell loss, and so indicates that other far less studied events may be occurring during progressive injury (Sedó-Cabezón et al., 2014).

Ototoxic studies of acute exposure to aminoglycosides and cisplatin, or other acute insults, are observed to cause numerous consequences. Hair cell death via apoptosis as seen in organ cultures is observed in both the vestibular and auditory systems; vestibular HCIs and auditory OHCs were predominately more affected than the other sensory hair cells (reviewed by Op de Beeck et al., 2011). Hair cell apoptosis or hair cell necrosis with *in vivo* models was also observed in both systems (Li et al., 1995; Forge and Schacht, 2000; Seoane et al., 2001a; Op de Beeck et al., 2011). Finally, acute excitotoxic damage from trans-tympanic injection of glutamate agonists was observed in the vestibular afferents (Gaboyard-Niay et al., 2016). Moderate dosages result in reversible swelling only (Brugeaud et al., 2007), while stronger dosages will cause total degeneration of the vestibular ganglion neurons (Raymond et al., 1988). Functional evidences have demonstrated a temporary loss of synaptic transmission, or “synaptic uncoupling” (Puel et al., 1995; Brugeaud et al., 2007; Sedó-Cabezón et al., 2015), for studied reversible damage to the terminals. Molecular studies of acute damage and degeneration or repair in the cochlea have been partly explored. Some noise exposure paradigms that do not cause hair cell degeneration may cause permanent damage to

the afferent terminals (Kujawa and Liberman, 2015). Likewise, patients with a familial history of hearing loss may also be more susceptible to hearing loss due to ototoxic exposure (Bitner-Glindzicz and Rahman, 2007).

3.17 The Introduction of Nitriles for Progressive Ototoxic Studies

These medical drugs, especially aminoglycosides, have been the main focus in the previous studies due to their importance to the population. However, rats and mice are comparatively more resilient to aminoglycoside-induced hair cell toxicity in *in vivo* studies (Oesterle et al., 2008; Taylor et al., 2008; Murillo-Cuesta et al., 2009, 2010) versus *in vitro* or trans-tympanic (acute) exposure studies (Forge and Schacht, 2000; Heydt, 2004). In response to this resilience, we decided to use nitriles as an alternative to the aminoglycoside ototoxic studies. It has been demonstrated that certain nitriles like IDPN (3,3'-iminodipropionitrile), allylnitrile, cis-crotonitrile, and cis-2-pentenenitrile are ototoxic in rats and mice (Llorens et al., 1993; Llorens and Demêmes, 1994; Balbuena and Llorens, 2001, 2003; Gagnaire et al., 2001; Boadas-Vaello et al., 2007, 2009; Saldaña-Ruíz et al., 2012). Data collected from these nitriles display significant similarity to aminoglycoside ototoxic compounds. In the cochlea, hair cell loss is observed from the beginning of the basal end to the apical end of the structure, and in the vestibular tissue from the striolar region towards the peripheral regions. These degenerative conditions observed with nitriles and aminoglycoside antibiotics are referred to as the “classic” pattern of ototoxicity (Lindemann, 1969; Wërsall et al., 1973; Llorens et al., 1993). This similarity allows us to study progressive ototoxic damage in rats and/or mice utilizing nitriles instead of aminoglycosides, and avoiding the difficulty of their resiliency.

The utilization of nitriles permits us to study ototoxic effects through a sub-chronic exposure model, rather than the more classic acute models. A sub-chronic model signifies an exposure protocol that consists of administering more than one dose, but will be exposed for less than a year. The majority of previous studies utilize an acute protocol such as *in vitro* or trans-tympanic injection experiments, but these models do not necessarily reflect what is occurring to humans that experience ototoxicity; the majority of human cases come from a sub-chronic intoxication, like with aminoglycoside antibiotic administration. These administrations can vary in dosage and duration, which led us to the conclusion that an acute model may not accurately reflect the ototoxic damage that may be occurring for progressive human cases. The amount of data pertaining to sub-chronic exposure to the vestibular sensorial hair cells and afferents and their ototoxic effects is few and far between. For these reasons, a new model of sub-chronic exposure to the nitrile IDPN through the drinking water for rats (Llorens and Rodríguez-Farré, 1997; Seoane et al., 2001a,b, 2003; Sedó-Cabezón et al., 2015) was developed. The sub-chronic exposure of IDPN for rats resulted in alterations in the behavior of the animals and alterations within the vestibular sensory epithelia and afferents, which included a loss of calyceal junctions between HCIs and their afferent terminals (fig. 16C-E), stereociliary coalescence (fig. 16D,E), the retraction and fragmentation of the afferent nerve terminals (Sedó-Cabezón et al., 2015) (fig. 16C-E), and finally, the detachment of the HCIs (Seoane et al., 2001b, fig. 16D-F). The detachment of HCIs is unique to the sub-chronic exposure compared to the acute experimentations. While the acute exposures result in hair cell apoptosis and/or necrosis, as previously mentioned, the sub-chronic exposure leads to hair cell extrusion. Hair cell extrusion is the ejection of a hair cell from the vestibular epithelium (fig. 16D-F). This occurs explicitly during sub-chronic exposure and is the culmination of the preceding alterations noted. However, molecular mechanisms and physiological understanding of this damage continues to be mostly unexplored and unanswered.

For this reason, this Thesis intends to characterize more thoroughly the progressive damage that occurs during sub-chronic intoxication of IDPN. Preliminary data (Deulofeu et al., 2014) were available to develop the mouse model established in this Thesis and IDPN was chosen because of its flexibility in

dosage within studies; it was demonstrated in high acute exposure studies (Llorens et al., 1993; Soler-Martín et al., 2007) and in sub-chronic drinking water exposures (Llorens and Rodríguez-Farré, 1997; Seoane et al., 2001a,b, 2003). By establishing and using a mouse model, functional, histological (ultra-structural, immunoconfocal), and molecular (RNA and protein) data were collected from the vestibular sensory epithelia and vestibular ganglia, which contain the cell bodies of the vestibular afferents that contact the hair cells of the vestibular epithelia. These studies were done to identify key molecular players involved in the synaptic pathology occurring during sub-chronic vestibular toxicity, and scrutinizing key proteins maintaining the calyceal junctions between HCIs and their calyces, along with proteins in charge of maintaining structural integrity of the hair cells and post-synaptic densities of the afferents. This Thesis also examined the recoverability of the system and whether molecular scarring occurred during sub-chronic intoxication, and if it persisted after the sub-chronic ototoxic insult was removed. In addition to vestibular ototoxic characterization, the first recorded sub-chronic intoxication experiment of the cochlea using the established sub-chronic IDPN protocol was completed, due to a newly formed collaboration. Functional and histological data were collected to compare synaptic pathology results with the vestibular system, and whether similar conclusions could be achieved in parallel to the two systems and/or where they diverged.

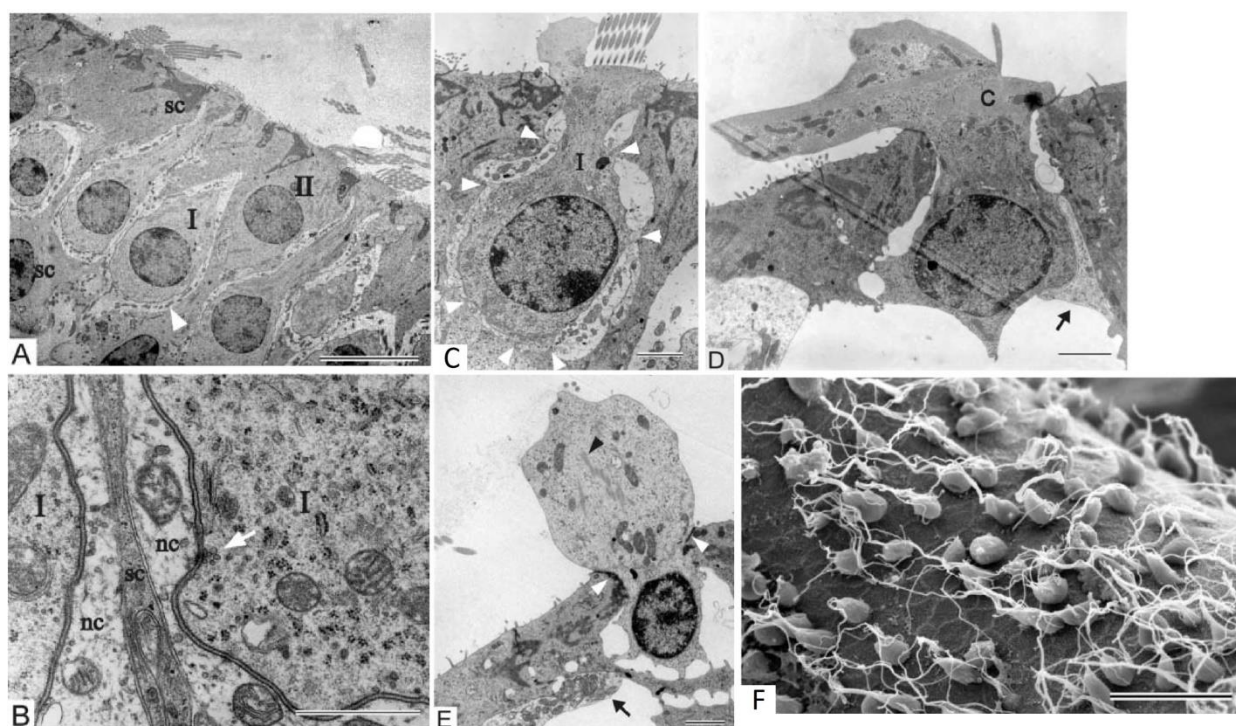


Figure 16: Transmission (A-E) or scanning (F) electron microscopy images of rat vestibular sensory epithelia after sub-chronic exposure to IDPN. **A** Image of the vestibular epithelium of a control rat. Type I hair cells (I) and a type II hair cell (II) are present, surrounded by supporting cells (sc). The calyx afferent nerve terminal is indicated (white arrowhead). **B** A magnified image of the calyceal junction between HCIs (I) and the calyx afferent nerve terminal (nc). The calyceal junction is electron dense (white arrow) and notable. **C** Type I hair cell (I) of the utricle of a rat exposed to 0.1% IDPN for 14 weeks. The afferent calyx surrounding the HCI is fragmenting (white arrowheads), an early alteration to the epithelium due to sub-chronic exposure. **D** Progressive damage to the HCI of a utricle of a rat exposed to 0.2% IDPN for 8 weeks. The stereocilia bundle has coalesced and the HCI is partially extruded passed the cuticular plate region (C). Cytoplasmic organelles can be seen in the protruded membrane. An afferent fiber (black arrow) can be seen making contact with the HCI, although without the calyceal junction in place. **E** HCI in a more advanced stage of extrusion in the crista of a rat exposed to 0.2% IDPN for 8 weeks. Stereociliary actin filaments (black arrowhead) are present in the protruded membrane, the apical tight junctions (white arrowheads), which anchor the hair cell to the epithelium, are present, and an afferent fiber (black arrow) is noted. **F** Protruding and extruding hair cells in a crista of a rat after 8 weeks of exposure to 0.2% IDPN. The supporting cells remain with a normal appearance with a high density of microvilli. Scale bars **A** 10 μ m, **B** 1 μ m, **C-E** 2 μ m, **F** 20 μ m. Images adapted from Seoane et al., 2001b.

4. Objectives

Objective 1: Determine how hair cell damage/loss due to sub-chronic exposure progresses in the mouse.

By following previous rat data (Sedó-Cabezón et al., 2015) on sub-chronic IDPN exposure, we wanted to identify the cellular basis of vestibular function loss in the mouse. To this end, we used ultra-structural techniques to visualize the progression of damage or loss. This includes observing for stereocilia coalescence and hair cell extrusion, characteristics described for the rat sub-chronic IDPN exposure. We expect to demonstrate stereociliary coalescence and hair cell extrusion if there is overt dysfunctional vestibular behavior.

Objective 2: Characterize the loss and potential recovery of calyceal junctions between HCIs and their afferents.

The previous rat data (Sedó-Cabezón et al., 2015) had characterized the loss of the calyceal junctions during IDPN exposure and then their recovery after a washout period. Utilizing ultra-structural techniques, we will demonstrate this loss and potential repair within the mouse vestibular epithelia. We will also utilize immunohistochemical techniques to quantify the loss and recovery of key/known proteins of the calyceal junction (caspr1), and the extracellular matrix protein (tenascin-c). We hypothesize that these proteins must be downregulated or mislocalized if we have observed ultrastructural calyceal junction dismantlement before.

Objective 3: Quantify the loss and potential recovery of synapses in sub-chronic vestibular toxicity.

We aimed to demonstrate that sub-chronic ototoxic exposure causes a loss of synapses in the vestibular sensory epithelium of the mouse, as previously demonstrated in the rat (Sedó-Cabezón et al., 2015). This includes the pre-synaptic ribbon, characterized by the core protein ribeye, and the post-synaptic clusters of glutamate receptors, specifically subunit GluA2, and in each of the three possible HC-afferent units (calyx-only units, HCII bouton afferent units, calyces from dimorphic afferents). Two additional post-synaptic density proteins will also be studied, PSD95 and Homer1, since both play an important role in PSD structure and organization. Determine if the loss of synapses is completely reversible, or becomes partially or fully permanent (Kujawa and Liberman, 2015; Sedó-Cabezón et al., 2015). We hypothesize that a complete recovery may or may not occur depending on the extent of the damage attained prior to the termination of the exposure. The extent of recovery may also be different within the different types of HC-afferent units.

Objective 4: Identification of molecular mechanisms implicated in the damage and repair processes occurring during sub-chronic ototoxicity.

By comparing RNAseq data from the vestibular sensory epithelia and vestibular sensory ganglia from control and exposed mice, we will identify possible molecular mechanisms being implicated in the damage and repair processes. This will be an initial analysis that should be extended in future studies.

Objective 5: Assess the toxicity of sub-chronic IDPN exposure on the cochlea.

A sub-chronic exposure experiment utilizing our established method has not been performed to study the cochlea up until now. The effects of sub-chronic IDPN exposure on the hearing of the mice will be assessed using auditory brainstem response measurements. If hearing loss is noted, immunofluorescent techniques will be utilized to determine for IHC or OHC loss and quantifying synaptic uncoupling. We hypothesize that hearing loss will occur with visible hair cell loss and/or synaptic damage, and that the extent of the damage will vary depending on the duration of the exposure.

5. Methodology

5.1 Animals

Two different strains of mouse were used for this thesis: the 129S1/SvImJ (129S1), which were from an established local colony at the University of Barcelona from previously purchased animals from Jackson Laboratory (Bar Harbor, ME, USA), and the 129S2/SvPasCrl (129S2), obtained from Charles River (Germany) and housed in the University Medical Center Groningen (UMCG) animal facility. In both facilities, the housing rooms were maintained at 22°C + 2°C with a 12:12 hr L:D cycle (0700-1900 hr) and they were allowed *ad libitum* access to food and filtered, sterilized tap water.

There were 190 129S1 mice used for experimentation, housed either individually or with up to 6 in a cage. They were placed in Makrolon cages (28x28x15 cm) with wood shavings as bedding and given standard diet pellets (TEKLAD 2014, Harlan Interfauna Ibérica, Sant Feliu de Codines, Spain). The use and care of the 129S1 mice at the University of Barcelona were approved by the Ethics Committee on Animal Experimentation of the University of Barcelona and performed in accordance with Law 5/1995 and Act 214/1997 of the Generalitat de Catalunya, EU Directive 2010/63, and Law 6/2013 and Act 53/2013 of the Gobierno de España.

There were 82 129S2 mice used for experimentation, and they were housed either individually or with up to 8 in a cage. Mice were received at 5 weeks of age, and given 1 week to acclimatize to the facility before starting any experimentation. All experiments for the 129S2 mice were approved by the animal ethics committee of the University of Groningen (UG) and UMCG, and complied with guidelines for animal experiments from the UG/UMCG, the Netherlands, and European animal welfare law.

All mice were monitored during exposure and weighed weekly in order to assess overall toxicity to limit suffering and to ensure quality of life. Mice found to have lost more than 20% of its initial body weight were terminated for ethical reasons. There was 1 129S1 mouse that died due to the IDPN exposure, and 1 129S2 mouse died due to poor recovery from the anesthetic after ABR evaluation.

5.2 Ototoxic IDPN Exposure

A total of 95 129S1 mice were exposed to 3,3'-iminodipropionitrile (IDPN, >98%, TCI Europe, Zwijndrecht, Belgium) in their drinking water, while 95 control mice received regular drinking water (see Table 1). Water bottles were changed weekly and weighed in order to estimate the dosage the mice were ingesting. Mice were evaluated weekly for any vestibular deficit caused by the exposure. There were 7 mice exposed to IDPN for 3 weeks, 17 mice exposed to IDPN for 5 weeks, and 71 mice exposed to IDPN for 8 weeks. Out of the 71 mice exposed to IDPN for 8 weeks, 21 mice that were exposed underwent a recovery ("washout") period of 11-13 weeks with standard drinking water and were utilized to model possible ototoxic recovery. Vestibular epithelia and ganglia were extracted from the mice and processed for immunofluorescent, ultrastructural, and/or molecular studies.

There were 38 129S2 mice exposed to IDPN for 2 (n=14), 4 (n=12), or 6 (n=12) weeks, 44 control mice receiving regular drinking water, and 7 of the mice that were exposed to IDPN for 2 weeks underwent a washout period of 4 weeks with standard drinking water to model potential ototoxic recovery (see Table 1). Water bottles were weighed and changed weekly, and the mice were evaluated for any auditory or vestibular deficits during weeks 2, 4, and 6 of the exposure. Washout animals were evaluated during the 2nd and 4th recovery week. Vestibular epithelia and the cochlea were extracted from these mice and processed for immunofluorescent studies.

	Study	Treatment Type	Number of Mice
129S1	Ototoxic Exposure, Body Weights, VDRs	Control	95
		IDPN 3	7
		IDPN 5	17
		IDPN 8	71
		WO	21
	First Immunostudy/Cristae, Calyceal Junctions	Control	6
		IDPN 8	3
		WO	5
	Second Immunostudy/Cristae, CtBP2/ribeye, GluA2, Colocalizations	Control	9
		IDPN 8	5
		WO	6
	Third Immunostudy/Cristae, CtBP2/ribeye, PSD95, Colocalizations	Control	6
		IDPN 8	6
		WO	6
	Fourth Immunostudy/Cristae, CtBP2/ribeye, Homer1, Colocalizations	Control	8
		IDPN 8	6
		WO	5
	SEM	Control	7
		IDPN 5	2
		IDPN 8	8
		WO	6
	TEM	Control	3
		IDPN 5	3
IDPN 8		4	
WO		3	
qRT-PCR	Control	46	
	IDPN 5	18	
	IDPN 8	44	
	WO	15	
RNA isolation (RNAseq)	Control	6	
	IDPN 8	6	
RNAseq	Control	3	
	IDPN 8	3	
RNA isolation study	Control	50	
129S2	Ototoxic Exposure, Body Weights, VDRs, ABRs	Control	44
		IDPN 2	14
		IDPN 4	12
		IDPN 6	12
		WO	7
	OHC Loss	Control	15
		IDPN 2	7
		IDPN 4	6
		IDPN 6	6
	Fifth Immunostudy/Utricle, Calyceal Junctions	Control	11
		IDPN 6	5
	Fifth Immunostudy/Organ of Corti, Caspr1 in first heminode	Control	15
		IDPN 4	6
		IDPN 6	5
	Fifth Immunostudy/Utricle, CtBP2/ribeye, GluA2, Colocalizations	Control	11
		IDPN 6	6
	Fifth Immunostudy/Organ of Corti, CtBP2/ribeye, GluA2, Colocalizations	Control	21
		IDPN 2	7
		IDPN 4	6
		IDPN 6	6

Table 1: Number of mice utilized per the different treatment groups for the various studies throughout the thesis.

5.3 Vestibular Dysfunction Ratings (VDRs)

In order to assess the vestibular deficit occurring in intoxicated animals, mice were tested with a well-established behavioral test battery, which has been validated in rats (Llorens et al., 1993; Llorens and Rodríguez-Farré, 1997; Boadas-Vaello et al., 2005; Sedó-Cabezón et al., 2015) and in mice (Soler-Martín et al., 2007; Boadas-Vaello et al., 2007, 2009; Saldaña-Ruíz et al., 2012b, 2013).

The behavioral test battery evaluated 6 different conducts: 3 spontaneous comportments observed in an open field and 3 anti-gravity reflexes. Each conduct was rated from 0 to 4, 0 as a normal vestibular response, and 4 signified a highly dysfunctional response. This allowed for a total vestibular dysfunction rating (VDR) that ranged from 0 to 24. Mice were placed in an empty rat cage and observed in silence for 1 minute in order to assess and rate the 3 open field measurements, which included: head bobbing (intermittent extreme backward extension of the neck), circling (stereotyped circulatory ambulation), and retropulsion (backward movement). Next, the 3 anti-gravity reflexes were assessed and rated. These included: the tail-lift reflex, the air-righting reflex, and contact inhibition of the righting reflex. For the tail-lift reflex, healthy mice demonstrated an extension of the body and forelimbs towards the Earth's center of gravity during the lift, while vestibular-deficient mice bend or curl the body ventrally. The air-righting reflex involved flipping mice into a supine position in midair, which resulted in the mice correcting themselves and dropping onto a foam cushion, landing on their paws. Vestibular-deficient mice did not right themselves from the supine position, causing them to land on the foam on their side or back. Contact inhibition of the righting reflex involved flipping a mouse into a supine position onto a horizontal surface. The mouse would then be trapped between the horizontal surface and a rigid sheet of plastic, where the soles of their paws touch the plastic. Healthy mice correct themselves, turning over to an upright position, while vestibular-deficient mice do not correct themselves, causing them to “walk” across the plastic sheet on the ventral surface.

5.4 Auditory Brainstem Response (ABR) Measurements

Auditory Brainstem Responses (ABRs) were measured as described previously (Reijntjes et al., 2018). Both click and pure tone (8, 16, 24, 32 kHz) ABRs were recorded from the right ear only to reduce the total time under anesthesia. Dedicated hardware and software were used to generate acoustic stimuli (Intelligent Hearing Systems (IHS)) with durations of 25 μ s (for click stimuli) or 5,000 μ s (for tone bursts) at a rate of 21.1 times/s. Peak to peak calibrations were used to determine the sound pressure level (in decibels, dB SPL), as previously described (Burkard, 2006). ABRs were recorded with an initial intensity of 20 dB SPL and then increased to 90 dB SPL in 5 dB SPL increments. An example intensity trace is shown in figure 17, at 75 dB SPL. Electrode recordings were amplified 100x, bandpass filtered between 30 and 3,000 Hz, and averaged over 512 recordings. Wave I absolute thresholds were set at the first intensity where it was distinguishable above the noise and appeared consistently in subsequent recordings. Wave I amplitudes were set by marking the crest of Wave I, and then its trough (fig. 17, blue solid arrows). Amplitudes were marked only when the trough was even with, or cleared, the noise floor. Wave I latencies were calculated as the time needed for Wave I to appear after receiving the click stimulus or tone burst; this was automatically calculated within the IHS program when marking the absolute threshold of Wave I.

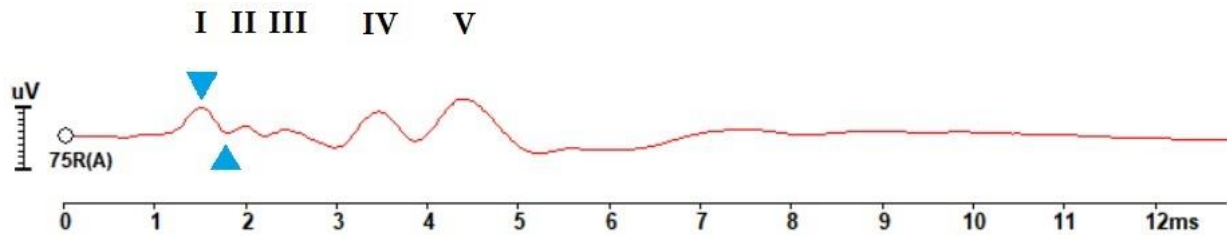


Figure 17: Example intensity trace at 75 dB SPL acquired during ABR measurement. The five Waves are labeled, but only Wave I was assessed. The x axis consists of time (ms) and the y axis of amplitude (μV). Using the IHS program, Wave I was manually labeled (inverted blue arrow) at its crest and the program would automatically calculate the latency of the Wave. The trough of Wave I was manually labeled (upright blue arrow) when it was equal to or below the noise floor ($\mu\text{V}=0$), and the program would automatically calculate the amplitude of Wave I.

Input/output (I/O) function slopes were calculated for Wave I amplitude and latency for the click stimuli and for each of the four tone bursts, when applicable. Slope values were calculated from individual mice over stimulus intensities ranging from 25-90 dB SPL and were analyzed for significance between the different treatment groups. Slopes were calculated as follows: first, the amplitude/latency of Wave I at each stimulus intensity was calculated from individual mouse ABRs (sample stimulus intensity, figure 17). Then, the amplitude/latency data of individual mice were plotted as a function of the stimulus intensity. Finally, the slope of each line was calculated per mouse and analyzed by treatment group.

5.5 Tissue Dissection and Epithelia/Ganglia Extraction

Tissue acquisition varied according to the experiment and study.

The vestibular epithelia and ganglia were isolated from 129S1 mice; mice were anaesthetized with an intraperitoneal injection of 400 mg/kg chloral hydrate and then decapitated. The skull was split, with the temporal bones uncovered and the bony labyrinth of the inner ear exposed, and then placed in cold 1x phosphate buffered saline (PBS) or fixatives. The vestibular ganglia were extracted from the surface of the labyrinth, while the 3 cristae, the utricle, and the saccule were excavated from the semicircular canals of each ear. The first ear was dissected within the first 5 minutes after decapitation, and the second ear was dissected within 15 minutes of decapitation.

The vestibular epithelia and the cochlea were isolated from 129S2 mice; mice were anaesthetized with 75 mg/kg dexmedetomidine via a subcutaneous injection into the loose skin between the shoulders and neck. The mouse was decapitated and the skull was split in half and placed in cold 1x PBS. The bony labyrinth of the inner ear was dissected out of the temporal bone and left intact. Two small holes were carved into the bony labyrinth: one hole at the apical end of the cochlea and one hole in the vestibule above where the utricle would lie. The tissue were fixed within the bone (explained in later text), and then put back into cold 1x PBS to be dissected. The vestibular epithelia (3 cristae, 1 utricle, 1 saccule) were dissected out of the bony labyrinth, and the organ of Corti was dissected out of the cochlea for each ear. The first ear was dissected within the first 5 minutes after decapitation, and the second ear was dissected within 15 minutes of decapitation.

5.6 Immunofluorescent Studies

After dissection, 129S1 vestibular tissues for immunostainings were fixed for 1 hr in 4% paraformaldehyde (PFA) in PBS with 15% picric acid at room temperature. The samples were rinsed and then stored in a cryoprotective solution (34.5% glycerol, 30% ethylene glycol, 20% PBS, 15.5% distilled water) at -20°C until processing for immunofluorescence. Immunofluorescent studies with vestibular epithelia for 129S1 mice varied in minor steps throughout the different protocols. In all cases, whole

vestibular cristae were immunostained with an equal number of specimens for each experimental group and processed in parallel to equal batch-to-batch differences in labeling. Primary and secondary antibody information is listed in Table 2 at the end of this section.

5.6.1 First Protocol/Study

Epithelia were rinsed from the cryoprotective solution in 2 washes of 500 μ l 1x PBS for 20 minutes each. The samples were then permeabilized and blocked in 500 μ l of 4% Triton-X-100 (Lysakowski et al., 2011) and 20% donkey serum in PBS for 90 minutes at room temperature. They were then incubated with the primary antibodies anti-caspr1 mouse monoclonal (IgG1), anti-tenascin-c rabbit polyclonal, and anti-Na⁺/K⁺-ATPase α 3 goat polyclonal in 200 μ l of 0.1% Triton-X-100 and 1% donkey serum in PBS for 48 hrs at 4°C. After incubation, the samples were rinsed 4 times in 500 μ l of PBS for 10 minutes each. The epithelia were then incubated with the secondary antibodies AlexaFluor 555 donkey anti-goat (IgG) and AlexaFluor 647 donkey anti-rabbit in 200 μ l of 0.1% Triton-X-100 in PBS for 2 hrs at room temperature. The samples were twice rinsed briefly in 500 μ l of PBS, and then incubated in the secondary antibody AlexaFluor 488 goat anti-mouse (IgG1) in 200 μ l of 0.1% Triton-X-100 in PBS for 2 hrs at room temperature. After the final incubation, the samples were rinsed 4 times in 500 μ l of PBS for 10 minutes each at room temperature. All incubations and rinses were done in slow agitation, and additionally in complete darkness after incubating with the secondary antibodies.

After staining, the samples were embedded in 0.49% gelatin, 30% bovine serum albumin, and 20% sucrose in 1x PBS overnight at 4°C. Finally, each sample was fixed within a gelatin block. The block was created by mixing 250 μ l of the previous gelatin solution and 22.5 μ l of 25% glutaraldehyde into a preconstructed mold, which solidified after 15 minutes. Once solidified, one epithelium was positioned and oriented on the block's surface (fig. 18), and a second block was formed over top of it. This layered block, with the specimen situated inside, was sectioned at 40 μ m tissue slices using a Leica VT100M vibrating microtome (Leica Microsystems CMS GmbH, Mannheim, Germany). The slices were mounted on glass slides in Mowiol medium, covered with a glass slip, and then stored at 4°C until viewing with a confocal microscope.

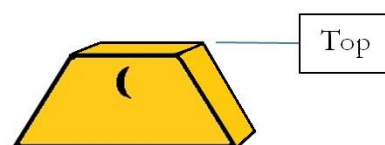


Figure 18: Block (side view). Cristae were orientated so that the visible line of cells seen with the use of a binocular microscope were laid out in a crescent shape; cuts to the block were made across the top allowing for correctly oriented hair cells (HCs) to be visualized and analyzed.

5.6.2 Second Protocol/Study

Vestibular epithelia were rinsed from the cryoprotective solution and then permeabilized and blocked for 90 minutes. The epithelia were incubated with the primary antibodies anti-GluA2 mouse monoclonal (IgG2a), anti-CtBP2/ribeye mouse monoclonal (IgG1), and anti-calretinin rabbit polyclonal for 48 hrs at 4°C. After incubation, they were rinsed with PBS, and then incubated with the secondary antibodies AlexaFluor 647 donkey anti-rabbit (IgG), AlexaFluor 555 goat anti-mouse (IgG1), and AlexaFluor 488 goat anti-mouse (IgG2a) in 200 μ l of 0.1% Triton-X-100 in PBS for 24 hrs at 4°C. The samples were then rinsed with PBS and embedded in the gelatin solution and stored overnight at 4°C. All incubations and rinses were done in slow agitation, and additionally in complete darkness after incubating with the

secondary antibodies. Blocks were formed and sliced as previously described, and then stored at 4°C until further processing.

5.6.3 Third Protocol/ Study

Vestibular epithelia were rinsed from the cryoprotective solution and then permeabilized and blocked in 300 µl of 4% Triton-X-100 and 5% donkey serum in PBS for 1 hr. Then, the epithelia were incubated overnight with the primary antibodies anti-CtBP2/ribeye mouse monoclonal (IgG1), anti-calretinin rabbit polyclonal, and anti-PSD95 mouse monoclonal (IgG2a) in 300 µl of the blocking buffer. The samples were then rinsed 3 times in 400 µl of PBS with 0.6% Triton-X 100 (PBT) for 10 minutes each. Epithelia were incubated with the secondary antibodies AlexaFluor 647 donkey anti-rabbit (IgG), AlexaFluor 555 goat anti-mouse (IgG1), and AlexaFluor 488 goat anti-mouse (IgG2a) in 300 µl of the blocking buffer for 4 hrs. After incubation, the samples were rinsed 3 times with 400 µl of PBT for 10 minutes each and then once in 400 µl of PBS for 10 minutes. The tissue was additionally fixed in 400 µl of 4% PFA for 30 minutes, and then rinsed twice in 400 µl of PBS for 10 minutes each. After rinsing, the samples were embedded in the gelatin solution and stored overnight in 4°C. All incubations and rinses were done in slow agitation at room temperature, and additionally in complete darkness after incubating with the secondary antibodies. Blocks were formed and sliced as previously described, and then stored at 4°C until further processing.

5.6.4 Fourth Protocol/ Study

Vestibular epithelia were rinsed from the cryoprotective solution and then preincubated for permeability in 500 µl of 4% Triton-X-100 in PBS for 1 hr at room temperature. Epithelia were then preincubated for blocking in 500 µl of 0.5% Triton-X-100 and 1% fish gelatin in PBS for 1 hr at room temperature. The samples were incubated with the primary antibodies anti-CtBP2/ribeye mouse monoclonal (IgG1), anti-homer1 rabbit polyclonal, and anti-calretinin goat polyclonal in 200 µl of 1% donkey serum and 1% fish gelatin in PBS for 24 hrs at 4°C. After incubation, the epithelia were rinsed 4 times in 500 µl of PBS for 10 minutes each. Then, they were incubated overnight with the secondary antibodies AlexaFluor 555 donkey anti-goat (IgG), AlexaFluor 647 donkey anti-rabbit (IgG), and AlexaFluor 488 donkey anti-mouse (IgG) in 200 µl of 0.1% Triton-X-100 and 1% fish gelatin in PBS at 4°C. The samples were then rinsed with PBS and embedded in the gelatin solution and stored overnight at 4°C. All incubations and rinses were done in slow agitation, and additionally in complete darkness after incubating with the secondary antibodies. Blocks were formed and sliced as previously described, and then stored at 4°C until further processing.

5.6.5 Fifth Protocol/ Study

The fifth immunofluorescent protocol was utilized for the vestibular epithelia and organs of Corti of 129S2 mice. As stated previously, during the dissection of the ears of the 129S2 mice, the whole inner ear bony labyrinth was extracted from the temporal bones of the skull. Two holes were chiseled into the bony labyrinth structure, and then placed into 4 mL of cold 4% PFA for 1 hr. The structure was agitated every 20 minutes in order to allow the PFA to penetrate the tissue and fix it evenly. Once fixed, the structure was placed back into cold PBS and the organ of Corti and the vestibular epithelia were carefully dissected out of the labyrinth for immunostaining.

Isolated sensory epithelia were placed in 400 µl of blocking buffer (5% normal goat serum, 4% Triton X-100, and 1% saponin in PBS) for at least 1 hr. The tissue was then incubated overnight with the following primary antibody combinations diluted in 300 µl of the blocking buffer: anti-prestin rabbit polyclonal, anti-CtBP2/ribeye mouse monoclonal (IgG1), anti-GluA2 mouse monoclonal (IgG2a) [cochlea]; anti-caspr1 mouse monoclonal (IgG1), anti-calretinin rabbit polyclonal [cochlea]; anti-CtBP2/ribeye mouse

monoclonal (IgG1), anti-GluA2 mouse monoclonal (IgG2a), anti-MyosinVIIa rabbit polyclonal [utricle]; anti-caspr1 mouse monoclonal (IgG1), anti-MyosinVIIa rabbit polyclonal [utricle]. Then, the samples were washed 3 times for 10 minutes each in 400 μ l of PBT. Epithelia were incubated with the secondary antibodies AlexaFluor 488 goat anti-mouse (IgG1), AlexaFluor 568 goat anti-rabbit (IgG), and AlexaFluor 647 goat anti-mouse (IgG2a) in 400 μ l blocking buffer for at least 4 hrs. The same secondary antibodies were used for all primary antibody combinations for both the organs of Corti and vestibular sensory epithelia. Then, the tissue was washed 3 times for 10 minutes each in 400 μ l of PBT and then once more for 10 minutes in 400 μ l of PBS. All incubations and rinses were done in slow agitation at room temperature, and additionally in complete darkness after incubating with the secondary antibodies.

The two ears, which included both organs of Corti and utricles, were mounted intact with VectaShield on a single glass slide per mouse. Glass cover slips were placed over the samples in VectaShield and sealed. Slides were stored in a 4°C refrigerator until light or confocal microscopy analysis.

Primary Antibody	Host and Type	Source	Catalog #	Concentration
Caspr1	Mouse Monoclonal (IgG1)	NeuroMab	75-001	1:400, 1:300
Tenascin-C	Rabbit Polyclonal	Millipore	AB19013	1:200
Na ⁺ /K ⁺ -ATPase α 3	Goat Polyclonal	Santa Cruz	SC16052	1:300
GluA2	Mouse Monoclonal (IgG2a)	Millipore	MAB397	1:200, 1:300
CtBP2/ribeye	Mouse Monoclonal (IgG1)	BD Bioscience	612044	1:200, 1:500
Calretinin	Rabbit Polyclonal	Swant	7699/3H	1:1000
PSD95	Mouse Monoclonal (IgG2a)	NeuroMab	75-028	1:200
Homer1	Rabbit Polyclonal	Synaptic Systems	160 002	1:500
Calretinin	Goat Polyclonal	Millipore	AB1550	1:400
Prestin	Rabbit Polyclonal	Gift from Dr. Mary Ann Cheatham		1:3000
Calretinin	Rabbit Polyclonal	Millipore	AB1550	1:500
MyosinVIIa	Rabbit Polyclonal	Prestige Antibodies	HPA028 918	1:500
Secondary Antibody	Host and Type	Source	Catalog #	Concentration
AlexaFluor 555	Donkey anti-goat (IgG)	Life Technologies	A21432	1:500
AlexaFluor 488	Goat anti-mouse (IgG1)	ThermoFisher	A21121	1:500
AlexaFluor 647	Donkey anti-rabbit (IgG)	ThermoFisher	A31573	1:500, 1:600
AlexaFluor 555	Goat anti-mouse (IgG1)	ThermoFisher	A21127	1:500
AlexaFluor 488	Goat anti-mouse (IgG2a)	Molecular Probes	A21131	1:500
AlexaFluor 488	Donkey anti-mouse (IgG)	Life Technologies	A21202	1:500
AlexaFluor 568	Goat anti-rabbit (IgG)	ThermoFisher	A11011	1:500
AlexaFluor 647	Goat anti-mouse (IgG2a)	ThermoFisher	A21241	1:500

Table 2: List of all primary and secondary antibodies used in the immunofluorescent studies.

5.7 Cochlear Place-Frequency Maps

The fifth immunofluorescent study utilized wholly mounted organ of Corti. To identify targeted frequencies in the organ of Corti, cochlear place-frequency (tonotopic) maps were determined for each organ of Corti from each ear of each 129S2 mouse. Low magnification micrographs were obtained with a Leica DM4000b microscope with the 5X objective. A compound image of individual cochlear sections (generally 2 to 3 sections) was constructed for each organ of Corti using Fiji ImageJ (Schindelin et al., 2012). Tonotopic maps were overlaid using the mouse cochlear frequency map determined previously (Müller et al., 2005) in Fiji ImageJ using the plugin found at:

<https://www.masseyeandear.org/research/otolaryngology/investigators/laboratories/eaton-peabody-laboratories/epl-histology-resources/imagej-plugin-for-cochlear-frequency-mapping-in-whole-mounts> .

The new, overlaid image was referenced during confocal microscopy in order to capture specific images at specific frequencies (8, 16, 24, 32 kHz) of the organ of Corti for quantification.

5.8 Confocal Microscopy and Image Analysis

A Leica TCS-SL confocal microscope was used for the first and second immunofluorescent study, a Zeiss LSM 880 confocal microscope was used for the third and fourth immunofluorescent study, and a Leica TCS SP8 confocal microscope was utilized for the fifth immunofluorescent study. The Leica TCS-SL and Zeiss LSM 880 confocal microscopes were provided by the Technological and Scientific Units (CCiT) of the University of Barcelona, and the Leica TCS SP8 confocal microscope was provided by the UMCG Microscope and Imaging Center (UMIC, Groningen, The Netherlands), by payment of service fees.

Quantitative data were obtained from ideally oriented sections from the central areas of the neuroepithelium and most accurately estimated frequency in the organ of Corti.

The calyceal junctions of the central areas of the cristae were studied in the first immunofluorescent study. For quantitative analysis, Z stacks of 50 images with 0.5 μm thick optical sections, spanning a total of 25 μm , were obtained from the individual 40 μm tissue slices. Two different tissue slices were analyzed for each of 6 control mice, 3 mice treated with IDPN for 8 weeks, and 5 mice after the washout period. Each Z stack was split into 5 serial snapshots by projecting 10 consecutive images onto one another; the 5 serial snapshots had a thickness of 5 μm each. From each snapshot, the total number of calyces with distinct caspr1 or tenascin-c immunoreactivities, and their colocalizations, were counted in ImageJ (Schneider et al., 2012). The number of HCs analyzed for control mice spanned from 525 to 893, the number of HCs for IDPN-treated mice spanned from 10 to 17, and the number of HCs for washout mice spanned from 396 to 470. All images were acquired at a 1024x1024 pixel resolution at a zoom level of 2 and from averaging 2 images together with the 63X oil immersion objective with the Leica TCS-SL confocal microscope.

The synaptic elements within three possible HC-afferent arrangements arrayed in the cristae were analyzed in the second, third, and fourth immunofluorescent studies. The three HC-afferent arrangements included: HCI-calyx-only units (identified by positive calretinin labeling of the calyx afferent), HCII-bouton units (identified by shape and calretinin-positive labeling of the HCII), and HCI-dimorphic units (calyces negative of calretinin labeling).

For quantitative analysis of CtBP2/ribeye and GluA2 puncta, the second immunofluorescent study was processed in a similar manner to the first immunostaining study. At least three different tissue slices (except for 1 control animal) were analyzed for each of 9 control mice, 5 mice treated with IDPN for 8 weeks, and 6 mice after the washout period. Z stacks consisting of 50 images with a 0.5 μm optical section thickness, spanning 25 μm in total thickness, were obtained from each 40 μm tissue slice. Each Z stack was split into 5 serial snapshots, as described previously. From each snapshot, the number of

CtBP2/ribeye puncta, GluA2 puncta, and the ribeye-GluA2 colocalizations were determined within synapses from the three different HC-afferent units using ImageJ. The number of puncta per HC were counted from 169 HCs of control mice, 147 HCs of IDPN-treated mice, and 188 HCs of washout mice, with the number of cells per unit type and treatment group varying between 25 to 74. All images were acquired at a 1024x1024 pixel resolution at a zoom level of 2 and from averaging 2 images together with the 63X oil immersion objective with the Leica TCS-SL confocal microscope.

Quantitative analysis of CtBP2/ribeye and either PSD95 or Homer1 puncta, and their colocalizations, were analyzed in the third and fourth immunofluorescent studies. At least two different tissue slices were analyzed for each mouse of each experimental group. All images acquired from each 40 μm tissue slice were taken with the 63X oil immersion objective at a zoom level of 1 with the Zeiss LSM 880 confocal microscope. Images were taken at a 1024x1024 pixel resolution and 2 images were averaged together at each step. Z stacks were obtained with a total thickness of 25 μm with 0.2 μm (CtBP2/ribeye/PSD95) or 0.4 μm (CtBP2/ribeye/Homer1) optimally optical section thicknesses, and then uploaded into Imaris v9.0 (Bitplane, Inc) for quantitative analysis. In Imaris, the “Spots” function was utilized to demarcate CtBP2/ribeye, PSD95, or Homer1 puncta with spot sizes of an estimated XY diameter of 0.6 μm , and an estimated Z diameter of 1.2 μm . Puncta demarcations were verified by hand to ensure accuracy of the function and adjusted when necessary. After verifying the puncta, the “Colocalize Spots” MatLab function integrated in the Imaris software was used to mark CtBP2/ribeye and PSD95 puncta colocalizations or CtBP2/ribeye and Homer1 puncta colocalizations that were within 1 μm of each other. These colocalizations were also verified by hand in order to ensure accuracy, and final counts were obtained directly from the program.

In the third study with CtBP2/ribeye and PSD95, there were 6 control mice, 6 mice treated with IDPN for 8 weeks, and 6 mice that underwent a washout period. The number of puncta per HC was obtained from 270 HCs of control mice, 237 HCs of IDPN-treated mice, and 239 HCs of washout mice. The number of cells per unit type and treatment group varied from 48 to 131.

In the fourth study with CtBP2/ribeye and Homer1, there were 8 control mice, 6 mice treated with IDPN for 8 weeks, and 5 washout mice. The number of puncta per HC was obtained from 355 HCs of control mice, 220 HCs of IDPN-treated mice, and 227 HCs of washout mice. The number of cells per unit type and treatment group varied from 52 to 170.

In the final immunofluorescent study, OHC quality, HC-afferent synapse integrity, and synaptic elements of the utricles and organs of Corti of 129S2 mice were studied. All images were taken with the 63X oil immersion objective at a zoom level of either 2 (striola of utricle) or 1 (organs of Corti) with the Leica TCS SP8 confocal microscope. Images were taken at a pixel resolution of 1024x1024 with an optimal optical section thickness of 0.3 μm resulting in Z stacks ranging in size of 6-13 μm (striola of utricle) or 25-50 μm (organs of Corti) in order to encompass the entire synaptic pole of the sensory hair cells. Z stacks were uploaded into either Fiji ImageJ or Imaris v7.6-9.0 for quantitative analysis. The striolar area of the utricle were imaged, while the cochlear segments most accurately estimated as the frequencies of 8, 16, 24, or 32 kHz were imaged using the frequency maps constructed earlier for each organ of Corti.

In order to assess OHC loss, snapshots of whole Z stacks with the immunostaining for prestin in the organ of Corti were made using the LAS AF Lite program, overlaying all images within the stack to create one, conglomerate image. A montage image was created for each selected frequency for each mouse of each treatment group when applicable. This assessment utilized 15 control mice and 19 mice treated with IDPN for 2 (n=7), 4 (n=6), or 6 (n=6) weeks. Each snapshot was uploaded into Fiji ImageJ in order to quantify the number of IHCs and OHCs. For every IHC, there are three OHCs. Ten IHCs were marked, and the corresponding OHCs to those IHCs were marked; missing OHCs were noted as a loss.

Assessment of HC-afferent synapse integrity noted the presence or absence of caspr1 immunoreactivity within calyceal junctions of the HCIs of utricles, and measuring the lengths of the first individual caspr1-labeled heminodes of type I afferent fibers making synapses with IHCs in the organ of Corti. In the utricle, MyosinVIIa was stained to demonstrate all HCIs, while caspr1 staining demonstrated the presence of a calyceal junction for HCIs. A total of 11 control mice and 5 mice treated with IDPN for 6 weeks were compared to one another to determine the presence or absence of calyceal junctions before and after IDPN exposure. A total of 1685 HCIs were analyzed for control mice, and 600 HCIs in IDPN-treated mice. In the organ of Corti, calretinin immunoreactivity marked the IHCs and caspr1 immunoreactivity was present in the first heminodes of the type I afferents. Using the “Measure” function of Imaris, caspr1 was measured in length due to their tube-like structure. At least 6 measurements were taken per IHC and at least 6 IHCs were measured per frequency per organ of Corti per mouse when applicable. The lengths of caspr1 were compared between the four frequencies within and between 15 control mice and 11 mice treated with IDPN for either 4 (n=6) or 6 (n=5) weeks. A total of 498 IHCs were analyzed with 3735 measurements for control mice, 159 IHCs with 889 measurements for mice treated with IDPN for 4 weeks, and 187 IHCs with 843 measurements for mice treated with IDPN for 6 weeks.

Finally, the synaptic elements CtBP2/ribeye and GluA2 were analyzed within the utricle and organ of Corti of control and IDPN-treated mice. Z stacks of the striolar region of the utricle and of the four selected frequency regions of the organ of Corti were uploaded into Imaris for quantification. The “Spots” function was used to demarcate the CtBP2/ribeye puncta and GluA2 puncta with spot sizes of an estimated XY diameter of 0.6 μm , and an estimated Z diameter of 1.2 μm . All marked puncta were verified manually to ensure accuracy of the function. Once identified, the integrated MatLab function “Colocalize Spots” was used to identify CtBP2/ribeye and GluA2 puncta colocalizations within 1 μm of each other. Colocalizations were verified manually to ensure accuracy. Puncta counts were extracted from the program. In the utricle, 11 control mice and 6 mice treated with IDPN for 6 weeks were analyzed. A total of 1682 HCIs were analyzed for the control mice, and 807 HCIs for the IDPN-treated mice. In the organ of Corti, 21 control mice and 19 mice treated with IDPN for 2 (n=7), 4 (n=6), and 6 (n=6) weeks at the four studied frequencies were analyzed, when applicable. A total of 1758 IHCs were analyzed for control mice, 492 IHCs were analyzed for mice treated with IDPN for 2 weeks, 781 IHCs were analyzed for mice treated with IDPN for 4 weeks, and 515 IHCs were analyzed for mice treated with IDPN for 6 weeks.

5.9 Scanning Electron Microscopy (SEM) Ultrastructural Studies

For ultrastructural studies, the first dissected ear of a chosen 129S1 mouse was used, while the second ear was used for immunofluorescent studies. At the time of dissection, the temporal bone with the bony labyrinth of the first ear was immersed in cold 2.5% glutaraldehyde in 0.1 M cacodylate buffer (pH 7.2) and the three cristae, the utricle, and the saccule were dissected out of the ear using a binocular microscope under a fume hood. The vestibular epithelia were fixed for 1.5 hrs, rinsed with the cacodylate buffer, post-fixed for 1 hr with 1% osmium tetroxide in the same buffer, rinsed again, and then placed in 70% ethanol and stored at 4°C until further processing.

The samples were dehydrated with increasing concentrations of ethanol up to 100%. The anterior and posterior cristae, the utricle, and the saccule were dried in a Polaron 3000 critical point apparatus using liquid CO₂, mounted and coated with carbon, and observed in a JEOL JSM-7001F field emission scanning electron microscope provided by the CCiT.

Each vestibular epithelium was examined and given a SEM Pathology Score ranging from 0-5. Scores are rated as follows: 0 = absent pathology; 1 = presence of membrane blebs behind the stereociliary bundles; 2 = presence of a small proportion (<5% of the population) of overtly damaged stereocilia bundles,

extruding, or missing HCs; 3 = significant presence (5-40%) of overtly damaged stereocilia bundles, extruding, or missing HCs; 4 = extensive presence (40-80%) of overtly damaged stereocilia bundles, extruding, or missing HCs; 5 = most HCs (>80% of the population) are missing, extruding, or showing fused stereociliary bundles. Cristae, utricle, and saccule samples were evaluated to assess HC and/or stereociliary damage between control epithelia, epithelia exposed to IDPN for 5 or 8 weeks, and epithelia from washout mice.

Finally, the total number of HCs in the utricle was assessed in Fiji ImageJ in order to gauge HC retention or loss due to ototoxic exposure. There were 7 control mice, 2 mice exposed to IDPN for 5 weeks, 8 mice exposed to IDPN for 8 weeks, and 6 washout mice.

5.10 Transmission Electron Microscopy (TEM) Ultrastructural Studies

Transmission electron microscope ultrastructural studies follow a similar protocol to SEM ultrastructural studies. The first dissected ear of a chosen 129S1 mouse would be immersed in cold 2.5% glutaraldehyde in 0.1 M cacodylate buffer and the vestibular epithelia was extracted from the bony labyrinth of the ear. The tissue would be fixed, rinsed, and dehydrated up to 100% ethanol as previously recorded in the SEM protocol. After dehydration, the lateral crista was embedded in Spurr resin. Semi-thin sections (1 μm) were stained with toluidine blue and observed in a light microscope to select specific regions of interest for TEM studies. Ultrathin sections were stained with uranyl acetate and lead citrate and examined in a JOEL 1010 electron microscope provided by the CCiT.

Using the “Measure” function in Imaris, the distance between the centers of adjacent membranes of the calyceal junction, the contact between HCIs and the calyx afferent, was measured in the TEM images (Sousa et al., 2009). Images were obtained from transverse sections, perpendicular to the surface of the epithelium, of the lateral crista at approximately 100-150 μm from its longitudinal edge. Control animals, animals exposed to IDPN for 5 or 8 weeks, and washout animals were compared to each other; 3 animals from each group were compared. There were 12-19 unique HCIs sequentially identified for each animal in the TEM images and analyzed. The localization of the HCIs analyzed varied in a pseudo-random distribution, due to the bars of the grids in which the tissue sections were mounted. For each HCI, 20-25 distances were measured at regularly distributed points along the basolateral membrane; the basolateral membrane extends from the basal end of the cell to the level of the upper end of the nucleus, where the calyceal junction is located in normal tissue (Sousa et al., 2009; Lysakowski et al., 2011; Sedó-Cabezón et al., 2015). For each point (total of 4,485 measurements), it was annotated whether the electrodense material, which characterizes the calyceal junction, was present or absent.

5.11 qRT-PCR Studies

A preliminary study was conducted to elect the most efficient protocol to isolate the greatest amount and best quality of RNA from vestibular epithelia and vestibular ganglia. A total of 50 129S1 mice were tested, with the vestibular epithelia and ganglia dissected out of both ears of each mouse in cold 1x PBS within the first 15 minutes after decapitation. Vestibular epithelia were either processed separately (3 cristae, 1 utricle), pooled together (6 cristae, 2 utricles), or pooled with multiple ears (12-24 cristae, 4-8 utricles). Vestibular ganglia were either processed separately (1 ganglia), pooled together (2 ganglia), or pooled with multiple ears (4-8 ganglia). Samples were placed within an Eppendorf to either be frozen in liquid nitrogen and stored in a -80°C freezer, or processed immediately after dissection.

The total RNA was isolated from these samples utilizing one of four protocols: the GE illustra RNAspin Mini Kit and its protocol from the manufacturer with a double DNase I digestion step, the standard GE illustra RNAspin Mini Kit and its protocol from the manufacturer, the Qiagen RNeasy Mini Kit and its protocol from the manufacturer, or a laboratory-established TRIZOL protocol.

The TRIZOL protocol was performed under a hood and with complete sterilization of the work area to avoid contamination. Tissue was taken from the -80°C freezer and 500 µl of the TRIZOL solution was added into the Eppendorf of the sample. Using a hand mixer, the tissue was disrupted for 30-35 seconds. A 20G needle and syringe were used to further disrupt the solution and then left for 5 minutes at room temperature. Then, 100 µl of chloroform was added to the solution and shaken vigorously for 15 seconds, followed by a 2-3 minute pause at room temperature. The solution was centrifuged for 15 minutes at 4°C at 12,000G. The top clear phase left after centrifugation was extracted and transferred to a new Eppendorf. Then, 250 µl of isopropanol was added and incubated for 10 minutes at room temperature. The solution was stored overnight in a -20°C freezer until the next day for further processing. In the next day, the solution was centrifuged for 10 minutes at 4°C at 12,000G, allowing the RNA to form into a pellet. The supernatant was removed and the pellet resuspended in 500 µl of 75% ethanol. It was centrifuged for 5 minutes at 4°C at 7,500G to wash the RNA. The supernatant was extracted and the pellet left to dry out. Finally, the pellet was resuspended in 20 µl of DEPC water and stored at -80°C until RNA quantity and quality processing.

Total RNA quantity and quality were assessed with an Agilent Bioanalyzer 2100 (Agilent Technologies, Santa Clara, CA, USA). The protocol that yielded the most consistent and effective results was established as the new laboratory protocol, and used for future qRT-PCR studies.

Once the preliminary study was completed, a total of five different qRT-PCR studies were performed comparing 46 control mice to 18 mice treated with IDPN for 5 weeks and 35 mice treated with IDPN for 8 weeks, and on occasion, with 15 mice that underwent a washout period as well.

Total RNA was extracted using the Qiagen RNeasy Mini Kit and protocol with the additional carrier RNA step. Samples were quantified with an Agilent Bioanalyzer 2100 and samples displaying a RIN of 7 or higher were processed further for qRT-PCR. Equal quantities of total RNA were reverse transcribed using a High-Capacity cDNA Reverse Transcription Kit (Applied Biosystems, Alcobendas, Spain). Equal amounts of cDNA (15 ng) were used for qRT-PCR analysis. Actin beta (Actb) or Glyceraldehyde-3-Phosphate Dehydrogenase (GAPDH) were used as the internal control gene. The qRT-PCR was performed with a SensiFAST Probe Hi-ROX kit (Bioline, Barcelona, Spain) in duplicate or triplicate with the Taqman assays (Life Technologies, Alcobendas, Spain) found in Table 3.

Gene	Assay ID
Actb	Mm00607939_s1
BDNF	Mm04230607_s1
Camk1G	Mm00460641_m1
Chrna6	Mm00517529_m1
Cntnap1	Mm00489702_m1
CtBP2	Mm00515572_m1
DLG4	Mm00492193_m1
DLGAP1	Mm00510688_m1
GAPDH	Mm99999915_g1
Gria2	Mm00442822_m1
Homer1	Mm00516275_m1
KCNQ5	Mm01226041_m1
NGFR	Mm00446296_m1
Nptx2	Mm00479438_m1
REST	Mm00803268_m1
SLC2A4	Mm00436615_m1
SLC17A6	Mm00499876_m1
Tnc	Mm00495662_m1

Table 3: Taqman Assays used in the various qRT-PCR studies.

Reaction mixtures (10 μ l) were first incubated at 50°C for 2 minutes and then at 95°C for another 10 minutes, followed by 40 cycles (95°C for 15 seconds and then 60°C for 1 minute) of PCR. Real-time fluorescence was detected using a 7900HT Real-Time PCR System (Applied Biosystems). Threshold cycles (Ct) were analyzed using Expression Suite software, and a relative quantification method ($\Delta\Delta$ Ct) was used to calculate target gene expression according to the Guide to performing Relative Quantitation of Gene Expression Using Real-Time Quantitative PCR (Applied Biosystems).

5.12 RNA-sequencing (RNAseq)

Throughout the qRT-PCR studies, the total RNA yield extracted from either the vestibular epithelia or vestibular ganglia was consistently low; these small yields only allowed for the study of 3-7 genes per mouse per qRT-PCR. For this reason, it was decided to implement a more viable protocol to maximize the amount of results to be obtained from each mouse. Thus, the first RNA-sequencing (RNAseq) studies were completed.

The total RNA of the vestibular ganglia from both ears from each of 6 control mice and 6 mice exposed to IDPN for 8 weeks were extracted using the Qiagen RNeasy Mini Kit and protocol with the additional carrier RNA step. They were quantified with an Agilent Bioanalyzer 2100 and the highest quality RNA (RIN >8) of 3 control mice and 3 treated mice were used for the first RNAseq study. The vestibular epithelia of the chosen mice also had the total RNA isolated, and as long as they were of high quality (RIN >8), they were processed in a second RNAseq study. These samples were processed by the National Center of Genomic Analysis (CNAG, Barcelona, Spain). Libraries were made from polyadenylated mRNA preparations, and sequenced to a depth of ≥ 40 M PE reads and read lengths of 2x75bp. Additional analyses are being carried out within the laboratory including: Gene Ontology (GO) analyses, Kyoto Encyclopedia of Genes and Genomes (KEGG) pathway enrichment analyses, and String functional protein association analyses. Future goals focus on identifying ontologies, pathways, transcription factors, and more involved with ototoxic exposure of the vestibular system.

5.13 Data Analysis-SPSS

Data are presented as mean \pm SE, except where indicated otherwise. Body weight and vestibular dysfunction data were analyzed with repeated-measures MANOVA (Wilks' criterion), repeated-measures ANOVA (Greenhouse-Geisser correction), or one-way ANOVA, depending on the number of degrees of freedom available. Day was the within-subject factor. Day-by-day analysis was performed after significant day-by-treatment interactions were recorded. Other data were analyzed by selected ANOVA designs and Duncan's post-hoc test, or by Student's *t* test. The IBM SPSS Statistics 25 program package was used.

6. Results

6.1 Preliminary Total RNA Isolation Study

6.1.1 Testing various protocols

The vestibular sensory epithelia and ganglia contain a small amount of cells, making total RNA extraction for downstream processes like qRT-PCR quite difficult. Previous total RNA extractions in the laboratory were completed using the GE illustra RNAspin Mini Kit and its protocol provided by the manufacturer with a double DNase I digestion step; the total RNA yield and quality were assessed using a NanoDrop ND-1000 Spectrophotometer, which was provided on site for the department. However, NanoDrop readings resulted in consistently low RNA quality and we concluded that the concentrations of RNA were too low to be read accurately by the NanoDrop. We began analyzing total RNA yields and quality via a picochip in an Agilent Bioanalyzer 2100. An exploratory study was conducted to elect the most efficient protocol to isolate the greatest amount and best quality of RNA from vestibular sensory epithelia and vestibular ganglia for the picochip analysis. A total of 50 129S1 male mice were utilized for the study. Vestibular sensory epithelia were either processed separately (3 cristae, 1 utricle [$\frac{1}{2}$ IVE]), pooled together (6 cristae, 2 utricles [IVE]), or pooled with multiple ears (12-24 cristae, 4-8 utricles [PVE(2), PVE(4)]). Vestibular ganglia were either processed separately (1 ganglia [$\frac{1}{2}$ Gang]), pooled together (2 ganglia [I Gang]), or pooled with multiple ears (4-8 ganglia [PGang(2), PGang(4)]). The total RNA was isolated from these samples utilizing one of four protocols: the GE illustra RNAspin Mini Kit and its protocol from the manufacturer with a double DNase I digestion step (GEx2), the standard GE illustra RNAspin Mini Kit and its protocol from the manufacturer (GE), the Qiagen RNeasy Mini Kit and its protocol from the manufacturer with the carrier RNA step (Q), or a laboratory-established TRIZOL protocol (T), which was described previously in the “Methodology” section.

Sample→	$\frac{1}{2}$ IVE	IVE	PVE(2)	PVE(4)	$\frac{1}{2}$ Gang	I Gang	PGang(2)	PGang(4)
Protocol↓								
GEx2		9	4	8		9	4	8
GE		7				7		
Q	2	4	2		2	4	2	4
T	2	4	2	4	2	4	2	4

Table 4: The total number of mice used in the preliminary total RNA isolation study for each protocol for each sample parameter.

After total RNA isolation of each sample, they were analyzed via a picochip with an Agilent Bioanalyzer 2100. The protocol that yielded the most consistent and effective RNA results was established as the new laboratory protocol, and used for future qRT-PCR studies, and later on, for RNAseq studies.

The Bioanalyzer is a chip-based capillary electrophoresis machine which analyzes RNA (or DNA or proteins) in quality control measurements. Each sample generates an individual RNA electropherogram that demonstrates the degradation quality of the RNA, the presence of genomic DNA contamination, the RNA concentration, the rRNA ratio (28s/18s), and the RNA Integrity number (RIN) (fig. 19a,b).

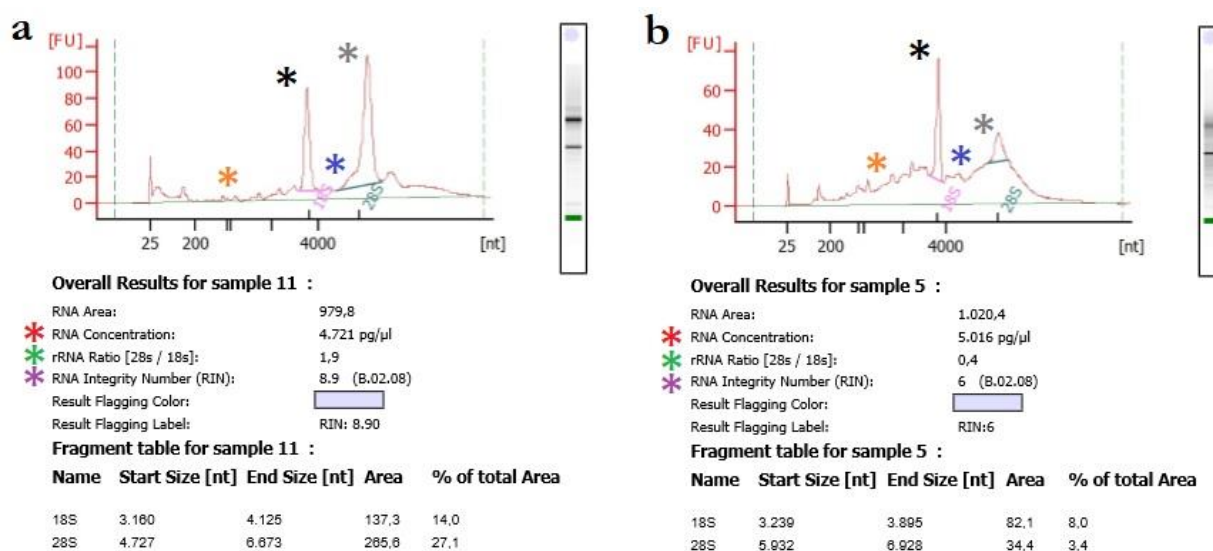


Figure 19: Example Bioanalyzer electropherograms. **a** Example of a high quality RNA sample. **b** Example of a poor quality RNA sample. **a,b** The electropherogram consists of two main peaks: the 18S peak (black asterisk) and the 28S peak (gray asterisk). Well-defined peaks represent less degraded and better quality RNA. The area in-between the two peaks (blue asterisk) needs to be as flat and as close to baseline as possible; spikes indicate contamination of genomic DNA. In general, the flatter and smoother the electropherogram, the better quality the RNA sample is (orange asterisk). The Bioanalyzer also measures the RNA concentration (red asterisk) of the sample, the rRNA ratio (green asterisk), and the RIN (purple asterisk). The RNA concentration is necessary in order to continue downstream processing, like qRT-PCR, for example. The rRNA ratio is the ratio of 28S:18S and is 2:1. This ratio indicates how intact the RNA is in the sample. Finally, a RIN is generated, which assigns an integrity value of 1 to 10 to the RNA sample. Samples assigned a 7+ are identified of being acceptable quality for downstream processing.

RNA degradation and genomic DNA contamination can be assessed using the individual electropherograms. In the graph, the taller and cleaner the 28s and 18s peaks are, the better quality the RNA is (fig. 19a,b, black and gray asterisks); when the trough in-between the two peaks is close to baseline, or 0, it demonstrates little to no genomic DNA contamination (fig. 19a,b, blue asterisk). The electropherogram generates the RNA concentration, rRNA ratio, and the RIN data (fig. 19a,b, red, green, and purple asterisks, respectively). The RNA concentration is important because it demonstrates how much total RNA was extracted from the samples; this concentration determines how many genes can be tested in the qRT-PCR downstream. The rRNA ratio is the ratio between 28s and 18s; a ratio of 2:1 indicates intact RNA. Finally, the RNA Integrity Number, or RIN is generated. The RIN assigns an integrity value to the RNA by evaluating a number of factors from the electropherogram, including the rRNA ratio, the 28s and 18s peaks, and the levels of degradation and/or contamination. Values of 1 to 10 are given, with 10 being the least degraded. As it stands, acceptable RINs start from 7.0 and include up to 10, although individual preferences can differ. In the case of the RNAseq studies, the CNAG required samples to be of at least an 8.0 or higher.

6.1.2 Qiagen proves to be the most consistent, efficient, and effective protocol

The first two protocols, the GE illustra RNAspin Mini Kit and its protocol from the manufacturer with a double DNase I digestion step and the standard GE illustra RNAspin Mini Kit and its protocol from the manufacturer, demonstrated extremely low RNA yields and low rRNA ratios that resulted in the majority of the samples with low RINs. These consistently low yields and low quality RNAs resulted in the rejection of these two protocols for future studies.

Next, the other two protocols, the Qiagen RNeasy Mini Kit and its protocol from the manufacturer and the laboratory-established TRIZOL protocol, were tested. Individual samples (IVE, I Gang), pooled samples (PVE2/4, PGang2/4), and singular samples ($\frac{1}{2}$ IVE, $\frac{1}{2}$ Gang) were tested with both protocols. The TRIZOL method demonstrated consistently good RINs, although the rRNA ratios were not optimal, for all sample types. The Qiagen protocol also demonstrated consistently good RINs, but also good rRNA ratios and higher RNA yields for both individual and pooled samples. Taking all factors into consideration, it was decided that the Qiagen protocol was the best protocol to be used for future total RNA isolations of vestibular sensory epithelia and ganglia because of its consistent quality and the fact that it yielded higher concentrations than the TRIZOL method.

6.2 Characterizing Vestibular Damage

6.2.1 Effects of sub-chronic IDPN on 129S1 body weight

The total number of male 129S1 mice utilized for body weight was a conglomerate of five different studies (see Table 1 in “Methodology”). Each study included two treatment groups of either control mice or those exposed to IDPN for either 3, 5, or 8 weeks. Of those mice treated with IDPN for 8 weeks, a subset of mice was selected to undergo the washout period to test for recoverability. As the exposures progressed, the number of mice decreased. In total, 41 mice were in the control group, and 95 mice were exposed to IDPN for 3 (n=7), 5 (n=17), and 8 (n=71) weeks. Of those mice exposed to IDPN for 8 weeks, 21 mice were selected for a washout period of 11-13 weeks.

Male 129S1 mice exposed to IDPN decreased in body weight from weeks 0 to week 3, (fig. 20a) and then demonstrated a small, steady increase as the exposure progressed. Meanwhile, control mice demonstrated a steady increase in body weight throughout the exposure. Washout mice gained weight from week 9 until the end of the recovery period, but they never recovered to control weights of the same time point. The maximal decrease in body weight for IDPN-treated mice was recorded at week 3 with 97.1% of their initial body weight. At weeks 5 and 8, body weights were recorded at 99.2%, and 100.4% of their initial body weight, respectively. After the washout period, recovered mice demonstrated an increase to 111.2% of their initial body at the end of the experiment. Likewise, control mice demonstrated body weights of 104.5%, 105.2%, and 108.4% at weeks 3, 5, and 8 to their initial body weight, respectively. At the end of the exposure, control mice were recorded at 122.3% of their initial body weight.

Body weight data were analyzed in four separate MANOVA tests. Data from the exposure period of week 0 to week 3 resulted in significant treatment ($F[1,134] = 21.8, p < 0.000$) and day by treatment interaction ($F[3,132] = 17.9, p < 0.000$) effects, but there was no significance for day effects. Data from the exposure period of weeks 4 to 5 resulted in significant day ($F[5,120] = 6.0, p < 0.000$), treatment ($F[1,124] = 19.3, p < 0.000$), and day by treatment interaction ($F[5,120] = 10.3, p < 0.000$) effects. Data from the exposure period of week 6 to week 8 resulted in significant day ($F[8,93] = 10.8, p < 0.000$), treatment ($F[1,100] = 19.4, p < 0.000$), and day by treatment interaction ($F[8,93] = 5.4, p < 0.000$) effects. Data from the recovery period of week 9 to week 20 resulted in significant treatment ($F[1,10] = 36.5, p < 0.000$) effects, but no significance for neither day nor day by treatment interaction effects. This indicates a similar evolution of the body weight for both control and recovery mice, although the two groups were not equal in weight during this period.

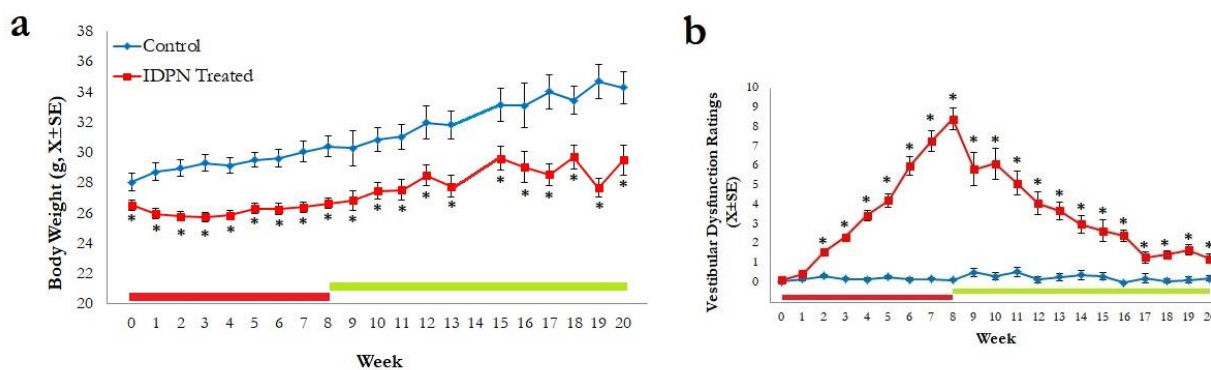


Figure 20: Effects of IDPN (30 mM in drinking water) on body weight and vestibular function of male 129S1/SvImJ mice. In both graphs, the (red) bar that runs across the x axis depicts IDPN exposure, while the (green) bar depicts the recovery period. The number of animals declined during the exposure. **a** Body weight. Control mouse weights steadily increased as time progressed, while IDPN-treated mice first decreased in weight from week 0 to week 3 and then steadily gained weight during the exposure. Washout mice continued to increase in weight during the recovery period, although they never matched weights with the control mice. **b** Vestibular Dysfunction Ratings. Data are tallied ratings from a battery of 6 items sensitive to vestibular dysfunction, each rated 0 (normal behavior) to 4 (highly dysfunctional response). IDPN-treated mice became more and more vestibularly dysfunctional as the exposure progressed, while control mice retained their normal behavior. Washout mice demonstrated a large capacity for recovery during the washout period; however it plateaued at the 9th week of recovery with almost control-like behavior. *IDPN-treated and washout mice significantly different from control mice, ($P < 0.000$), post-hoc Duncan's tests performed after significant repeated-measures MANOVA.

6.2.2 Effects of sub-chronic IDPN on 129S1 vestibular function

Mice exposed to IDPN for up to 8 weeks displayed progressive loss of vestibular function; those mice selected for the washout period demonstrated a potential for full functional, vestibular recovery (fig. 20b). VDRs were recorded each week throughout the exposure period and then after during the recovery. Mice exposed to IDPN demonstrated VDRs of 2.3 ± 0.1 , 4.2 ± 0.3 , and 8.4 ± 0.6 at weeks 3, 5, and 8 of the exposure, respectively. Maximal scores of VDR were observed at week 8, although they did not reach the highest scoring total of 24. Washout mice displayed a gradual decline in VDRs during the recovery period with a score of 1.2 ± 0.2 recorded at the end of the experiment. Control mice did not show any vestibular deficiency throughout the exposure. The number of mice utilized for these recordings were the same as the ones used for body weight.

VDR data were analyzed in three separate MANOVA tests. Data from the exposure period of week 0 to week 5 resulted in significant day ($F[2,107] = 64.1$, $p < 0.000$), treatment ($F[1,108] = 77.6$, $p < 0.000$), and day by treatment interaction ($F[2,107] = 46.7$, $p < 0.000$) effects. Data from the exposure period of week 6 to week 8 resulted in significant day ($F[2,99] = 52.4$, $p < 0.000$), treatment ($F[1,100] = 75.4$, $p < 0.000$), and day by treatment interaction ($F[2,99] = 53.2$, $p < 0.000$) effects. Data from the recovery period of week 9 to week 20 resulted in significant treatment ($F[1,10] = 35.7$, $p < 0.000$) effects, but no day or day by treatment interaction effects. This indicates a difference between the two treatment groups, but not necessarily dependent on the time line, since controls remained unchanging throughout the exposure.

6.2.3 SEM analysis of stereociliary damage and HC loss following sub-chronic IDPN exposure

SEM observation of the vestibular sensory epithelia revealed the apical surfaces of the HCs, characterized by the stereociliary bundles protruding from the cell's cuticular plate, and of the supporting cells, characterized by their abundant microvilli. The appearance and density of the stereociliary bundles in most control specimens (fig. 21A) matched previous literature descriptions for the epithelia from healthy adult rats and mice (Dechesne et al., 1986; Soler-Martín et al., 2007; Saldaña-Ruíz et al., 2013). They were given a pathology score of 0. However, some control samples attained SEM Pathology Scores of 1 or 2, as they had displayed blebs or stereociliary fusion in a small number of HCs, respectively. Blebs are minor pathological alterations often recorded in control vestibular epithelia, likely due to hypoxia during dissection, as they are known to be formed within a few minutes of HC stress (Shi et al., 2005; Goodyear et al., 2008).

The effect of drinking 30 mM of IDPN on the surface morphology varied according to how long the mouse was exposed for, and the vestibular sensory epithelia considered. In all cases, the saccules from IDPN animals presented a control-like morphology. In contrast, IDPN had an observable impact on the utricles, which are pictured in figure 21. At 5 weeks of IDPN exposure, when the mice were starting to show the initial loss of vestibular function, the surface morphology was similar to that of control animals. Similar control-like morphological features were recorded in 4 mice exposed for 8 weeks and showing low (3 to 6) VDRs (fig. 21B). In contrast, 3 mice that showed VDRs of 10 to 11 at 8 weeks of exposure displayed some loss of cells, stereocilia fusion, and HC extrusion in the peristriolar area. These were given SEM Pathology Scores of 2 to 3 (fig. 21C-E). The worst-case example (fig. 21F,G; SEM Pathology Score of 4) corresponded to a mouse exposed for 8 weeks, and had resulted in a VDR of 18. Washout mice examined at 13 weeks after the end of the 8-week exposure period displayed intact morphology (SEM Pathology Score of 0, fig. 21H) or limited pathological alterations (SEM Pathology Scores of 1 to 2, fig. 21I,J).

Figure 21K summarizes the relationship between the vestibular dysfunction of the animals at the end of the ototoxic exposure period and the SEM Pathology Scores. In figure 21L, the relationship between the VDRs at both the end of the exposure period and after recovery, and the SEM Pathology Scores is shown. The data indicate that a significant loss of function occurs before a significant proportion of HCs are severely damaged or lost, and that this initial dysfunction is fully or largely reversible.

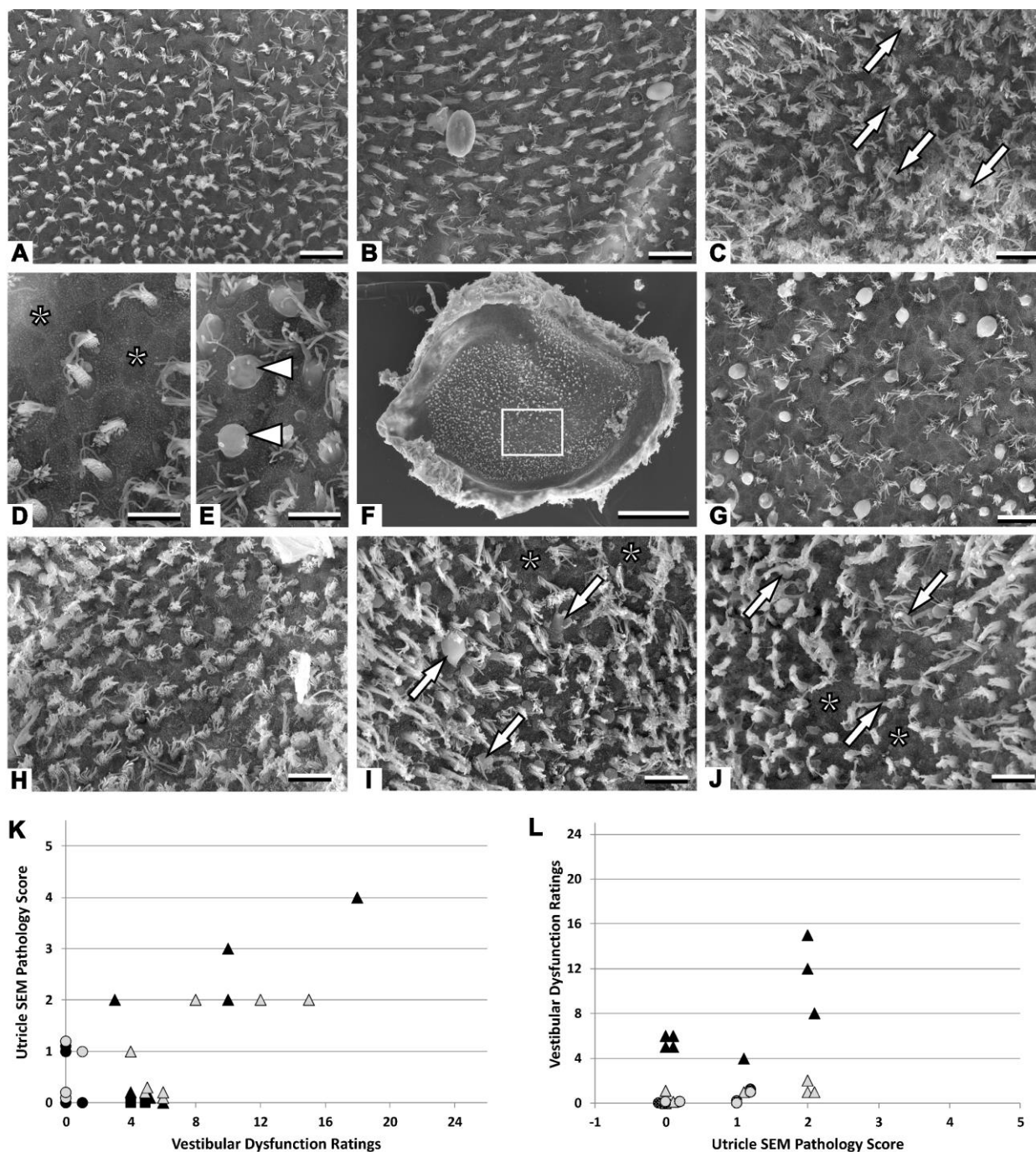


Figure 21: Effects of IDPN (30 mM in the drinking water) on the utricle as assessed by SEM analysis of the surfaces of the sensory epithelia. All images correspond to the central (striolar) part of the utricle except in **F**, which depicts the whole utricle and indicates the peristriolar region. **A** Control mouse. A normal density of HCs with a uniform distribution of stereociliary bundles emerging from a field of microvilli, which indicate supporting cells. **B-G** Utricles from mice exposed to IDPN for 8 weeks with diverse pathological stages. **B** Utricle with a SEM Pathology score of 0 from a mouse with a VDR of 4. **C** Utricle with a SEM Pathology score of 2 from a mouse with a VDR of 10; presence of coalescent hair bundles are noted (white arrows). **D,E** Details of a utricle with a SEM pathology score of 3 from a mouse with a VDR of 10, with a lack of HCs (asterisks in **D**) and extruding HCs (white arrowheads in **E**). **F** Utricle of the worst-case mouse, displaying a VDR of 18 and a SEM pathology score of 4, with widespread loss of and ongoing extrusion of HCs. **G** Higher magnification of the area defined by the white rectangle in **F**. **H-J** Utricles from mice exposed to IDPN for 8 weeks followed by a washout period of 13 weeks. In **I** and **J**, asterisks signal spaces lacking a HC, and white arrows signal coalescent stereociliary bundles. **H** SEM Pathology Score of 0 in a mouse presenting a VDR of 6 at 8 weeks, and a VDR of 1 after washout. **I** SEM Pathology Score of 2 in a mouse presenting a VDR of 8 at 8 weeks, and a VDR of 1 after washout. **J** SEM Pathology Score of 2 in a mouse presenting a VDR of 15 at 8 weeks, and a VDR of 1 after washout. **K** Relationship between VDRs at the end of the exposure period and the SEM Pathology

Scores in control mice (circles) and in mice exposed to 30 mM IDPN for 5 (squares) or 8 (triangles) weeks; animals were examined at the end of the IDPN exposure (black symbols) or after a washout period (light grey symbols). **L** Relationship between SEM Pathology Scores and VDR recovery in mice exposed to 30 mM IDPN and assessed after washout. Each animal is represented by two symbols showing the VDR at the end of the IDPN exposure period (black), and at the end of the washout (light gray). Scale bars: 10 μ m in **A, B, C, G, H, I, and J**; 5 μ m in **D and E**; 250 μ m in **F**.

The effect of the treatment on the crista was similar or larger than in the utricles, resulting in the same or same+1 pathology scores (fig. 22A-I). Control cristae demonstrated a normal distribution of HCs and intact stereocilia bundles (fig. 22A, SEM Pathology Score of 0). Cristae from mice exposed to IDPN for 8 weeks displayed a variety of pathological damage, depending on the extent of the ototoxicity and VDRs (fig. 22B-F). While more mildly affected mice demonstrated control-like morphology (fig. 22B, VDR of 5 and SEM Pathology Score of 0), mice with VDRs of 10 had varying cases of HC extrusion and/or loss and/or stereociliary bundle coalescence (fig. 22C-E, SEM Pathology Scores of 2). The mouse with the worst case of ototoxicity (VDR of 18), displayed large losses of HCs and continued HC extrusion (fig. 22F, SEM Pathology Score of 5). For mice that underwent a washout period (fig. 22G-I), those with mild VDRs displayed control-like morphologies (fig. 22G, VDR of 6). Whereas cristae from mice more affected (VDRs of 8 or 15) had pathological hair bundles or hair bundles that were absent (fig. 22H,I).

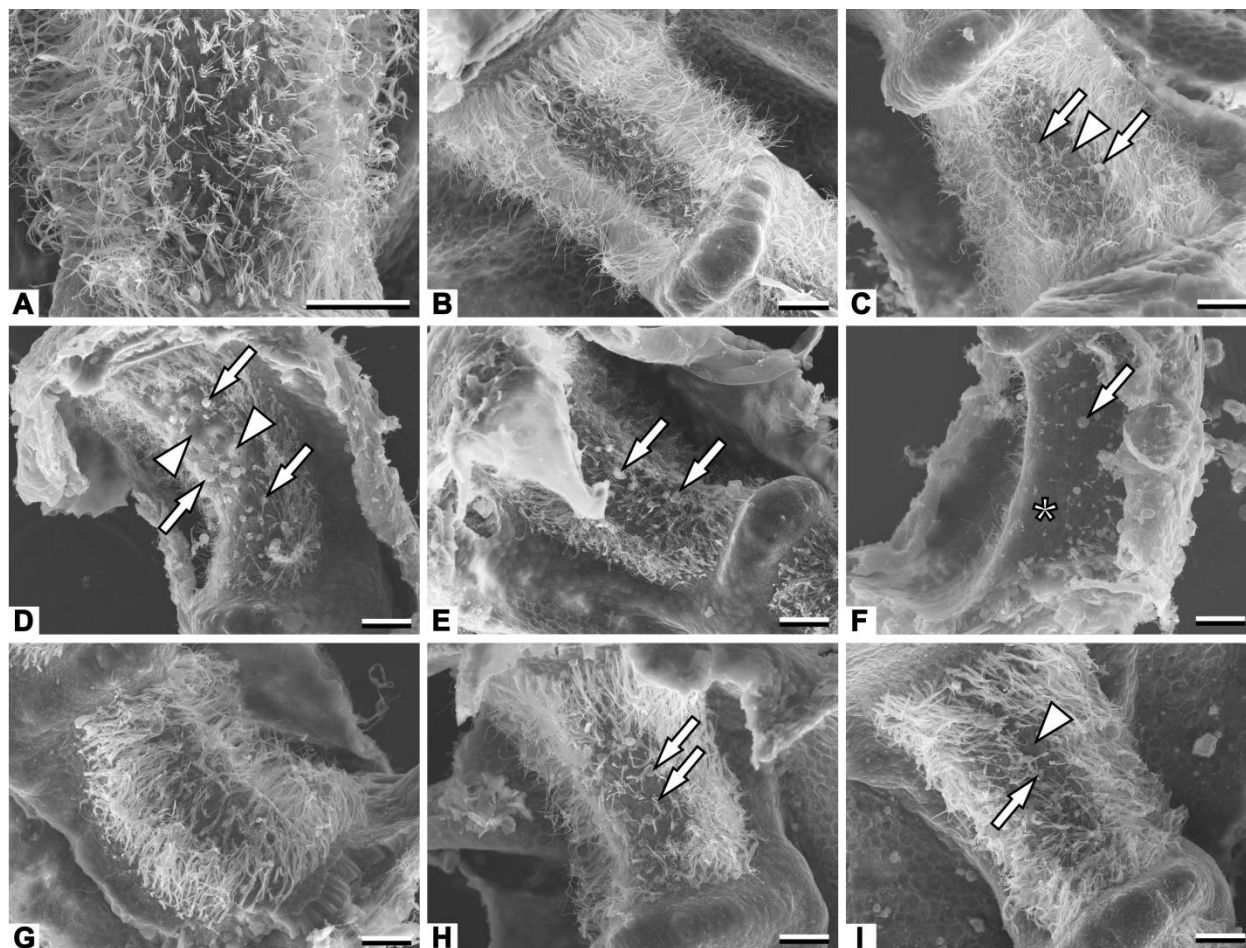


Figure 22: Effects of IDPN (30 mM in drinking water) on the vestibular cristae by SEM observation of the surface of the sensory epithelium. **A** Control crista. Homogenous spread of stereociliary bundles indicates a normal distribution of HCs and supporting cells. **B-F** Cristae from mice exposed to IDPN for 8 weeks with varying pathological degrees. **B** Crista with a SEM Pathological Score of 0; mouse with a VDR of 5. **C** Crista with a SEM Pathological Score of 2; mouse with a VDR of 10. White arrows denote the presence of coalescent stereociliary bundles and the white arrowhead showing absent HCs. **D,E** Two cristae from the same mouse that had a VDR of 10. There were extruding (white arrows) and absent (white arrowheads) HCs. **F** Crista of the

worst-case mouse, which had a VDR of 18 and a SEM Pathology Score of 5. There was extensive loss of cells (asterisk) and ongoing extrusion of HCs (white arrow). **G-I** Cristae from mice exposed to IDPN for 8 weeks, and then completed a washout period of 13 weeks. **G** Crista with a SEM Pathology Score of 0 from a mouse with a VDR of 6 after the IDPN exposure, and then a VDR of 1 after the washout period. **H** Crista with a SEM Pathology Score of 2 from a mouse with a VDR of 8 after the IDPN exposure, and then a VDR of 1 after the washout period. Pathological hair bundles are noted (white arrows). **I** Crista with a SEM Pathology Score of 2 from a mouse with a VDR of 15 after the IDPN exposure, and then a VDR of 1 after the washout period. There were pathological (white arrow) and absent (white arrowhead) hair bundles.

6.2.4 Light Microscopy and TEM analysis of calyceal junction loss, stereociliary fusion, and HC extrusion following sub-chronic IDPN exposure

Transverse sections of the lateral crista examined by light microscopy and TEM displayed morphological features matching previously described vestibular cristae from adult healthy mice (fig. 23A-C, Desai et al., 2005b). The vestibular sensory epithelium contains HCIs and HCIIIs, which differ in shape and afferent innervation.

In mice exposed to IDPN for 5 weeks, the epithelium had an overall control-like appearance; however, some of the individual HCI-calyx afferent contacts were altered. These alterations consisted of partial to complete absence of the calyceal junction and fragmentation of the afferent (fig. 23D). These morphologies are not recorded in healthy sensory epithelia. After 8 weeks of exposure to IDPN, morphological abnormalities were diverse in different mice. Mice exposed for this amount of time and showing low (3 to 6) VDRs displayed a similar morphology to that described for 5-week animals, with occasional loss of the calyceal junction (fig. 23E) and calyx fragmentation. In the 3 mice with VDRs in the 10-11 range, there was widespread calyceal junction dismantlement, and some extruding HCs were recorded in one of them (fig. 23F). In semi-thin sections from the crista of the worst-case example exposed for 8 weeks (VDR=18), we recorded widespread loss of HCs, the presence of completely extruded HCs in the endolymphatic cavity, and extruding HCs (fig. 23G). Under TEM observation, dismantlement of the calyceal junctions and calyceal fragmentation was extensive. Some of the extruding HCs showed signs of degeneration and vacuolization (fig. 23H), while others kept an apparently undamaged cytoplasm and nucleus, as illustrated in figure 23F. The ultrastructural morphology of cristae from animals examined after the washout resembled that of control animals, with clearly visible calyceal junctions (fig. 23I).

The dismantlement of the calyceal junctions was assessed by measuring membrane-to-membrane distances in the HCI-calyx afferent contacts. Where the calyceal junction is present and intact, the distances are smaller and more regular in places (fig. 23J); characteristically, both membranes are electron dense in healthy mice. Areas identified that did not have an intact junction had larger membrane-to-membrane distances and lacked electron dense membranes (fig. 23K). The mean distance measured at intact junctions was only slightly larger in 8-week mice (29.5 ± 0.4 nm) and slightly lower in 5-week mice (26.0 ± 0.2 nm) compared to the mean in control mice (26.8 ± 0.2 nm, Duncan's test after significant ANOVA, $F[3,2875] = 33.8$, $p < 0.000$). The mean distance in washout animals (26.5 ± 0.2 nm) did not differ from that in controls. These values agree with previous literature data (28 ± 4 nm, Sousa et al., 2009). However, the proportion of areas that were identified as presenting an intact calyceal junction versus no junction was lower in 8-week animals (40%) than in control (71%) and washout (76%) mice. Consequently, when the distances for both intact and dismantled calyceal junctions were compared, it was found that IDPN animals had a 60% increase in mean membrane-to-membrane distance compared to controls ($p < 0.05$), and that this was reduced to a 17% increase after washout. The comparison of distances that included all intact and dismantled junction measurements can be seen in figure 23L. ANOVA results for the data in figure 23L are $F[3,4479]=112.0$, $p<0.000$.

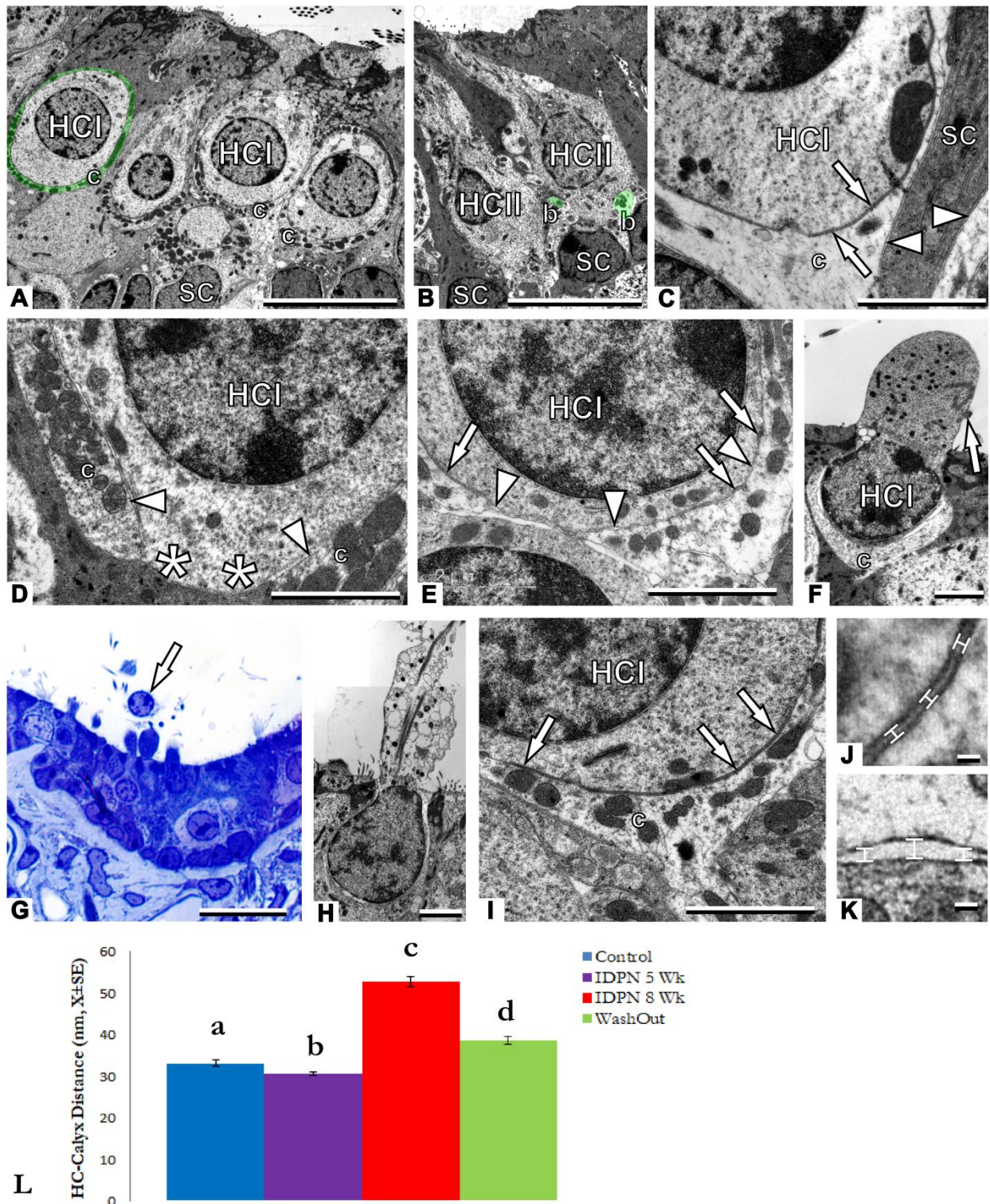


Figure 23: Effects of IDPN (30 mM in the drinking water) on the lateral vestibular crista as assessed by light microscopy (G) and TEM (A-F, H-K). A-C Control epithelium. Note the calyceal afferent endings (c, in A and C, highlighted in green in A) encasing HCIs. Supporting cells (SC) fill in the basal end of the epithelium and extend apically to separate HCs. In B, HCII are shown with bouton afferents (also highlighted in green). In the higher magnification of C, note the difference in electron density of the membranes in the calyceal junction area (white arrows) compared to other plasma membranes elsewhere in the epithelium (white arrowheads). D Crista from a mouse treated to IDPN for 5 weeks. In this HCI-afferent contact, the calyx ending (c) is fragmented and does not cover the bottom end of the HCI (asterisks) like a control. The calyceal junction is missing for most of the HCI-afferent contact (white arrowheads). E Representative image of a crista from a mouse exposed to IDPN for 8 weeks. In this HCI-calyx afferent contact, the calyceal junction is observed in some segments (white arrows) and is lacking in others (white

arrowheads). **F** An extruding HCI in a mouse exposed to IDPN for 8 weeks. Note the calyx afferent (c), and the kinocilium (white arrow). **G** An extruding cell in the crista from the worst-case animal exposed to IDPN for 8 weeks. Note the remnants of a completely extruded cell (white arrow) in the endolymphatic cavity. **H** Extensive vacuolization in a partially extruded HC, from the same crista shown in **G**. **I** Representative image of a crista after a washout period of 13 weeks. The calyceal junctions are distinctly visible in most basolateral membranes of the HCI. **J** High magnification image of the calyceal junction in a control mouse. The three marks represent example membrane-to-membrane distance measurements; they're small and uniform. **K** High magnification of the loss of a calyceal junction of a mouse exposed to IDPN for 8 weeks. Note the membrane-to-membrane measurements have increased in distance and reduced in uniformity. **L** Mean membrane-to-membrane distances including all points throughout the HCI-calyx contact. a, b, c, d: groups not sharing a letter are significantly different, $P < 0.05$, Duncan's test after significant ANOVA. Scale bars: 10 μm in **A**, **B**, and **G**; 2 μm in **C**, **D**, **E**, **F**, **H** and **I**; 100 nm in **J** and **K**.

6.2.5 Molecular analysis of calyceal junction dismantlement following sub-chronic IDPN exposure

The first immunofluorescent analysis (fig. 24A) studied two important proteins which characterize the calyceal junctions of HCIs in the vestibular sensory epithelium: caspr1, which localizes at the neuronal membrane of the calyceal junction (Sousa et al., 2009), and tenascin-c, which localizes in the extracellular matrix of the junction, within the synaptic cleft between the HCIs and their corresponding post-synaptic afferents (Lysakowski et al., 2011). Additionally, the plasma membrane of the afferent terminals was immunolabeled with antibodies against the Na^+/K^+ ATPase $\alpha 3$ subunit (NaKAa3) (Schuth et al., 2014) (fig. 24C). Previous results in SEM and TEM had demonstrated that breakdown and loss of calyceal junctions for HCIs, but not the actual loss of the HCIs themselves (except in extreme cases). The cristae of 6 control mice, 3 mice treated with IDPN for 8 weeks, and 5 washout mice were examined and the calyceal junctions were examined by immunolabeling of caspr1 and tenascin-c. Mice exposed to IDPN for 8 weeks (fig. 24e-h) demonstrated a dramatic loss in both caspr1 and tenascin-c, and their colocalizations. One-way ANOVA comparisons indicated significant group differences in caspr1 ($F[2,132] = 233.4$, $p < 0.000$), tenascin-c ($F[2,132] = 69.6$, $p < 0.000$), and their colocalizations ($F[2,132] = 62.6$, $p < 0.000$). When compared to control mice (fig. 24a-d), IDPN mice lost 97% of recorded caspr1, 93% of recorded tenascin-c, and 95% of their recorded colocalizations. The mice that underwent a washout period (fig. 24i-l) demonstrated a large capacity for recovery with losses of only 37%, 4%, and 9% of caspr1, tenascin-c, and their colocalizations, respectively. The results of the immunofluorescent study coordinates with the TEM results analyzed. In TEM, we see the dismantlement and loss of the calyceal junctions, and immunofluorescent data reaffirms the calyceal junction loss with the loss of caspr1, an identified junction protein, and tenascin-c, the extracellular matrix protein. The recovery of the calyceal junctions were also recorded (and observed in the TEM studies), with tenascin-c and its colocalizations with caspr1 recovering to control-like numbers, but with caspr1 only partially recovering (fig. 24B). Whether there are any implications involving the lack of caspr1 after washout have not been studied.

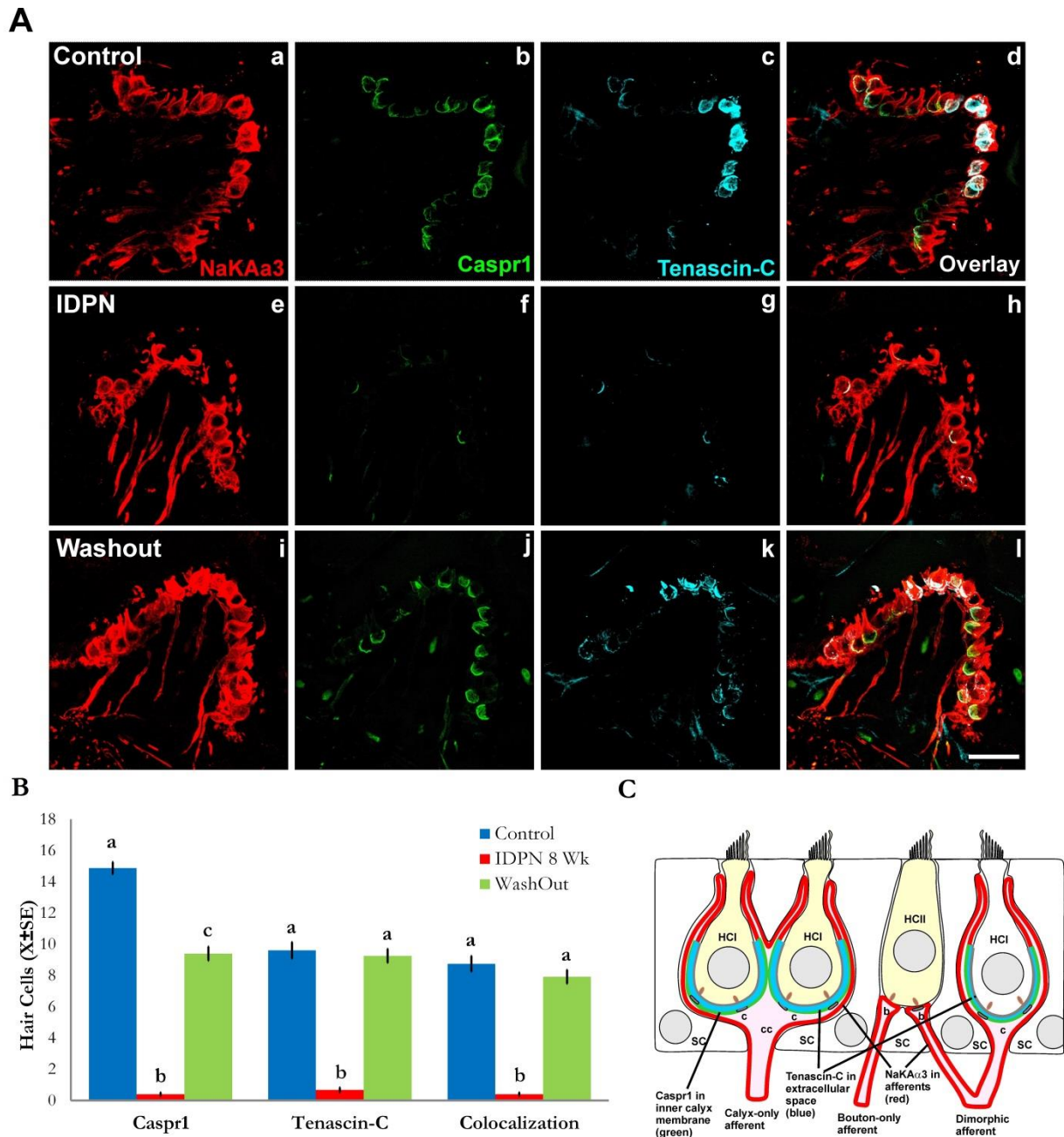


Figure 24: Effects of IDPN (30 mM in drinking water) on the calyceal junctions of HCIs in the cristae of the vestibular sensory epithelia of male 129S1/SvImJ mice. Mice treated with IDPN for 8 weeks demonstrated a profound loss of caspr1 and tenascin-c, two known, associated proteins of calyceal junctions. **A** Immunofluorescent study focusing on caspr1 (green) and tenascin-c (blue), with the afferent terminals labeled with Na⁺/K⁺ATPase α 3 subunit (red). **a-d** Control crista displaying intact calyceal junctions, labeled with caspr1 and/or tenascin-c and their colocalizations. **e-h** Crista from a mouse treated with IDPN for 8 weeks. The structure of the HCs and the afferents remain intact as observed with the NaKAa3 labeling, but there is a dramatic loss of caspr1 and tenascin-c labeling, and their colocalizations, demonstrating the loss of calyceal junctions of HCIs. **i-l** Crista from a mouse exposed to IDPN for 8 weeks and then underwent a washout period of 13 weeks, indicating a recuperation of the calyceal junctions, due to the presence of caspr1 and tenascin-c labeling, and their colocalizations. **B** Graph depicting the number of HCs per snapshot (5 snapshots per slice) with caspr1, tenascin-c, and their colocalizations compared to the three treatment groups. There is an almost complete loss of caspr1, tenascin-c, and their colocalizations for IDPN-treated mice, with full recoveries of tenascin-c and the colocalizations for washout mice. Caspr1 only partially recovers for the washout mice. **C** Schematic of the supporting cells (SC), and HCs and HCIIs with the three different afferent units (c= calyx, cc= complex calyx, b= bouton). a, b, c: groups not sharing a letter are significantly different, $P < 0.000$, Duncan's test after significant ANOVA.

6.2.6 mRNA expression of tenascin-c in the vestibular sensory epithelia is altered following sub-chronic IDPN exposure

The vestibular sensory epithelia and ganglia of male 129S1 mice were processed with qRT-PCR to observe changes in the mRNA expression of caspr1 (Cntnap1) and tenascin-c (Tnc), known calyceal junction proteins and visualized in the previous immunofluorescent study, during the exposure (fig. 25). For the vestibular ganglia, a total of 9 control mice, 8 mice treated with IDPN for 5 weeks, 8 mice treated with IDPN for 8 weeks, and 8 recovery mice were analyzed. One-way ANOVA of the results indicated no significant alterations of mRNA expression for the two genes between the different treatment groups, although an apparent increase (1.7 fold) was observed for Tnc during the 8 week IDPN treatment. In the vestibular sensory epithelia, Tnc mRNA expression was analyzed; it is not known whether tenascin-c is secreted from the afferent or the epithelium, and so expression was analyzed from both tissues. Likewise, caspr1 is present in the afferent side of the calyceal junction, so its expression was not analyzed in the vestibular epithelium. A total of 8 control mice, 7 mice treated with IDPN for 5 weeks, 8 mice treated with IDPN for 8 weeks, and 5 recovery mice were analyzed. ANOVA comparisons resulted in significant group differences for Tnc ($F[3,24] = 5.1, p = 0.007$). Tnc had a gradual decline in mRNA expression compared to control mice, where 5 week IDPN-treated mice had a 0.8 ± 0.0 fold and then progressed to a 0.7 ± 0.1 fold for 8 week IDPN-treated mice. Washout mice demonstrated a full recovery in fold for Tnc. So, while the vestibular ganglia is not altering mRNA expression of caspr1 or tenascin-c during the exposure, tenascin-c expression is being downregulated in the vestibular sensory epithelia, demonstrating a downgrading of calyceal junction support and/or structure.

The observed downregulation of Tnc mRNA expression after exposure and a full recovery after washout reflects the immunofluorescent data previously observed.

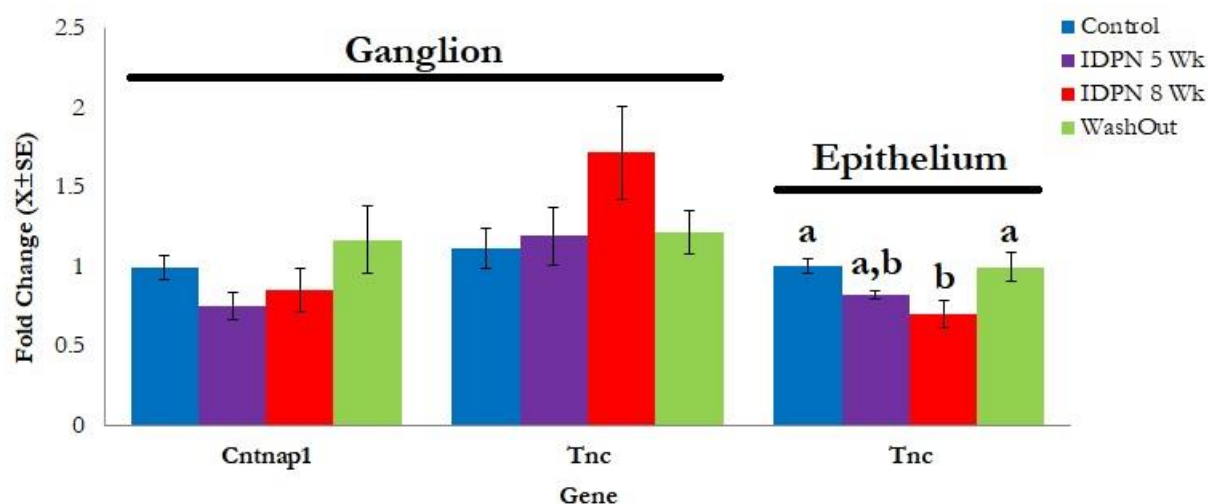


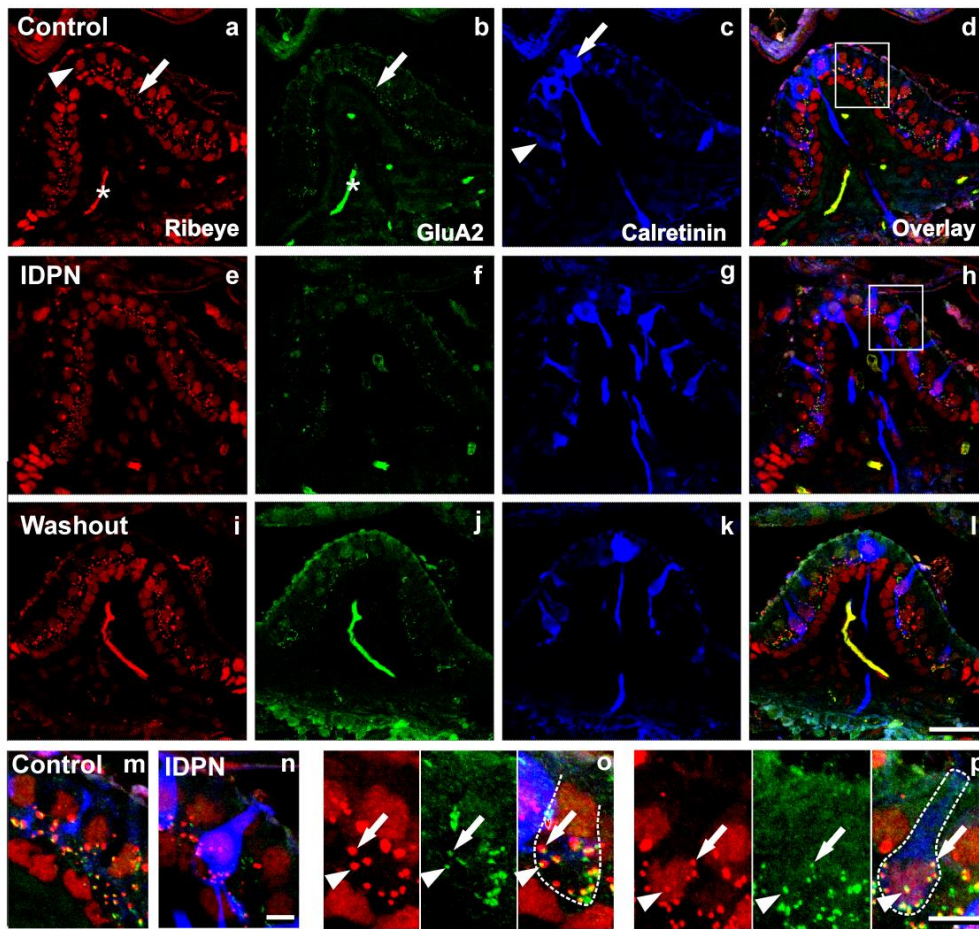
Figure 25: Alterations of mRNA expression of the calyceal junction protein caspr1 in the vestibular sensory ganglion, and the extracellular matrix protein tenascin-c in the vestibular sensory epithelium and ganglion from IDPN exposure of male 129S1/SvImJ mice. No significant effects were found for the genes examined in the vestibular ganglion. The mRNA expression of tenascin-c (Tnc) in the vestibular sensory epithelium demonstrated a decline in expression after 8 weeks of IDPN, and recovered to control levels after the washout period. This indicates a downregulation of tenascin-c in the epithelium during intoxication, which may contribute to the calyceal junction loss seen in the immunofluorescent studies. a, b: groups not sharing a letter are significantly different, $P < 0.01$, Duncan's test after significant ANOVA.

6.2.7 Molecular analysis of synaptic uncoupling and post-synaptic density protein alterations following sub-chronic IDPN exposure

The integrity of HC-afferent synapses and post-synaptic density proteins were examined. First, the synapses were examined using immunofluorescent studies of ribeye, the core ribbon protein of ribbon synapses, and GluA2, the most abundant subunit of the ionotropic AMPA receptor, in the three HC-afferent units within the cristae of control mice, mice treated with IDPN for 8 weeks, and washout mice (fig. 26A). One-way ANOVA comparisons for the three HC-afferent units resulted in significant group differences for calyx-only ($F[2,115] = 14.7, p < 0.000$), the calyces of dimorphic units ($F[2,202] = 15.8, p < 0.000$), and HCII units ($F[2,179] = 12.7, p < 0.000$) for ribeye. Mice treated with IDPN resulted in a decline in ribeye puncta for all three HC-afferent units. Washout mice demonstrated partial recovery of ribeye puncta for calyx-only and HCII units, and a full recovery of puncta for the calyces of dimorphic units. Calyces of dimorphic units also displayed a decrease in ribeye and GluA2 colocalizations ($F[2,202] = 4.0, p = 0.020$), which were fully recovered after the recovery period. Moreover, HCII units demonstrated a decrease in GluA2 puncta ($F[2,179] = 3.6, p = 0.029$) and ribeye and GluA2 colocalizations ($F[2,179] = 4.4, p = 0.013$), with partial recoveries for both (fig. 26B).

These results demonstrated a general decrease in ribeye puncta across the cristae, while the loss of receptors and/or synapses was recorded in two of the three HC-afferent units only; IDPN affects the HC-afferent units differently.

A



B

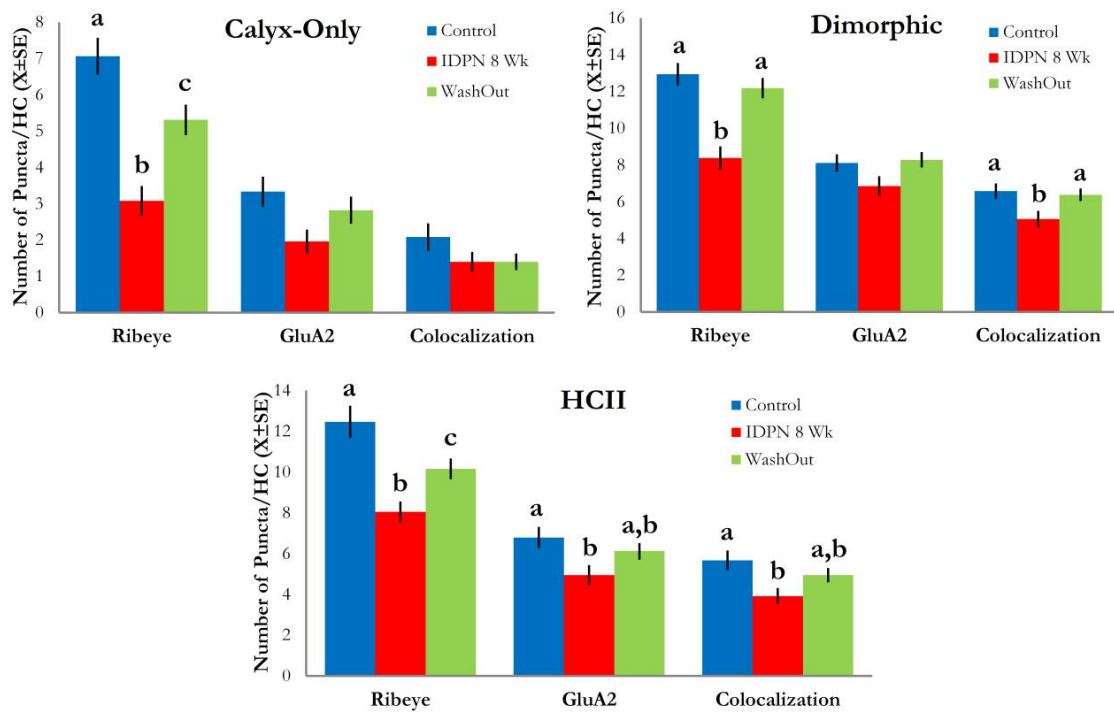


Figure 26: Effects of IDPN (30 mM in drinking water) on the active synapses of the three HC-afferent units within the vestibular cristae of control, IDPN-treated, and washout male 129S1/SvImJ mice. A Immunofluorescent study focusing on CtBP2/ribeye

(red) as the pre-synaptic marker, GluA2 (green) as the post-synaptic marker, and calretinin-labeling (blue) to identify the different HC-afferent units. **a-d** Control crista. **a** Ribeye-labeled image with individual puncta (white arrow) and the nuclei staining (white arrowhead). Blood vessels of mice are known to be marked when utilizing mouse isotype antibodies (asterisk). **b** GluA2-labeled image with individual puncta (white arrow). **c** Calretinin-labeled image with visible HC-afferent units including calyx only units (white arrow) and HCII units (white arrowhead). **d** Overlaid image of all three stainings. The white box refers to image **m**, which is a higher magnification of the area. **e-h** IDPN-treated crista. **e** Overlay with a white box, which refers to image **n**, a higher magnification of that area. **i-l** Washout crista. **l** Scale bar is 25 μm and refers to all previous images. **m-p** Higher magnifications of HC-afferent units. **m** Higher magnification of a HC for a control crista. **n** Higher magnification of a HC for an IDPN-treated crista. Scale bar is 5 μm and also refers to **m**. **o** Example HC with the calyx dimorphic unit with ribeye puncta, GluA2 puncta, and their colocalizations labeled (white arrows and arrowheads). A white dotted line indicates the shape and limits of the HC. **p** Example HCII with ribeye puncta, GluA2 puncta, and their colocalizations labeled (white arrows and arrowheads). A white dotted line indicates the borders of the HC. Scale bar is 5 μm and also refers to **o**. **B** Ribeye, GluA2, and colocalization puncta counts per HC-afferent unit for the different treatment groups. Calyx only units demonstrated a loss of ribeye after IDPN treatment, with only a partial recovery after washout. The calyces of dimorphic units demonstrated a loss of ribeye and colocalizations after IDPN treatment, which recovered to control levels after the washout period. HCII units demonstrated a loss for ribeye, GluA2, and their colocalizations after IDPN treatment, with varying degrees of recovery after the washout period. a, b, c: groups not sharing a letter are significantly different, $P < 0.03$, Duncan's test after significant ANOVA.

Next, the integrity of the post-synaptic density was examined. Ribeye was used as the marker of the pre-synaptic apparatus within the HC, and its colocalizations with either PSD95 or Homer1 were compared between the three HC-afferent units within the cristae of control, IDPN-treated (8 weeks), and washout mice. In immunofluorescent PSD95 data (fig. 27A), one-way ANOVA comparisons for the three HC-afferent units were analyzed with the different treatment groups. Mice treated with IDPN for 8 weeks noted a significant decrease in ribeye puncta in calyx-only units ($F[2,34] = 14.9$, $p < 0.000$); a decrease is noted for ribeye puncta in the calyces of dimorphic units, but it was not statistically significant. There was a significant increase in PSD95 puncta ($F[2,31] = 3.3$, $p = 0.049$) and their colocalizations with ribeye ($F[2,31] = 3.5$, $p = 0.044$) in HCII units for treated mice. Washout mice showed puncta and colocalization numbers returning to control levels, demonstrating the capacity for recovery (fig. 27B). No significant effects were seen for ribeye, PSD95, or their colocalizations in the calyces of dimorphic units.

These results continue to uphold the hypothesis that IDPN ototoxicity affects the HC-afferent units differently. There is marked ribeye puncta reduction, which had been noted previously, but there is an increase in PSD95, strengthening post-synaptic density structure.

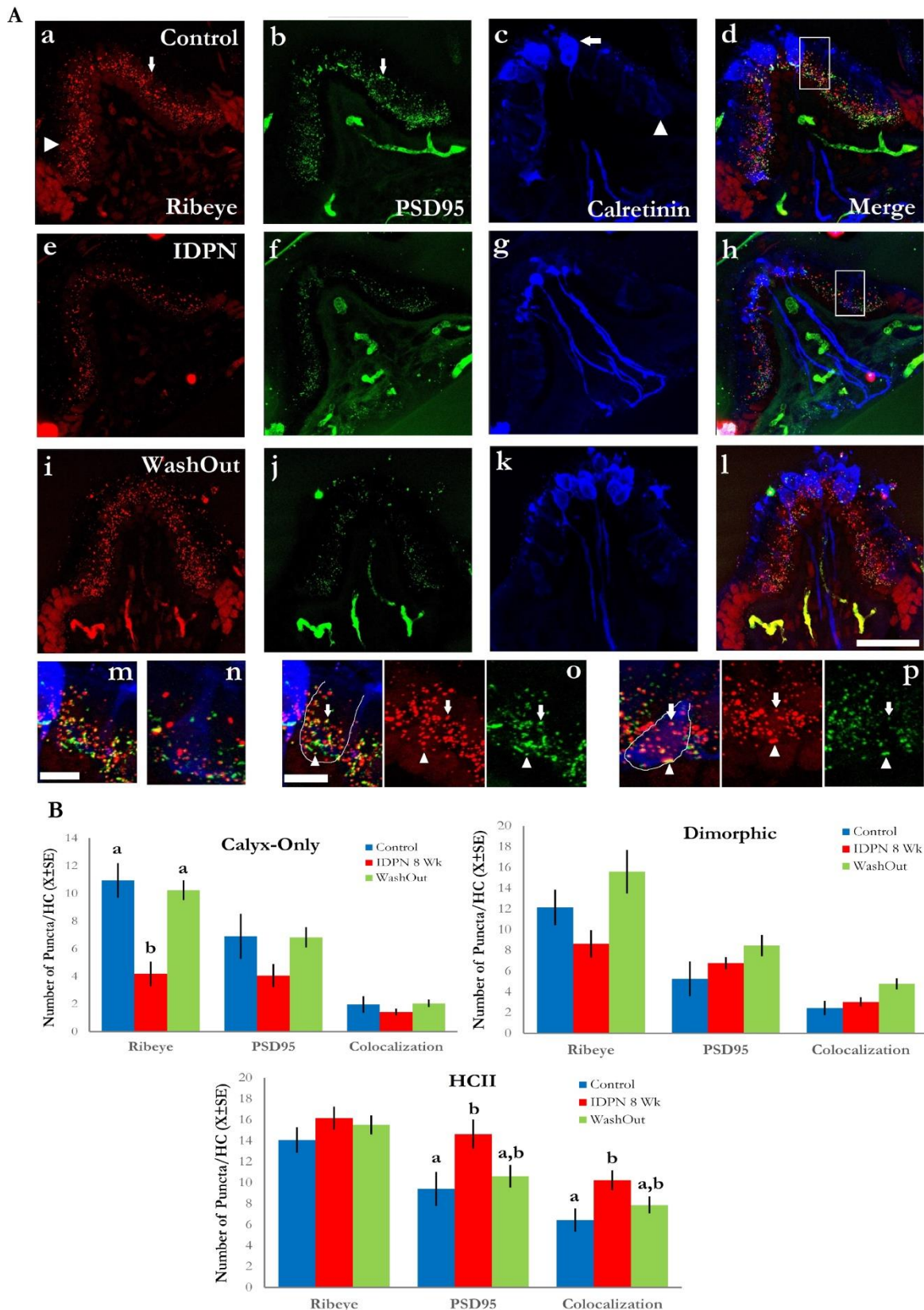


Figure 27: Effects of IDPN (30 mM in drinking water) on synaptic proteins of the three HC-afferent units within the vestibular cristae of control, IDPN-treated, and washout male 129S1/SvImJ mice. **A** Immunofluorescent study focusing on the CtBP2/ribeye (red) as the presynaptic marker, PSD95 (green) as the post-synaptic marker, and calretinin-labeling (blue) to identify the different HC-afferent units. **a-d** Control crista. **a** Ribeye-labeled image with individual puncta (white arrow) and the nuclei staining (white arrowhead). **b** PSD95-labeled image with individual puncta (white arrow). **c** Calretinin-labeled image with

visible HC-afferent units including calyx only units (white arrow) and HCII units (white arrowhead). **d** Overlaid image with all three stainings. The white box refers to image **m**, which is a higher magnification of the area. **e-h** IDPN-treated crista. **h** Overlay with a white box, which refers to image **n**, a higher magnification of that area. **i-l** Washout crista. **l** Scale bar is 20 μm and refers to all previous images. **m-p** Higher magnifications of HC-afferent units. **m** Higher magnification of a HC for a control crista. **n** Higher magnification of a HC for an IDPN-treated crista. Scale bar is 5 μm and also refers to **m**. **o** Example of a HC with the calyx of a dimorphic unit with ribeye puncta, PSD95 puncta, and their colocalizations labeled (white arrows and arrowheads). A white line indicates the shape and limits of the HC. **p** Example HCII with ribeye puncta, PSD95 puncta, and their colocalizations labeled (white arrows and arrowheads). A white line indicates the borders of the HC. Scale bar is 5 μm and also refers to **o**. **B** Ribeye, PSD95, and colocalization puncta counts per HC-afferent unit for the different treatment groups. Calyx only units demonstrated a loss of ribeye after IDPN treatment, with complete recovery after washout. The calyces of dimorphic units did not indicate any significant effects on ribeye, PSD95, or their colocalizations between the three treatment groups. HCII units demonstrated an increase in PSD95 and their colocalizations after IDPN treatment, with varying degrees of recovery after the washout period. a, b: groups not sharing a letter are significantly different, $P < 0.05$, Duncan's test after significant ANOVA.

Finally, the immunofluorescent study of ribeye puncta and Homer1 puncta, and their colocalizations, were compared within the three HC-afferent units between control, IDPN-treated (8 weeks), and washout mice. In the immunofluorescent Homer1 data (fig. 28A), one-way ANOVA comparisons of the three HC-afferent units were analyzed with the different treatment groups. Mice treated with IDPN noted a significant decrease in ribeye puncta in calyx-only units ($F[2,37] = 4.7$, $p = 0.015$); this number returned to control-like levels after washout. In all remaining HC-afferent units, no significant effects were found in puncta numbers for ribeye between the different treatment groups. Likewise, no significant effects of Homer1 puncta numbers, or for their colocalizations, were found in any of the three HC-afferent units (fig. 28B).

These results demonstrated that although ribeye puncta were affected by the IDPN intoxication (mostly in calyx-only units), protein levels of Homer1 remained the same. Homer1, a scaffolding protein in the post-synaptic density of vestibular afferents, remained unaffected by the ototoxic insult at the protein level.

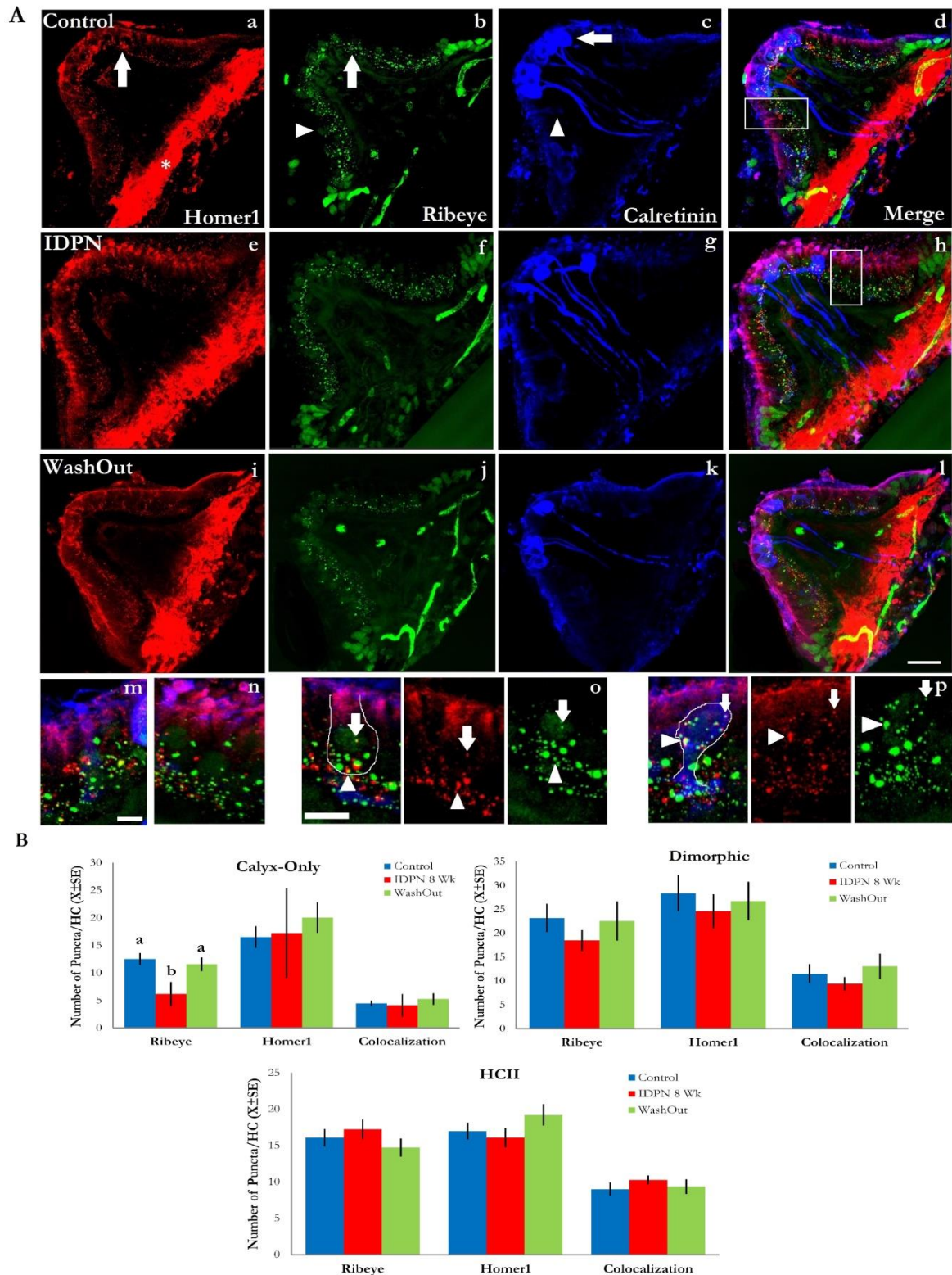


Figure 28: Effects of IDPN (30 mM in drinking water) on synaptic proteins of the three HC-afferent units within the vestibular cristae of control, IDPN-treated, and washout male 129S1/SvImJ mice. **A** Immunofluorescent study focusing on CtBP2/ribeye (green) as the pre-synaptic marker, Homer1 (red) as the post-synaptic marker, and calretinin-labeling (blue) to identify the different HC-afferent units. **a-d** Control crista. **a** Homer1-labeled image with individual puncta (white arrow). Excessive labeling of the membrane can be seen for Homer1 (asterisk). **b** Ribeye-labeled image with individual puncta (white arrow) and the nuclei staining (white arrowhead). **c** Calretinin-labeled image with visible HC-afferent units including calyx only units (white arrow) and HCII units (white arrowhead). **d** Overlaid image with all three stainings. The white box refers to image **m**, which is a higher

magnification of the area. **e-h** IDPN-treated crista. **h** Overlay with a white box, which refers to image **n**, a higher magnification of that area. **i-l** Washout crista. **l** Scale bar is 20 μm and refers to all previous images. **m-p** Higher magnifications of HC-afferent units. **m** Higher magnification of a HC for a control crista. **n** Higher magnification of a HC for an IDPN-treated crista. Scale bar is 5 μm and also refers to **m**. **o** Example HC with a calyx dimorphic unit with ribeye puncta, Homer1 puncta, and their colocalizations labeled (white arrows and arrowheads). A white line indicates the shape and limits of the HC. **p** Example HCII with ribeye puncta, Homer1 puncta, and their colocalizations labeled (white arrows and arrowheads). A white line indicates the borders of the HC. Scale bar is 5 μm and also refers to **o**. **B** Ribeye, Homer1, and colocalization puncta counts per HC-afferent unit for the different treatment groups. Calyx only units demonstrated a loss of ribeye after IDPN treatment, with complete recovery after washout. The calyces of dimorphic units and HCII units did not indicate any significant effects on ribeye, Homer1, or their colocalizations between the three treatment groups. a, b: groups not sharing a letter are significantly different, $P < 0.02$, Duncan's test after significant ANOVA.

6.2.8 mRNA expression of various synaptic, scaffolding, and signaling proteins in the vestibular sensory epithelia and ganglia are altered following sub-chronic IDPN exposure

The vestibular sensory epithelia and ganglia of male 129S1 mice were processed with qRT-PCR to observe changes in the mRNA expression of specific synaptic, scaffolding, and signaling proteins during the exposure. The number of control mice and mice treated with IDPN for 8 weeks varied for the different genes; mice treated with IDPN for 5 weeks and washout mice were compared when applicable (Table 5).

Gene						
	Ganglion					Epithelium
Treatment↓	Gria2	DLG4	Homer1	DLGAP1	REST	CtBP2
Control	9	9	8	8	9	8
IDPN 5 Wk	8	8			8	7
IDPN 8 Wk	8	8	7	7	8	8
WashOut	8	8			6	5

Table 5: Number of mice utilized per gene in the qRT-PCR study of synaptic, scaffolding, and signaling proteins for control mice, mice treated with IDPN for 5 weeks, mice treated with IDPN for 8 weeks, and washout mice in vestibular sensory ganglion and epithelium.

In the vestibular ganglion, the mRNA expression of 5 different genes was examined (fig. 29). Of those 5 genes, 1 gene (Homer1) demonstrated an increase in mRNA expression for mice treated with IDPN for 8 weeks, and the other 2 genes showed an increase in mRNA expression for only washout mice (Gria2) or an increase in expression for treated mice and washout mice (DLG4). Of the remaining 2 genes (REST, DLGAP1), they demonstrated no significant alteration in mRNA expression. Vestibular sensory ganglia data were analyzed in two separate one way ANOVA tests, since qRT-PCR analyses were carried out in multiple studies. ANOVA comparisons resulted in significant group differences for Gria2 ($F[3,29] = 4.1$, $p = 0.016$), DLG4 ($F[3,29] = 8.5$, $p < 0.000$), and Homer1 ($F[1,13] = 5.2$, $p = 0.040$). Overall, there was an upregulation of various synaptic and scaffolding genes in the afferent due to the IDPN exposure.

In the vestibular sensory epithelium, the mRNA expression of ribeye (CtBP2) was examined (fig. 29). There was a decrease in expression for CtBP2 after 5 weeks of IDPN treatment, and then remained in a decreased state even after washout, when compared to control mice. The loss of ribeye had also been noted in the immunofluorescent studies. Vestibular sensory epithelium data were analyzed by one way ANOVA and resulted in significant group differences for CtBP2 ($F[3,24] = 6.6$, $p = 0.002$).

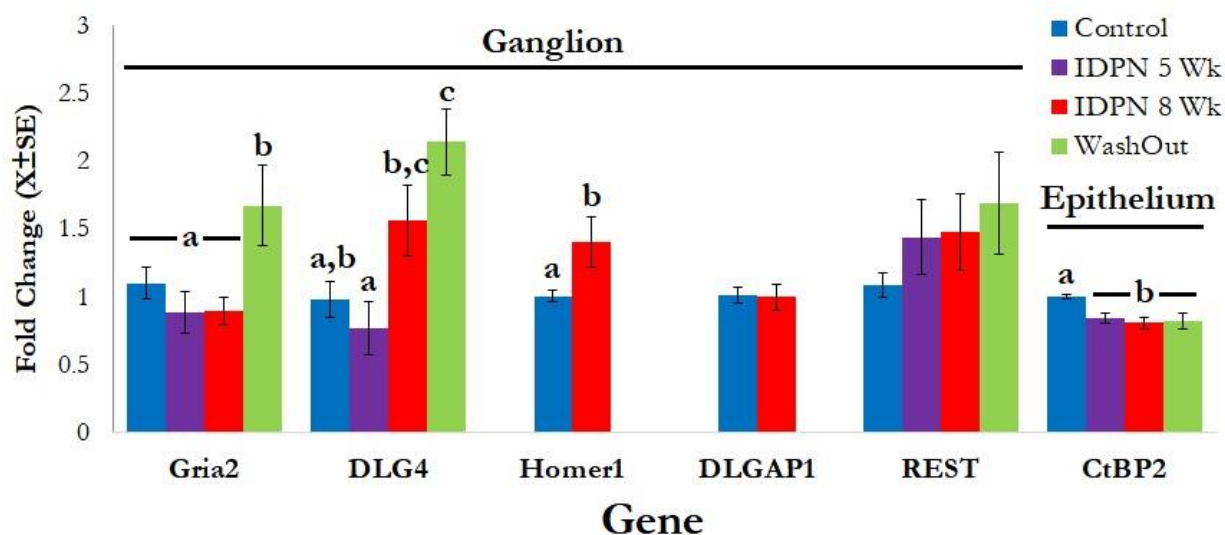


Figure 29: Alterations of mRNA expression of synaptic, scaffolding, and signaling proteins in vestibular sensory ganglia and epithelia after IDPN exposure of male 129S1/SvImJ mice. A total of 3 genes demonstrated an increase in mRNA expression after the IDPN exposure and/or washout period in the vestibular ganglia (Homer1, DLG4, Gria2). In the vestibular sensory epithelia, ribeye (CtBP2) demonstrated a decrease in expression, which did not recover to control levels after the washout period. Two genes (REST, DLGAP1) did not demonstrate any significance from the exposure. a, b, c: groups not sharing a letter are significantly different, $P < 0.04$, Duncan's test after significant ANOVA.

6.2.9 Preliminary RNAseq data of the vestibular ganglia and vestibular sensory epithelia demonstrate a depression in signal transmission in the afferent and cell-cell adhesion in the epithelia following sub-chronic IDPN exposure

The first RNAseq study compared the vestibular ganglion of 3 control mice with 3 mice treated with IDPN for 8 weeks (VDRs of 7, 14, 14). There were 13,532 mRNA sequences available to compare expressions between treatment groups, which resulted in 956 differentially expressed (DE) genes showing significance (fig. 30a). Of these 956 DE genes, 436 were upregulated, while 520 were downregulated (fig. 30b). A heat map (fig. 30c) of the most significantly altered DE genes ($n=50$) demonstrated that the mice treated with IDPN showed a downregulation of the majority (96%) of these top genes compared to control mice.

Functional enrichment analyses led to numerous pathways being affected by the ototoxic exposure; the “synaptic vesicle cycle” pathway emerged as highly significant ($p = 1.22E-05$, FDR = 0.015726) in the vestibular ganglia, and was examined for further processing. The DE genes listed in this pathway include: SYT1, STXBP1, ATP6V1B2, CLTC, STX1B, ATP6V1A, AP2B1, SLC17a6, AP2A1, ATP6V0A1, VAMP2, UNC13B, and UNC13A. All of these genes were downregulated, except for the isomer UNC13B, which was upregulated. All the downregulated genes aid in neurotransmitter release, calcium sensing, vesicle structure, and/or vesicle linkage for the exocytotic process. The UNC13 gene in particular is the priming step in vesicle exocytosis; while UNC13A promotes the close linkage of a vesicle to the plasma membrane, UNC13B promotes a more distant linkage, potentially restraining vesicle release. This noted depression in the synaptic vesicle cycle led to the examination of the “endocytosis” pathway, which had also been marked as being significant ($p = 0.0024$, FDR = 3.050741).

The DE genes implicated in the endocytosis pathway demonstrated a mix of downregulated and upregulated gene expression. Downregulated DE genes included: KIF5A, ASAP2, CLTC, LDLRAP1, EPS15, AP2B1, TFRC, AP2A1, DNAJC6, PDCD6IP, SH3GL2, and F2R. These genes aid in the process of neurotransmitter, molecular, or vesicular transport and/or the formation of vesicles. Upregulated DE

genes included: FGFR2, H2-K1, H2-D1, PRKCI, ARPC1B, RAB11FIP2, ARF3, RAB5A, GRK2, EHD2, and AGAP3. These genes aid in vesicle trafficking at the plasma membrane, activating various signaling cascades, vesicle formation, cell locomotion, and/or returning molecules and/or neurotransmitters to the endoplasmic reticulum (ER) or Golgi apparatus (Stelzer et al., 2016). When examining all the DE genes affected in the “endocytic” pathway, it can be argued that endocytosis is being depressed, neurotransmitter reuptake is depressed, and the process of neurotransmitter release is depressed; cessation of these mechanisms results in no new vesicles being formed for exocytosis and neurotransmitter release, less molecules and/or neurotransmitters are extracted from the synaptic cleft, and molecules/neurotransmitters in the pre-synaptic cell are being brought back to the ER or Golgi apparatus for storage instead of released.

By examining these two pathways, the argument can be made that the afferents in the ganglion of IDPN-treated mice are being depressed. The mechanisms utilized to transmit a signal are being downregulated with less vesicle formation for neurotransmitter release and fewer reuptakes from the synaptic cleft. This strengthens the hypothesis that sub-chronic IDPN exposure is causing a depression in the vestibular afferents, leading to less signal transduction to the parts of the brain that further process this information.

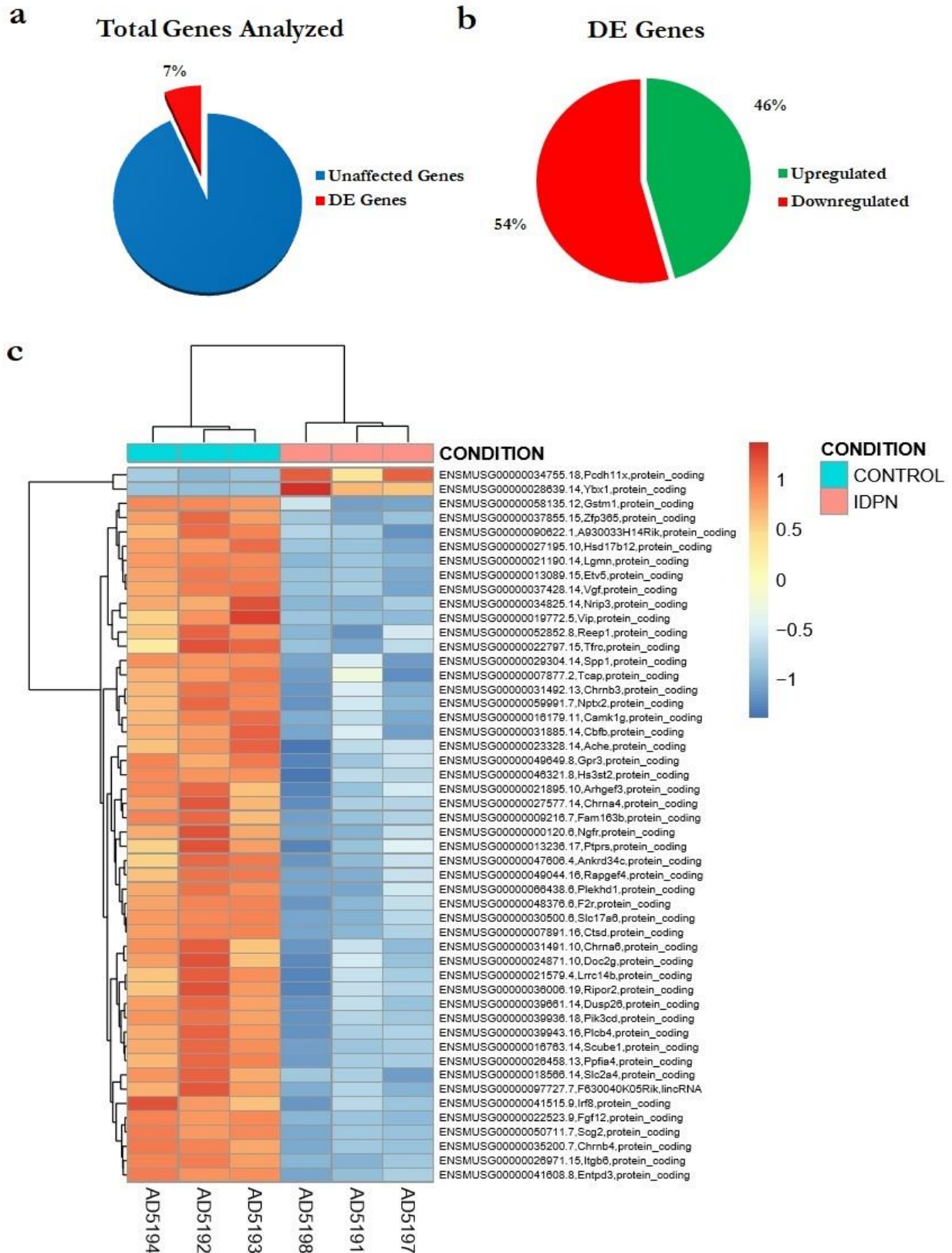


Figure 30: Effects of IDPN (30 mM in drinking water) on the transcriptome of the vestibular ganglia of male 129S1/SvImJ mice. **a** Percentage of genes differentially expressed (red) compared to the total number of genes (blue) examined in the RNAseq study. **b** Percentages of the differentially expressed genes that were either upregulated (green) or downregulated (red). **c** Heat map of the most significantly altered DE genes ($n=50$); the majority of these DE genes were downregulated for the IDPN-treated mice compared to control mice.

The second RNAseq study compared the vestibular sensory epithelium of the same 3 control mice and 3 mice treated with IDPN for 8 weeks. There were 17,219 mRNA sequences available to compare expressions between treatment groups, which resulted in 1,134 differentially expressed (DE) genes showing significance (fig. 31a). Of these 1,134 DE genes, 439 were upregulated, while 695 were downregulated (fig. 31b). A heat map (fig. 31c) of the most significantly altered DE genes (n=50) demonstrated that the mice treated with IDPN showed a downregulation of the majority (84%) of these top genes compared to control mice.

Functional enrichment analyses led to numerous pathways being affected by the ototoxic exposure; the “cell-cell adhesion via plasma-membrane adhesion molecules” pathway emerged as highly significant ($p = 2.21E-16$), and was examined for further processing. A total of 51 DE genes were listed in this pathway; 5 of the DE genes were upregulated, while the remaining 46 DE genes were downregulated. The majority of these downregulated genes coded for cadherin or protocadherin proteins; cadherin and protocadherin are calcium-dependent cell-cell adhesion glycoproteins or proteins, integrated into neuronal synapse connections. The significance of this pathway leads to the hypothesis that the sensory HCs are losing cell-cell adhesion with its corresponding afferent, as seen in the TEM and immunofluorescent studies of calyceal junctions. This loss of adhesion contributes to junction breakdown, afferent retraction from the HC, and potentially to HC extrusion.

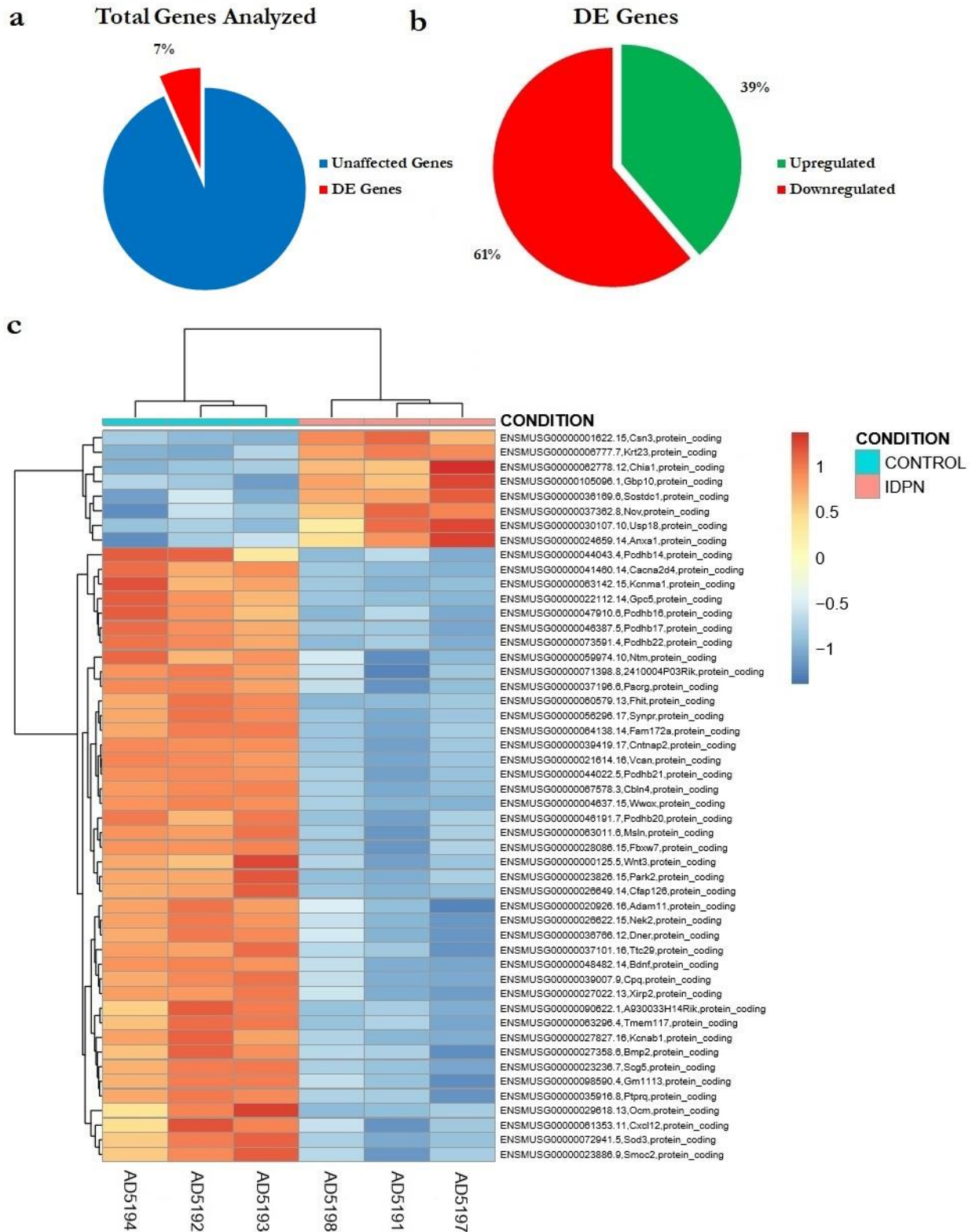


Figure 31: Effects of IDPN (30 mM in drinking water) on the transcriptome of the vestibular sensory epithelia of male 129S1/SvImJ mice. **a** Percentage of genes differentially expressed (red) compared to the total number of genes (blue) examined in the RNAseq study. **b** Percentages of the differentially expressed genes that were either upregulated (green) or downregulated (red). **c** Heat map of the most significantly altered DE genes ($n=50$); the majority of these DE genes were downregulated for the IDPN-treated mice compared to control mice.

6.2.10 Corroborating RNAseq results with qRT-PCR analyses of selected neurotrophic factors, synaptic, receptor, and kinase proteins, and proteins associated with molecule transport

The vestibular sensory epithelia and ganglia of male 129S1 mice were processed with qRT-PCR techniques to corroborate alterations in the mRNA expression of specific synaptic, receptor, transport, and signaling proteins during the exposure, due to their relevance observed in the two RNAseq studies. The specific genes chosen demonstrated highly significant values from the studies and overlapped with various synaptic signaling mechanisms of interest. The number of control mice and mice treated with IDPN for 8 weeks varied for the different genes (Table 6).

Treatment↓	Gene							
	Ganglion						Epithelium	
	SLC17a6	SLC2a4	Camk1G	NGFR	KCNQ5	Chrna6	Nptx2	BDNF
Control	7	8	8	8	9	9	9	8
IDPN 8 Wk	6	7	6	6	9	9	9	8

Table 6: Number of mice utilized per gene in the qRT-PCR study of selected neurotrophic factors, synaptic, receptor, and kinase proteins, and proteins associated with molecule transport distinguished from the RNAseq studies for control mice and mice treated with IDPN for 8 weeks in vestibular sensory ganglion and epithelium.

In the vestibular ganglion, the mRNA expression of 7 different genes was examined (fig. 32). All 7 genes demonstrated a decrease in mRNA expression for mice treated with IDPN for 8 weeks, compared to control mice. Vestibular sensory ganglion data were analyzed in two separate one way ANOVA tests, and comparisons resulted in significant group differences for SLC17a6 ($F[1,11] = 93.2, p < 0.000$), SLC2a4 ($F[1,13] = 40.4, p < 0.000$), Camk1G ($F[1,12] = 56.4, p < 0.000$), NGFR ($F[1,12] = 16.0, p = 0.002$), KCNQ5 ($F[1,16] = 10.3, p = 0.006$), Chrna6 ($F[1,16] = 12.5, p = 0.003$), and Nptx2 ($F[1,16] = 41.1, p < 0.000$).

In the vestibular sensory epithelium, the mRNA expression of BDNF was examined (fig. 32); BDNF also demonstrated a decrease in mRNA expression for mice treated with IDPN for 8 weeks, compared to control mice. Vestibular sensory epithelium data were analyzed with a one way ANOVA test, and comparisons resulted in significant group differences for BDNF ($F[1,14] = 131.7, p < 0.000$). Overall, there was a downregulation of various synaptic and signaling genes in both tissues, which match the downregulation seen in the RNAseq results.

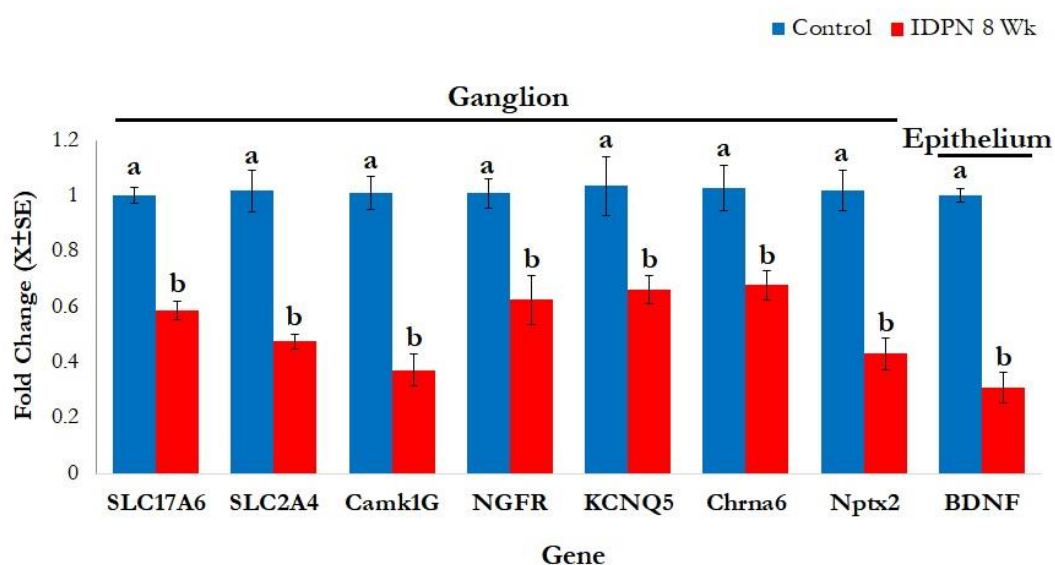


Figure 32: Alterations of mRNA expression of specific synaptic, receptor, transport, and signaling proteins in vestibular sensory epithelia and ganglia after IDPN exposure of male 129S1/SvImJ mice. All 7 genes demonstrated a decrease in mRNA expression after the IDPN exposure in the vestibular ganglia (SLC17a6, SLC2a4, Camk1G, NGFR, KCNQ5, Chrna6, Nptx2). In the vestibular sensory epithelia, BDNF also demonstrated a decrease in expression. a, b: groups not sharing a letter are significantly different, $P < 0.006$, Duncan's test after significant ANOVA.

6.3 Characterizing Auditory Damage

6.3.1 Effects of sub-chronic IDPN on 129S2 body weight

The number of male 129S2 mice utilized for this collaborative experiment decreased as the exposure progressed (see Table 1 in "Methodology"). There were 44 controls at week 0, 32 at week 2, 24 at week 4, and the exposure completed with 18 controls at week 6. The number of IDPN mice during the exposure was 31 for weeks 0 to 2, 24 at week 4, and 12 at the end of the exposure. The number of washout mice throughout the exposure was 7 from week 0 to week 2, and 6 mice until the end of the exposure at week 6.

Male 129S2 mice exposed to 30 mM IDPN demonstrated a decrease in body weight as exposure progressed from week 0 to week 4, and a slight increase from week 5 to week 6 (fig. 33a). Likewise, control mice demonstrated an increase in body weight throughout the 6 weeks of the study. In the washout experiment, animals lost body weight during treatment from week 0 to week 2, as recorded in the previous experiment, but then recovered significantly to control levels during the washout period from week 3 through to week 6. The maximal decrease in weight for IDPN-treated animals was recorded on week 4 where they had 85.6% of their initial weight compared to control mice which had 111.8% of their initial weight. At the end of the 6 week exposure, control mice and IDPN-treated mice had 113.1% and 87.8% of their initial weight, respectively. The washout mice demonstrated 89.9% of their initial weight on their final exposure week (week 2) and then had a full recovery in body weight after the four weeks of recovery. At week 6, recovery mice had 114.9% of their initial body weight.

Body weight data were analyzed in three separate MANOVA tests. Data from the exposure period of week 0 to week 2 resulted in significant day ($F[2,66] = 21.7$, $p < 0.000$), treatment ($F[2,67] = 10.1$, $p < 0.000$), and day by treatment interaction ($F[4,132] = 37.7$, $p < 0.000$) effects. Data from the exposure period of week 3 to week 4 resulted in significant day ($F[1,51] = 6.9$, $p = 0.011$), treatment ($F[2,51] = 38.4$, $p < 0.000$), and day by treatment interaction ($F[2,51] = 4.4$, $p = 0.018$) effects. Finally, data from the exposure period of week 5 to week 6 resulted in significant day ($F[1,33] = 9.6$, $p = 0.004$), treatment ($F[2,33] = 30.8$, $p < 0.000$), and day by treatment interaction ($F[2,33] = 4.8$, $p = 0.015$) effects.

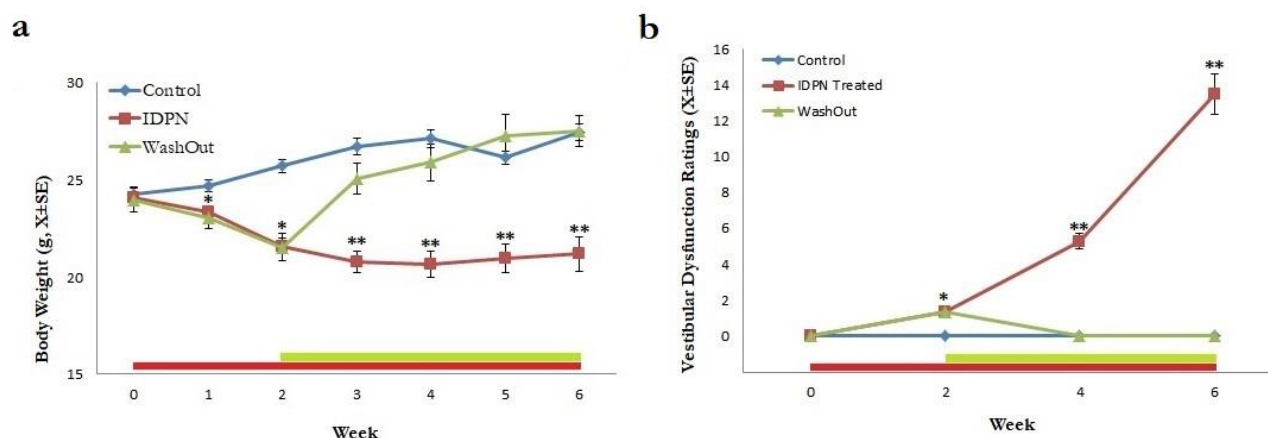


Figure 33: Effects of IDPN (30 mM in drinking water) on body weight and vestibular function of male 129S2/SvPasCrl mice. In both graphs, the (red) bar that runs fully across the x axis depicts IDPN exposure, while the shorter (green) bar depicts a subset

of mice treated with IDPN for 2 weeks and then underwent a recovery period. The number of animals declined during the exposure. **a** Body weight. Control mouse weights steadily increased as time progressed, while IDPN-treated mice decreased in weight during the exposure. Washout mice decreased in weight during the 2 week exposure, but then recovered to control mouse weights during the recovery period. **b** Vestibular Dysfunction Ratings. Data are tallied ratings from a battery of 6 items sensitive to vestibular dysfunction, each rated 0 (normal behavior) to 4 (highly dysfunctional response). IDPN-treated mice became more vestibularly dysfunctional as the exposure progressed, while control mice retained their normal behavior. Washout mice showed a small deficiency after the 2 week exposure, but then returned to control mouse numbers during the recovery period. *IDPN-treated and washout mice significantly different from control mice, ** IDPN-treated mice significantly different from the other experimental groups, ($P < 0.02$), post-hoc Duncan's tests performed after significant repeated-measures MANOVA

6.3.2 Effects of sub-chronic IDPN on 129S2 vestibular function

Mice exposed to IDPN for up to 6 weeks showed a loss of vestibular function that progressed over time; VDRs were recorded at week 2, 4, and 6 with progressively increasing scores (fig. 33b). The maximal VDRs were observed at week 6 of the exposure, but it was well below the highest possible score of 24. Likewise, washout mice, which were exposed to IDPN for 2 weeks, demonstrated a very small vestibular deficit; the mice were completely recovered after the 4 weeks of standard water. Control animals showed no vestibular dysfunction throughout the exposure. The number of mice used for each time point was the same as mentioned in the body weight data.

VDR data were analyzed in three separate MANOVA tests. Data from the initial exposure period (weeks 0-2) resulted in significant day ($F[1,39] = 72.8, p < 0.000$), treatment ($F[2,39] = 18.2, p < 0.000$), and day by treatment interaction ($F[2,39] = 18.2, p < 0.000$) effects. Data from the fourth exposure week resulted in significant day ($F[1,52] = 52.8, p < 0.000$), treatment ($F[2,52] = 88.8, p < 0.000$), and day by treatment interaction ($F[2,52] = 88.8, p < 0.000$) effects. Data from the end of the exposure compared to the initiation (week 0, 4, and 6) resulted in significant day ($F[2,33] = 71.1, p < 0.000$), treatment ($F[2,34] = 170.5, p < 0.000$), and day by treatment interaction ($F[4,66] = 39.6, p < 0.000$) effects. These data demonstrate that drinking-water IDPN readily causes sub-chronic ototoxicity in 129S2 male mice.

6.3.3 IDPN exposure strongly affects the hearing of treated mice

The absolute thresholds were determined from weeks 0, 2, 4, and 6 between the control, IDPN-treated, and recovery mice. The number of mice per treatment for each time point was the same as mentioned for the body weight data. Data is presented in 2 approaches: as a sub-chronic exposure and as a recovery model. The sub-chronic exposure (fig. 34a) compared the absolute thresholds of control mice and mice treated with IDPN for 2, 4, or 6 weeks. During the exposure period, mice demonstrated a robust loss of hearing that began as early as 2 weeks of exposure, and propagated from 32 to 8 kHz. The recovery model (fig. 34b) compared control mice, mice treated with IDPN for 2 weeks, and mice that underwent a washout period of either 2 or 4 weeks after 2 weeks of IDPN exposure. As noted in the sub-chronic model, a deficit in hearing was recorded after 2 weeks of IDPN exposure; washout mice of 2 weeks demonstrated a small capacity for recovery, while washout mice of 4 weeks recovered more, although not completely.

Absolute threshold data were analyzed with one-way ANOVA comparing the click stimuli and the four frequencies between the different treatment groups. Click stimuli data and data for 8, 16, and 24 kHz demonstrated significant effects between the treatment groups ($F[5,179] = 258.2, F[5,179] = 70.6, F[5,179] = 322.7, F[5,179] = 45.4$, respectively, all $p < 0.000$). Control data displayed no significance when compared to each other. These results indicate that longer IDPN exposure causes deeper and more profound hearing loss, although only 2 weeks of exposure was sufficient to cause hearing loss. An extensive washout period after 2 weeks of IDPN exposure demonstrated the capacity for recoverability, but any recovery after 4 or 6 weeks of IDPN exposure has yet to be examined.

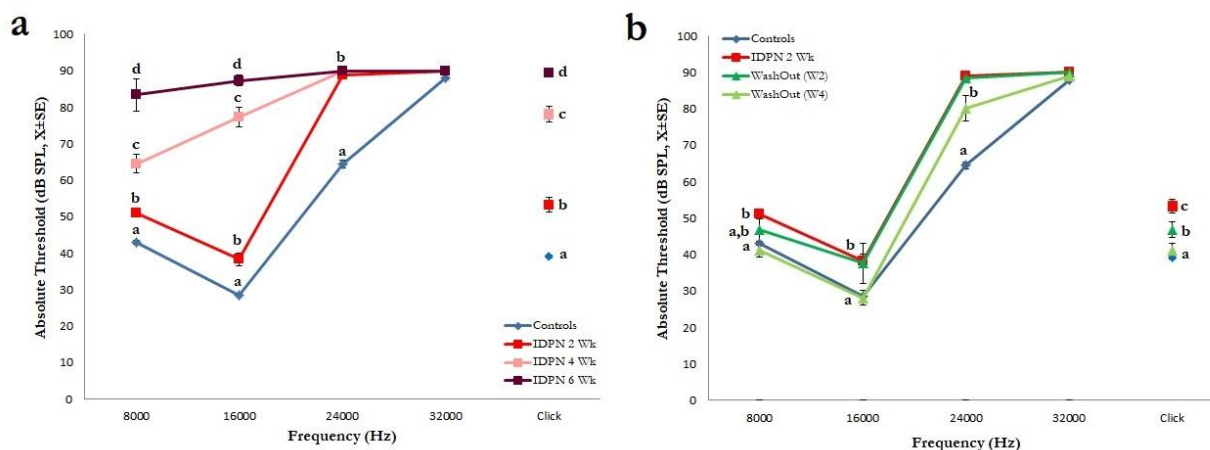


Figure 34: Effects of IDPN (30 mM in drinking water) on absolute thresholds for click stimuli and at the four frequencies (8, 16, 24, 32 kHz) of male 129S2/SvPasCrl mice. **a** Absolute thresholds of sub-chronic ototoxicity. A significant difference in absolute threshold can be seen for the mice treated with IDPN: those treated for 2 weeks were worse in hearing than control mice, those treated for 4 weeks were worse in hearing compared to control and IDPN-treated 2 week mice, and those treated for 6 weeks were the worst in hearing (deaf) compared to all other experimental groups. **b** Absolute thresholds of recovery mice. Washout mice showed a potential for recovery, showing small recovery after 2 weeks of standard water, and then an almost complete recovery after 4 weeks of standard water. a, b, c, d: groups not sharing a letter are significantly different, $P < 0.000$, Duncan's test after significant ANOVA.

The amplitudes of Wave I were determined and compared with input/output function slopes for the sub-chronic exposure (fig. 35a) and the recovery model (fig. 35b). For the sub-chronic exposure (fig. 35a), 44 control mice, 14 mice treated with IDPN for 2 weeks, and 9-15 mice treated with IDPN for 4 weeks were compared for the click stimuli, and at 8 and 16 kHz; data for mice treated with IDPN for 6 weeks were not included due to a lack of sample number. Input/output function slopes were not calculated at 24 or 32 kHz due to the extremely elevated absolute thresholds (+60 dB SPL) for these frequencies. One-way ANOVA comparisons for 8 kHz data and 16 kHz data resulted in significant effects between treatment groups, but not for the click stimuli. At 8kHz, there was a reduction in amplitude for IDPN mice compared to controls ($F[2,70] = 8.7$, $p < 0.000$). At 16 kHz, there was a reduction in amplitude after 2 weeks of IDPN exposure, but this recovered to control levels despite continued IDPN exposure ($F[2,64] = 6.6$, $p = 0.003$).

For the recovery model (fig. 35b), 53 control mice, 14 mice exposed to IDPN for 2 weeks, and 4 washout mice with a recovery time of 4 weeks were compared for the click stimuli, and at 8 and 16 kHz; washout mice with a recovery time of 2 weeks were not included due to a lack of sample number. Input/output function slopes were not calculated at 24 or 32 kHz due to the extremely elevated absolute thresholds (+60 dB SPL) for these frequencies. One-way ANOVA comparisons at 16 kHz resulted in significant effects between treatment groups, but not for the click stimuli (all washout mice excluded due to a lack of sample number) or at 8 kHz. There was a reduction in amplitude size after IDPN treatment, as seen previously, but it remained decreased after a 4 week washout period ($F[2,68] = 8.2$, $p = 0.001$).

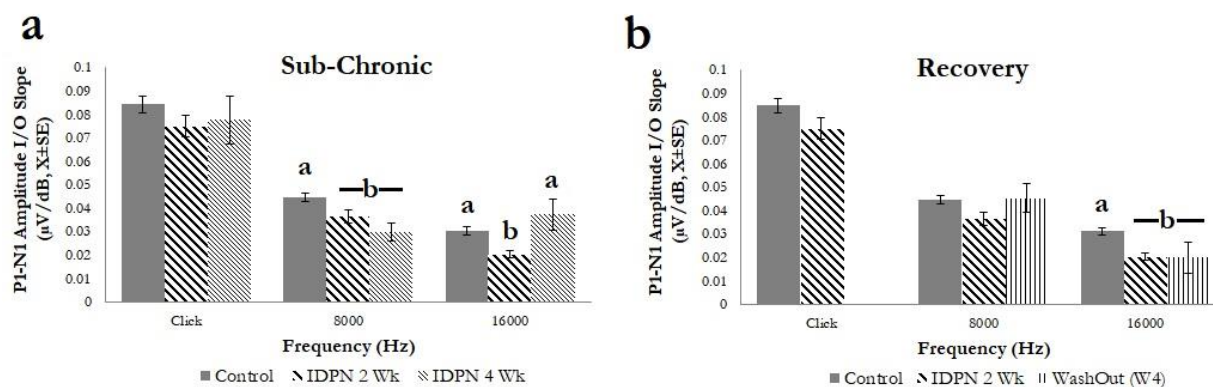


Figure 35: Effects of IDPN (30 mM in drinking water) on the input/output function slopes of the amplitudes of Wave I for click stimuli and at two of the frequencies (8, 16 kHz) of male 129S2/SvPasCrl mice. **a** Input/output function slopes for control mice and mice treated with IDPN for 2 or 4 weeks. A significant effect was noted for the different treatment groups at 8 and 16 kHz. At 8 kHz, mice treated with IDPN decreased in Wave I amplitude size. At 16 kHz, mice treated with IDPN for 2 weeks declined in Wave I amplitude, but returned to control size despite continued IDPN exposure. **b** Input/output function slopes for control mice, mice treated with IDPN for 2 weeks, and washout mice with a recovery of 4 weeks (except for click stimuli). Significant effects were seen between treatment groups at 16 kHz. Mice treated with IDPN for 2 weeks and washout mice decreased in Wave I amplitude size, compared to control mice. a, b: groups not sharing a letter are significantly different, $P < 0.005$, Duncan's test after significant ANOVA.

The latencies of Wave I were determined and compared with input/output function slopes for the sub-chronic exposure (fig. 36a) and the recovery model (fig. 36b). For the sub-chronic exposure (fig. 36a), 44 control mice, 14 mice treated with IDPN for 2 weeks, and 12-17 mice treated with IDPN for 4 weeks were compared for the click stimuli, and at 8 and 16 kHz; data for mice treated with IDPN for 6 weeks were not included due to a lack of sample number. Input/output function slopes were not calculated at 24 or 32 kHz due to the extremely elevated absolute thresholds (+60 dB SPL) for these frequencies. One-way ANOVA comparisons at 16 kHz yielded significant effects between treatment groups, but not for the click stimuli or at 8 kHz. The results demonstrate a large decrease in slope for mice treated with IDPN for 4 weeks ($F[2,67] = 13.1$, $p < 0.000$), compared to controls and mice exposed to IDPN for 2 weeks, indicating that latency times for the Wave I peak increased for these animals.

For the recovery model (fig. 36b), 56 control mice, 14 mice exposed to IDPN for 2 weeks, and 11 washout mice with a recovery time of 2 ($n=6$) or 4 ($n=5$) weeks were compared for the click stimuli, and at 8 and 16 kHz. Input/output function slopes were not calculated at 24 or 32 kHz due to the extremely elevated absolute thresholds (+60 dB SPL) for these frequencies. One-way ANOVA comparisons at 8 kHz yielded small significant effects between the IDPN-treated mice and 4 week recovered mice compared to the mice that only recovered for 2 weeks ($F[3,77] = 3.4$, $p = 0.022$); however, the alterations of mean latency values for these mice did not reach statistically significant differences with control mean values. No significant effects were found for the click stimuli or at 16 kHz.

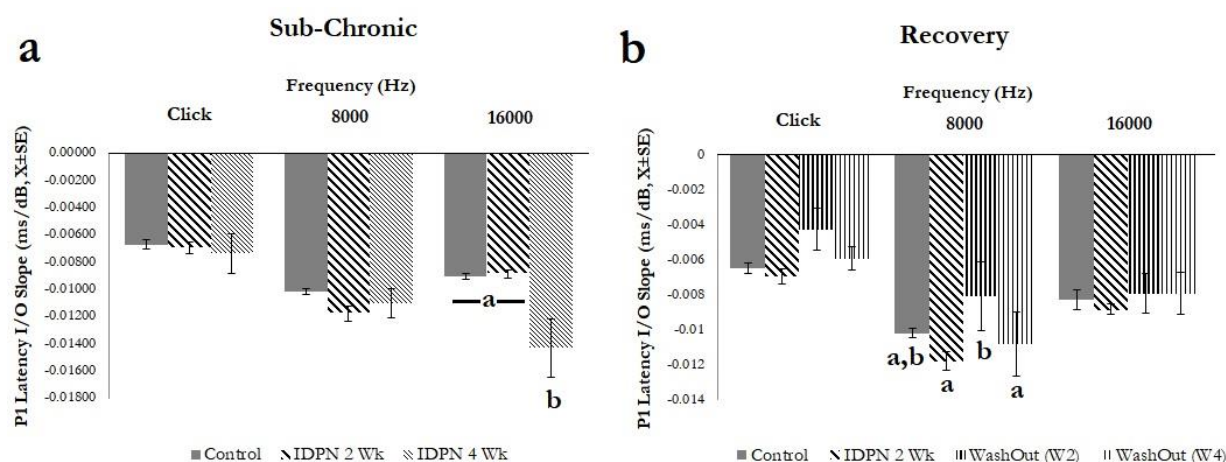


Figure 36: Effects of IDPN (30 mM in drinking water) on the input/output function slopes of the Wave I latencies for click stimuli and at the four frequencies (8, 16 kHz) of male 129S2/SvPasCrl mice. **a** Input/output function slopes for control mice and mice treated with IDPN for 2 or 4 weeks. A significant effect was noted for the different treatment groups at 16 kHz. Mice treated with IDPN for 4 weeks showed a significant decrease in slope, resulting in longer latency times compared to control mice or mice treated with IDPN for 2 weeks. **b** Input/output function slopes for control mice, mice treated with IDPN for 2 weeks, and washout mice with either a 2 or 4 week recovery. Significant effects between treatment groups are indicated at 8 kHz. Data indicates a significant decrease in slopes for IDPN-treated mice and washout mice with a recovery of 4 weeks compared to washout mice with a 2 week recovery, although they are all categorized as being at control levels. a, b: groups not sharing a letter are significantly different, $P < 0.03$, Duncan's test after significant ANOVA.

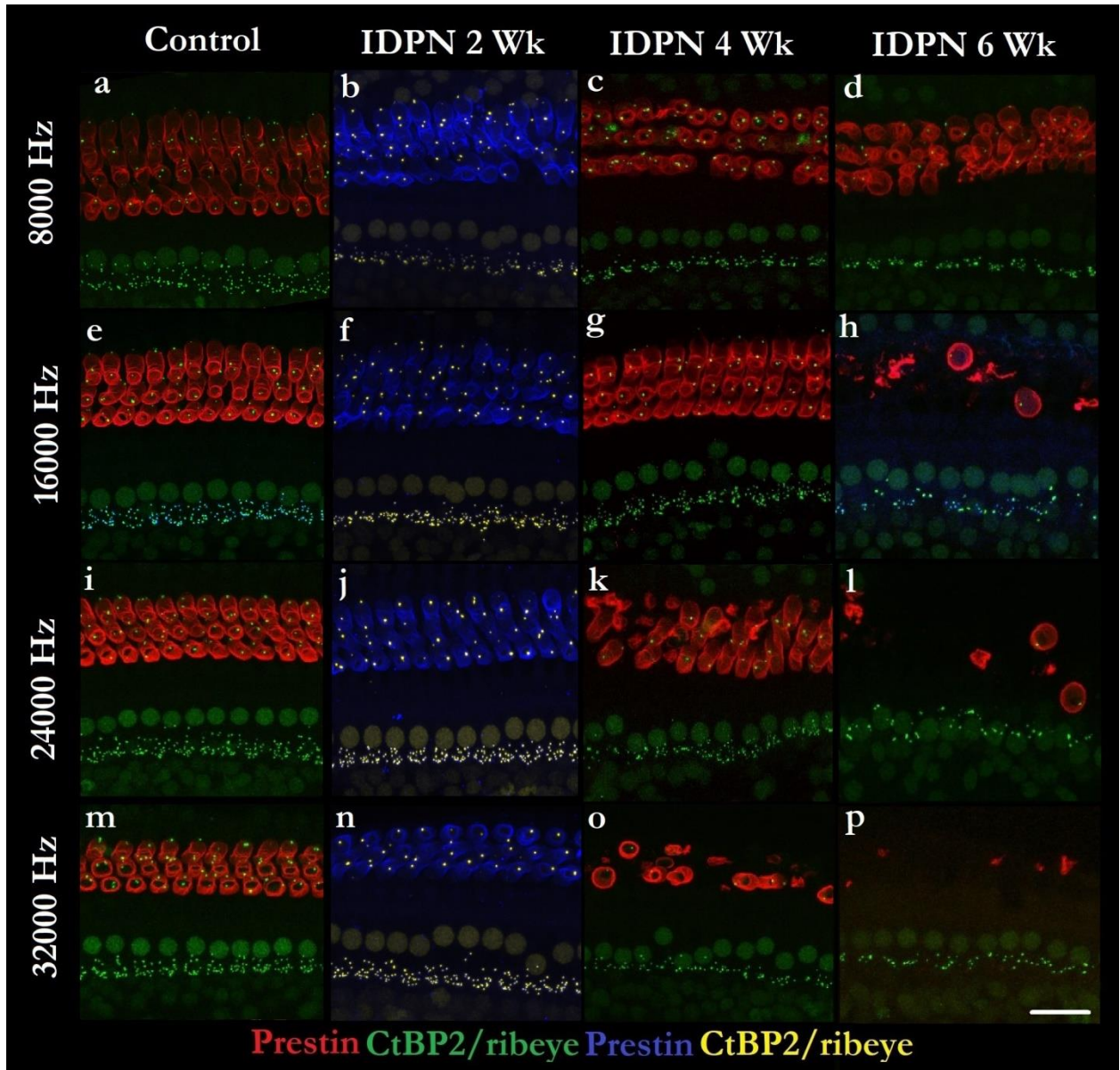
6.3.4 IDPN exposure causes a robust loss of OHCs, but IHCs remain intact

An immunofluorescent study examined the number of OHCs and IHCs in control mice and mice treated with IDPN for 2, 4, or 6 weeks at the four distinct frequencies; OHCs were immunolabeled with antibodies against prestin, while IHC nuclei were immunolabeled with CtBP2/ribeye. In healthy mice, every IHC is paired with three OHCs; in this study, a segment expanding the length of 10 IHCs was selected and the number of corresponding OHCs was recorded (fig. 37q). OHC data were analyzed with a one-way ANOVA test.

The number of IHCs remained unchanged throughout the exposure, regardless of IDPN exposure. In all cochlear sections (fig. 37a-p), IHC nuclei showed the regular placement that characterizes control cochlea. On the contrary, mice exposed to IDPN demonstrated a loss of OHCs that varied as a function of the time of exposure and the frequency zone (fig. 37a-p, fig. 37q).

At 8000 Hz, 5 mice treated with IDPN for 6 weeks were recorded with a 16% loss of OHCs (fig. 37d), whereas the 6 mice treated with IDPN for 4 weeks (fig. 37c), and the 6 mice treated with IDPN for 2 weeks (fig. 37b), remained at control animal ($n=15$) levels ($F[3,28] = 6.4$, $p = 0.002$). At 16000 Hz, 5 mice treated with IDPN for 6 weeks were observed with a 69% loss of OHCs (fig. 37h), whereas the 6 mice treated with IDPN for 4 weeks (fig. 37g), and the 7 mice treated with IDPN for 2 weeks (fig. 37f), remained at control animal ($n=14$) levels ($F[3,28] = 25.4$, $p < 0.000$). At 24000 Hz, 5 mice treated with IDPN for 6 weeks were observed with a 86% loss of OHCs (fig. 37l) and 5 mice treated with IDPN for 4 weeks had a 38% loss of OHCs ($F[3,25] = 37$, $p < 0.000$) (fig. 37k). At this frequency, the 6 mice treated with IDPN for 2 weeks (fig. 37j) remained at control animal ($n=13$) levels. At 32000 Hz, 5 mice treated with IDPN for 6 weeks were recorded with a 97% loss of OHCs (fig. 37p), and 5 mice treated with IDPN for 4 weeks had a 77% loss of OHCs ($F[3,26] = 462.8$, $p < 0.000$) (fig. 37o). At this frequency, the 5 mice treated with IDPN for 2 weeks (fig. 37n) remained at control animal ($n=15$) levels.

This result demonstrates that this IDPN exposure, at least up until 6 weeks of intoxication, does not result in any IHC loss. However, OHC loss occurs. This OHC effect is tonotopic and time-dependent. The highest frequencies demonstrate loss first, and the longer the IDPN exposure, the more OHCs are lost.



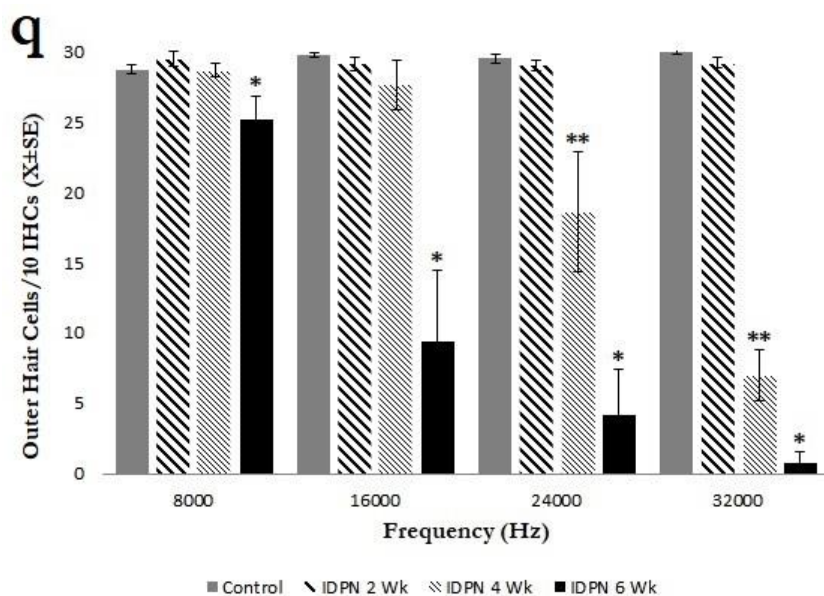


Figure 37: Effects of IDPN (30 mM in drinking water) on outer/inner hair cell counts of male 129S2/SvPasCrl mice. Inner hair cell counts remained at control levels, regardless of IDPN exposure of up to 6 weeks. **a-p** Ten inner hair cells were marked with CtBP2/ribeye (green/yellow) and the corresponding outer hair cells were marked with prestin (red/blue). **a,e,i,m** Control mice displayed 10 inner hair cells and 30 outer hair cells; **b,f,j,n** Mice treated with IDPN for 2 weeks displayed 10 inner hair cells, and 30 outer hair cells. **c,g,k,o** Mice treated with IDPN for 4 weeks displayed 10 inner hair cells, and control-like numbers of outer hair cells at 8 and 16 kHz, and significantly decreased numbers of outer hair cells at 24 and 32 kHz. **d,h,l,p** Mice treated with IDPN for 6 weeks displayed 10 inner hair cells, and significantly decreased numbers of outer hair cells at 8, 16, 24, and 32 kHz. **p** Scale bar is equal to 20 μ m and applies to all previous images. **q** Data are average outer hair cell counts for control and IDPN-treated mice for 2, 4, and 6 weeks at the four specified frequencies (8, 16, 24, 32 kHz). Ten inner hair cells were identified and the corresponding outer hair cells were marked and counted; missing cells were noted as a loss. *IDPN-treated mice for 6 weeks significantly different from other treatment groups; **IDPN-treated mice for 4 weeks significantly different from other treatment groups, $P < 0.000$, post-hoc Duncan's tests performed after significant one-way ANOVA

6.3.5 IDPN exposure causes a loss of *Caspr1* in vestibular sensory epithelia, but not in the organ of Corti

The calyceal junctions of HCIs from the striola of the utricle of the vestibular sensory epithelia were analyzed during the IDPN exposure for male 129S2 mice. The total HCs were identified with myosinVIIa-labeling and HCI-calyx afferent units were identified by *caspr1*-labeling, which marked the calyceal junctions (fig. 38c,d). Control mice showed *caspr1* fluorescence (fig. 38c), indicating intact calyceal junctions. A large percentage of the HCs examined for the control mice demonstrated positive *caspr1*-labeling (fig. 38a). Mice treated with IDPN for 6 weeks displayed a noted loss in *caspr1* fluorescence (fig. 38d) and a noted decline in positive *caspr1*-labeling when compared to control mice (fig. 38a). This indicates a loss of calyceal junctions, which had been observed in previous studies for the cristae, but now have been observed in the utricle.

There were 5 control mice from week 0 with a total of 125.6 ± 0.7 HCs, where 73% were identified as HCs (*caspr1*-labeled) and 27% were HCs without *caspr1*-labeling. There were 6 control mice from week 6 with a total of 134.3 ± 11.6 HCs, where 70% were identified as HCs (*caspr1*-labeled) and 30% were HCs without *caspr1*-labeling. One-way ANOVA determined that there were no significant differences between the two control groups. Finally, 5 mice exposed to IDPN for 6 weeks were compared to controls; one-way ANOVA comparison resulted in significant effects between the two treatment groups. IDPN-treated mice were recorded with a total of 120.0 ± 15.6 HCs, where only 1% were identified as HCs (*caspr1*-labeled), a large decrease compared to controls ($F[1,16] = 612.1$, $p < 0.000$) (fig. 38a). Meanwhile, 99% of the total HCs were HCs without *caspr1*-labeling, a significant increase when

compared to controls ($F[1,16] = 612.1, p < 0.000$) (fig. 38a). Despite the IDPN exposure, the total number of HCs in both control and IDPN-treated mice remained unchanged and equal (fig. 38b).

This result indicates that the 6 week IDPN exposure did not result in any HC loss for the utricle of the vestibular sensory epithelia of the mice. However, the loss of caspr1 is observed, and thus, the loss of the calyceal junctions of HCIs.

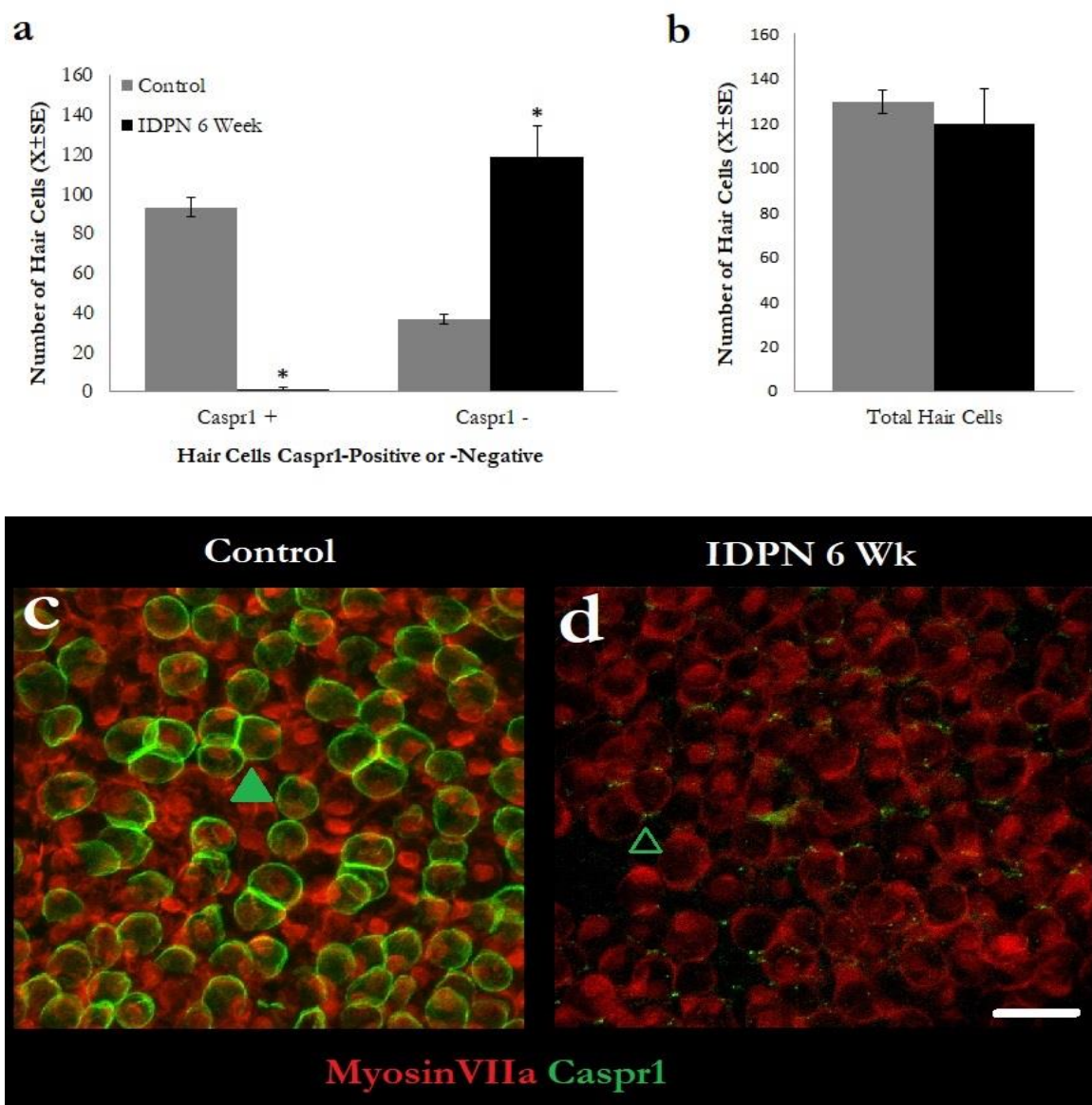


Figure 38: Effects of IDPN (30 mM in drinking water) on caspr1-labeling of the calyceal junctions of type I hair cells from the striola of the utricle of the vestibular sensory epithelia of male 129S2/SvPasCrl mice. **a** Comparison of treatment groups of hair cells identified by caspr1-labeling or the absence of caspr1-labeling (myosinVIIa-labeling only). The control group demonstrated a large number of hair cells labeled with caspr1, compared to hair cells lacking caspr1-labeling. After the 6 week IDPN exposure, the number of hair cells with identifiable caspr1-labeling decreased immensely, and the number of hair cells identified without caspr1-labeling increased dramatically. **b** The total number of complete hair cells in the striola of the utricle, identified by myosinVIIa-labeling. No significance was found between control and IDPN-treated mice. **c,d** Snapshots of the striola of the utricle with caspr1-labeling (green) and myosinVIIa-labeling (red). **c** Snapshot of a control mouse. Solid green arrow indicates the caspr1-labeling of the calyceal junction of a type I hair cell. **d** Snapshot of an IDPN-treated mouse. Open green arrow indicates the absence of caspr1-labeling of a hair cell, demonstrating the loss of calyceal junctions. Scale bar is 15 μm . *IDPN-treated mice for 6 weeks significantly different from the control mice, $P < 0.000$, post-hoc Duncan's tests performed after significant one-way ANOVA

The caspr1-labeling of the organ of Corti identifies the first heminode of type I afferent fibers contacting with IHCs (fig. 39b). Due to the shape of the afferent, this results in the caspr1-labeling having a tube-like structure that can be measured in length (fig. 39a). At least 6 different measurements were made per IHC, and at least 6 IHCs were analyzed per frequency. The number of mice per treatment group per frequency varied (Table 7).

	Frequency (Hz)			
Treatment↓	8000	16000	24000	32000
Control	14	15	14	14
IDPN 4 Wk	6	5	5	5
IDPN 6 Wk	5	5	5	5

Table 7: Number of mice utilized per treatment group per frequency for caspr1 length measurements in the cochlea.

One-way ANOVA was performed and resulted in no significant effects occurring between treatment groups at any of the frequencies studied. Caspr1 lengths at the first heminode in the type I afferent, which contacts with the IHCs, resulted in no change throughout the IDPN exposure.

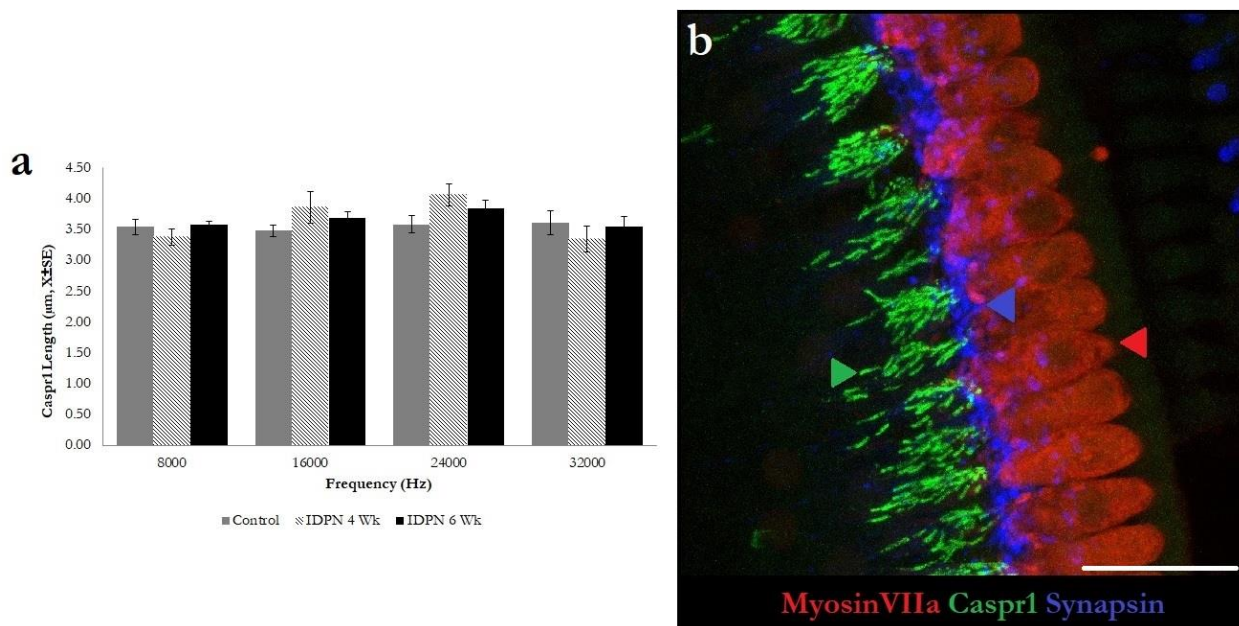


Figure 39: No effects of IDPN (30 mM in drinking water) exposure to the caspr1 protein in type I afferent filaments in the organ of Corti of male 129S2/SvPasCrl mice. **a** The lengths of the caspr1 were measured and compared between control mice and IDPN-treated mice (4 or 6 week exposure) across the four frequencies (8, 16, 24, 32 kHz). No significant differences were found. **b** Representative image of the immunostaining of the organ of Corti. Inner hair cells were identified by myosinVIIa (red, solid red arrow), the efferents making contact with the inner hair cells were identified by synapsin (blue, solid blue arrow), and caspr1-labeling was present in the first heminode of the type I afferent fibers that contact with the inner hair cells (green, solid green arrow). Scale bar is 20 µm.

6.3.6 IDPN exposure causes a decrease in active synapses in both cochlear and vestibular sensory epithelia

Active synapses, characterized by the core ribbon protein ribeye and the GluA2 subunit of the ionotropic AMPA receptor, were analyzed within HCs of the striola of the utricle (fig. 40b,c) and within IHCs of the organ of Corti at the four studied frequencies (fig. 41d-u). In the utricle, 11 control mice and 6 mice treated with IDPN for 6 weeks were compared. The number of puncta for ribeye, GluA2, and their colocalizations all decreased after IDPN exposure, compared to control mice (fig. 40a). One-way ANOVA was performed and active synapse data resulted in significant effects occurring between treatment groups for the number of ribeye puncta ($F[1,16] = 70.6, p < 0.000$), GluA2 puncta ($F[1,15] = 14.6, p = 0.002$), and their colocalizations ($F[1,15] = 14.2, p = 0.002$). These results indicate that the overall number of active synapses is decreasing in the utricles of IDPN exposed mice; this is comparable to the active synapse loss seen in the cristae, recorded in previous studies.

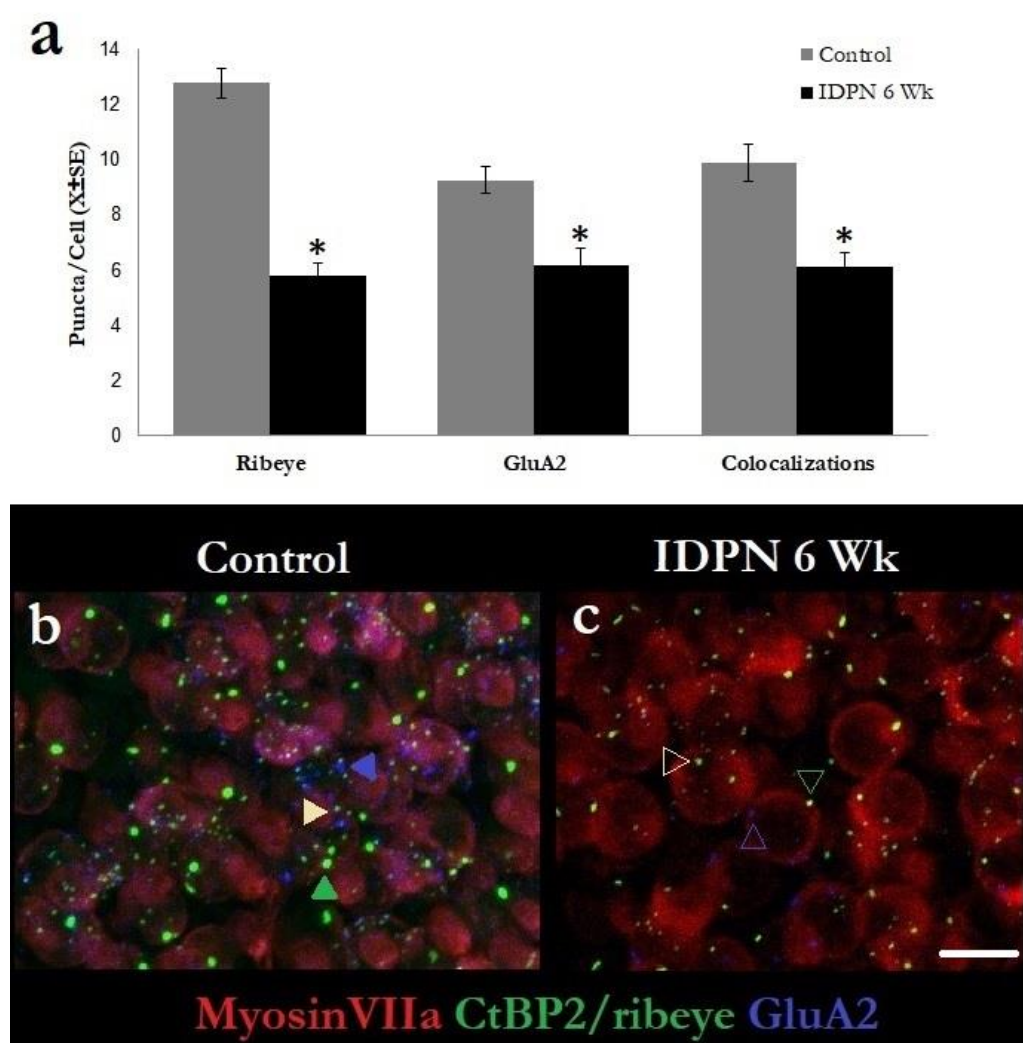


Figure 40: Effects of IDPN (30 mM in drinking water) exposure on active synapses analyzed within the striola of the utricle of the vestibular sensory epithelia of male 129S2/SvPasCrl mice. The number of active synapses decreased between control mice and mice treated with IDPN for 6 weeks. **a** The number of ribeye puncta, GluA2 puncta, and their colocalizations decreased after mice were exposed to IDPN for 6 weeks. **b,c** Representative images of the immunostainings of the active synapses for control and IDPN-treated mice. Hair cells were identified by myosin VIIa-labeling (red), ribeye puncta were marked by CtBP2/ribeye-labeling (green), and GluA2 puncta were marked by GluA2-labeling (blue). Scale bar is 6 μ m. **b** Control utricles displayed numerous puncta for both ribeye and GluA2; an example of a singular puncta for ribeye (solid green arrow), GluA2 (solid blue arrow), and a colocalization (solid beige arrow) are indicated. **c** IDPN-treated utricles (6 weeks) displayed significantly

less puncta for ribeye and GluA2, and their colocalizations. Example singular puncta for ribeye (open green arrow), GluA2 (open blue arrow), and a colocalization (open beige arrow) are indicated. *IDPN-treated mice for 6 weeks significantly different from the control mice, $P < 0.003$, post-hoc Duncan's tests performed after significant one-way ANOVA.

Active synapses were analyzed in the four studied frequencies for the organs of Corti between control mice, mice treated with IDPN for 2 weeks, mice treated with IDPN for 4 weeks, and mice treated with IDPN for 6 weeks (fig. 41d-u). There were 21 control mice (fig. 41d-g), 7 mice treated with IDPN for 2 weeks (fig. 41h-k), 6 mice treated with IDPN for 4 weeks (fig. 41l-o), and 6 mice treated with IDPN for 6 weeks (fig. 41p-s) for this study; all four frequencies were analyzed for each mouse. Ribeye puncta declined for mice treated with IDPN for 6 weeks at 16000, 24000, and 32000 Hz; ribeye puncta also decreased for mice treated with IDPN for 4 weeks at 32000 Hz (fig. 41a). GluA2 puncta declined for mice treated with IDPN for 6 weeks at 16000, 24000, and 32000 Hz; GluA2 puncta also decreased for mice treated with IDPN for 4 weeks at 24000 and 32000 Hz (fig. 41b). Colocalizations declined for mice treated with IDPN for 6 weeks at 16000, 24000, and 32000 Hz; colocalizations also decreased for mice treated with IDPN for 4 weeks at 32000 Hz (fig. 41c). No puncta or colocalization numbers were altered at 8000 Hz.

Three one-way ANOVA tests were completed in order to analyze ribeye puncta, GluA2 puncta, and colocalization data separately across the four frequencies. Ribeye data resulted in significant effects of IDPN exposure for 6 weeks compared to the other 3 groups at 16000 Hz ($F[3,37] = 19.6$, $p < 0.000$) and 24000 Hz ($F[3,40] = 13.3$, $p < 0.000$), and significant effects of IDPN exposure for 4 and 6 weeks at 32000 Hz ($F[3,40] = 44.2$, $p < 0.000$). GluA2 data resulted in significant effects of IDPN exposure for 6 weeks at 16000 Hz ($F[3,37] = 24.4$, $p < 0.000$) and significant effects of IDPN exposure for 4 and 6 weeks at 24000 Hz ($F[3,40] = 12.4$, $p < 0.000$) and 32000 Hz ($F[3,40] = 47.0$, $p < 0.000$). Colocalization data resulted in significant effects of IDPN exposure for 6 weeks at 16000 Hz ($F[3,37] = 20.2$, $p < 0.000$) and 24000 Hz ($F[3,40] = 11.5$, $p < 0.000$), and significant effects of IDPN exposure for 4 and 6 weeks at 32000 Hz ($F[3,40] = 46.4$, $p < 0.000$). No significant effects were indicated at 8000 Hz and no significant effects were found for mice treated with IDPN for 2 weeks at any of the studied frequencies.

These results indicate a loss of active synapses in a tonotopic pattern, similar to OHC loss. The higher frequencies lost their active synapses more readily compared to lower frequencies, and a longer IDPN exposure time resulted in more frequencies being affected. This indicates that sub-chronic ototoxicity affects the active synapses of higher frequencies in the organs of Corti first and, depending on the exposure time, affects the lower frequencies as well.

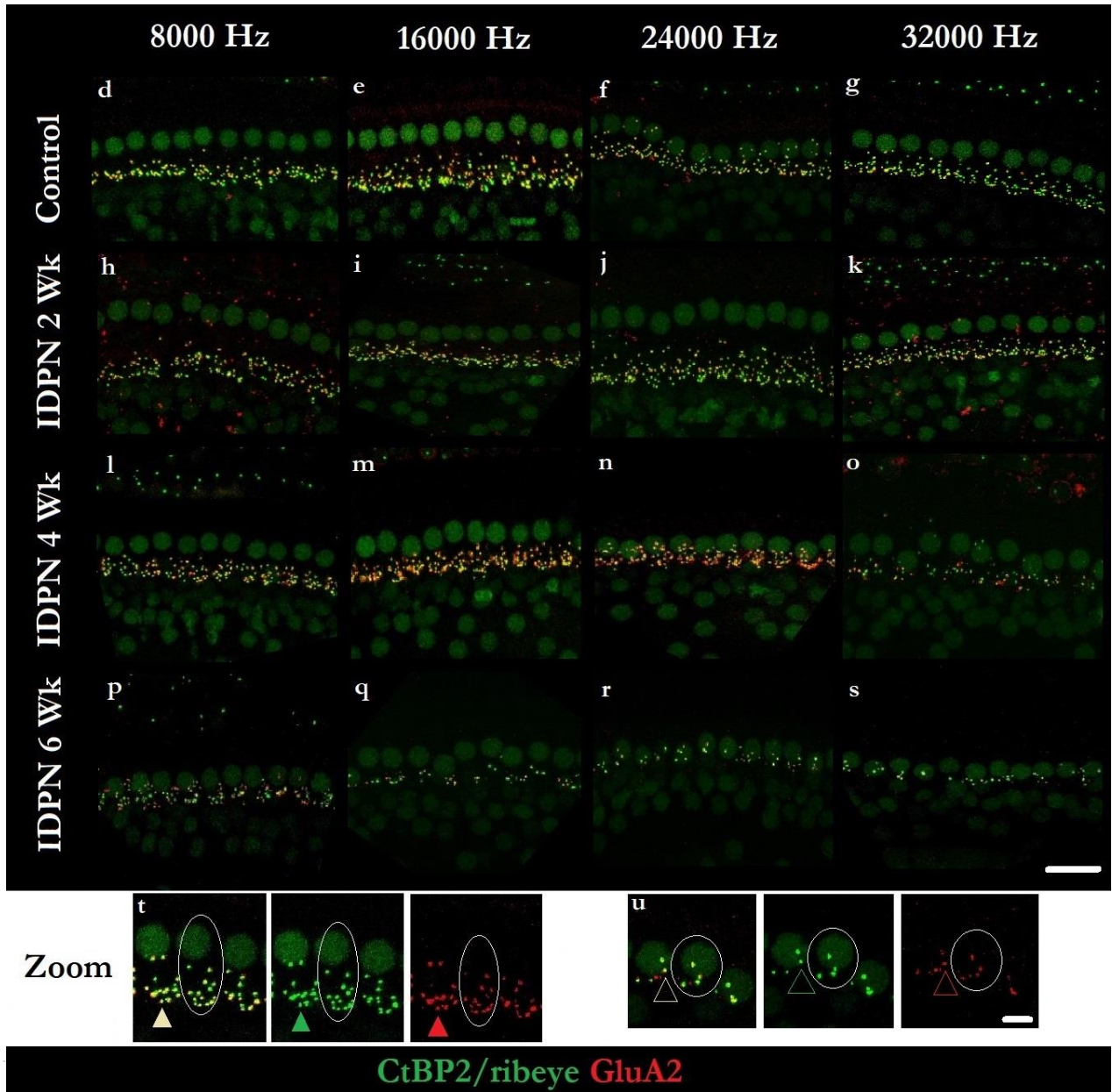
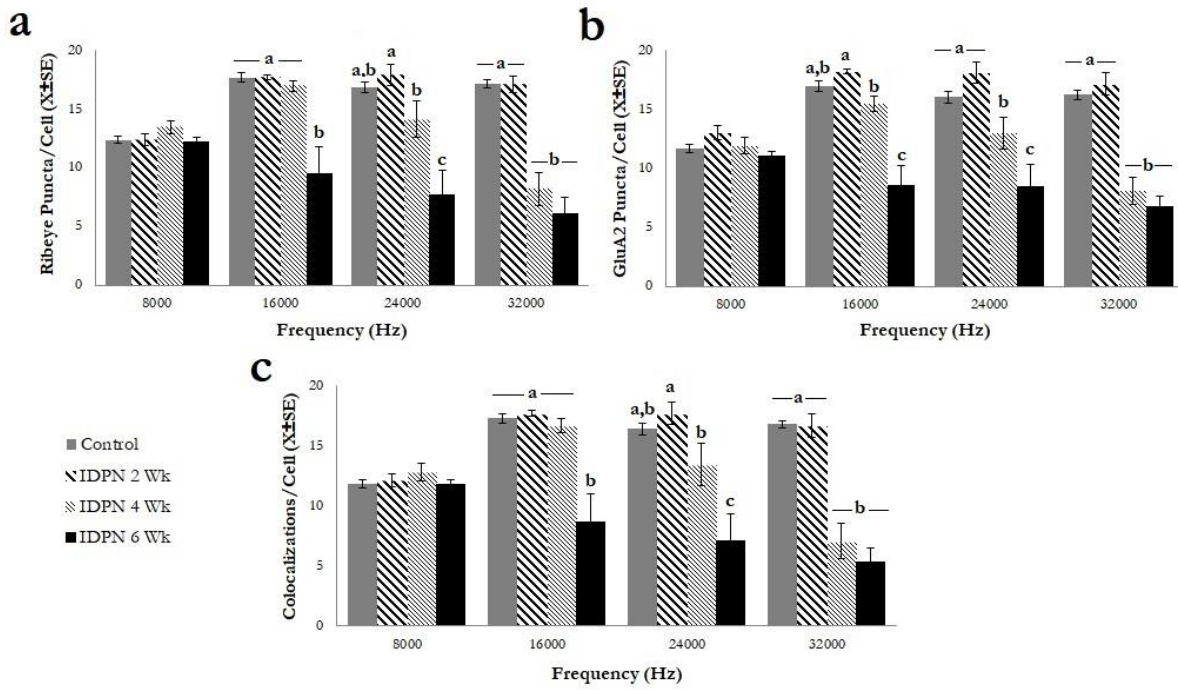


Figure 41: Effects of IDPN (30 mM in drinking water) on the active synapses of the IHCs of the organ of Corti at the four studied frequencies (8, 16, 24, 32 kHz) of male 129S2/SvPasCrl mice. The number of active synapses decreased at 16, 24, and 32 kHz for mice treated with IDPN for 6 weeks. The number of active synapses decreased at 24 and 32 kHz for mice treated with IDPN for 4 weeks. Mice treated with IDPN for 2 weeks remained at control levels across all frequencies. **a-c** Number of ribeye puncta (**a**), GluA2 puncta (**b**), and their colocalizations (**c**) per IHC across the four studied frequencies. **d-u** Immunostaining of the organs of Corti for control and IDPN-treated mice at the four studied frequencies. Ribeye puncta were immunolabeled with CtBP2/ribeye (green) and the nuclear stainings were used to distinguish individual IHC. The GluA2 receptor was labeled in red. **d-g** Control organ of Corti at the four frequencies. **h-k** Organ of Corti of mice treated with IDPN for 2 weeks at the four frequencies, where active synapse numbers remained at control levels. **l-o** Organ of Corti of mice treated with IDPN for 4 weeks. **l,m** (8, 16 kHz) demonstrated control-like numbers of active synapses. **n,o** (24, 32 kHz) demonstrated a decline in all puncta following the exposure. **p-s** Organ of Corti of mice treated with IDPN for 6 weeks. **p** (8 kHz) demonstrated control-like numbers of active synapses. **q-s** (16, 24, 32 kHz) demonstrated a decline in all puncta following the exposure. **s** Scale bar is 20 μm and applies to all previous images. **t,u** Magnified views of control IHCs at 32 kHz (**t**) and of IDPN-treated IHCs from 6 weeks of exposure at 32 kHz (**u**). Individual puncta are identified for ribeye (solid green arrow, open green arrow), GluA2 (solid red arrow, open red arrow), and a colocalization (solid beige arrow, open beige arrow) in both treatment group magnifications. Scale bar is 6 μm . a, b, c: groups not sharing a letter are significantly different, $P < 0.000$, Duncan's test after significant ANOVA.

7. Discussion

7.1 Sub-Chronic IDPN Intoxication

The overall objective of this Thesis was to establish a mouse model of sub-chronic IDPN exposure based on the previous rat data (Sedó-Cabezón et al., 2015) and preliminary mouse data, and further characterize the vestibular damage accrued during intoxication and its subsequent recovery. A first study of the auditory damage occurring in this model was also included. The knowledge gathered during this Thesis is set to advance the field of nitrile toxicity and progressive ototoxicity of the inner ear. A multitude of studies utilized functional, histological, and molecular techniques to procure this knowledge and advance in its understanding.

7.2 The Vestibular Model

7.2.1 Establishing the sub-chronic IDPN mouse exposure model

The study of aminoglycoside antibiotics for progressive inner ear damage is difficult to realize due to the resiliency rodents demonstrate towards aminoglycoside treatment (Sedó-Cabezón et al., 2014). For this reason, we turned to nitriles, specifically IDPN, because they demonstrate the “classic” pattern of ototoxicity as seen in progressive aminoglycoside administration (see “Introduction”, Lindemann, 1969; Wersall et al., 1973; Llorens et al., 1993). This led to the establishment of the sub-chronic IDPN rat exposure model (Llorens and Rodríguez-Farré, 1997) and identifying various types of damage accrued during the intoxication (Seoane et al., 2001a,b; Seoane et al., 2003) and their capacity to recover when the ototoxic insult was removed (Sedó-Cabezón et al., 2015). To further validate the sub-chronic IDPN exposure model, a second species, the mouse, was chosen to be established.

Preliminary mouse data for sub-chronic IDPN intoxication examined male and female 129S1/SvImJ (129S1) and RjOrl:Swiss/CD-1 (Swiss) mice. They were tested with 20-40 mM IDPN in their drinking water for 3, 5, or 8 weeks and their vestibular function were evaluated. Female Swiss mice were tested with lower IDPN dosages, while male Swiss mice had been tested with a spectrum of IDPN dosages (20-40 mM). The ensuing results did not produce systemic toxicity within the Swiss mice, but there were no overt effects on vestibular function either. Female 129S1 mice tested with lower IDPN dosages (20-35 mM IDPN) showed a weak loss of vestibular function, while those tested with 40 mM IDPN reached a 20% loss of body weight after a short exposure time, requiring termination. Finally, male 129S1 mice were tested with the varying dosages and durations. Those mice tested with 20 and 25 mM IDPN displayed no overt loss of vestibular function, while those tested with 30, 35, and 40 mM IDPN did experience overt loss of vestibular function. However, male 129S1 mice treated with the higher doses of IDPN (35, 40) reached a 20% loss of body weight, requiring termination. In the end, the best combination which produced maximal loss of vestibular function, but without losing 20% of body weight, was intoxicating male 129S1 mice with 30 mM IDPN for up to 8 weeks.

The stability of male 129S1 mice with 30 mM IDPN and an exposure of up to 8 weeks permitted for numerous studies on sub-chronic ototoxic exposure and vestibular dysfunction characterization, which is the core of this Thesis. We observed that the sub-chronic IDPN exposure on male 129S1 mice caused an initial loss of weight at the start of the exposure, which then slowly recovered over time. Additionally, the previously established vestibular test battery indicated a loss of vestibular function, which continued to decline throughout the exposure. The loss in weight and the overt, progressive dysfunction observed during the sub-chronic IDPN exposure is characteristic to the sub-chronic IDPN rat model. One marked difference between the rat and mouse data were the VDR scores. Rats underwent a sub-chronic IDPN exposure of 20 mM IDPN for 4 weeks and resulted in mean VDRs of 13-14 (Sedó-Cabezón et al., 2015), while the mouse sub-chronic IDPN exposure demonstrated average VDRs of 8.4 ± 0.6 over a maximum

value of 24; the VDR range is significantly less in mice compared to rats, and this difference is reflected upon in the later studies.

7.2.2 Sub-chronic IDPN effects on the morphology of the vestibular sensory epithelia and ganglia

In the ultrastructural results, we observed that mice treated with IDPN for 5 weeks and a few treated with IDPN for 8 weeks displayed control-like morphologies in the SEM studies. These mice had low VDR (3-6) scores. However, mice exposed for 8 weeks with higher VDRs displayed the characteristic vestibular alterations as seen in rats: stereociliary coalescence and hair cell extrusion. Mice that underwent a recovery period showed intact morphology or minimal pathological alterations, which were comparable to the rat data (Sedó-Cabezón et al., 2015). However, rats more commonly acquired VDRs higher than the most affected mice. These rats demonstrated more stereociliar coalescence and hair cell extrusion, and their recovery depended on whether vestibular function was restored after the washout period. If a rat with a high VDR score regained vestibular function after the washout period, control-like morphology was seen in the SEM images. However, if vestibular function did not recover, stereociliar coalescence and hair cell extrusion was observed. Since the majority of the treated mice did not achieve high VDRs like the rats, they would recover vestibular function after the washout period and thus, show intact morphology. Additionally, the extent of the damage depended on which vestibular tissue was being considered. The most affected tissue were the cristae, then the utricle, and then the saccule, which demonstrated control-like morphologies throughout the exposure (cristae>utricle>saccule). Damage occurred more abundantly in the striolar region of either the cristae or utricle, and moved towards the peripheral regions depending on the extent of the VDR. This was demonstrated in previously established results and is the “classic” pattern of ototoxicity for nitriles and aminoglycoside antibiotics (Lindemann, 1969; Wërsall et al., 1973; Llorens et al., 1993).

In the TEM data, we observed more progressive damage in the cristae. Mice treated for 5 weeks showed mostly control-like morphology, although some individual HCI-calyx afferent contacts were altered with either partial or complete absence of the calyceal junction, and fragmentation of the afferent. The contacts with absent calyceal junctions resembled those described for caspr1-null mice (Sousa et al., 2009). Mice exposed for 8 weeks varied in morphological alterations. Those with low VDRs showed similar characteristics to the 5 week exposed mice. Mice exposed for 8 weeks and with higher VDRs displayed widespread calyceal junction dismantlement, afferent fragmentation and detachment, and a few extruding hair cells into the endolymphatic cavity. A mouse with the highest VDR of 18 displayed a large loss of hair cells, completely extruded hair cells, and hair cells in the process of extrusion. TEM visualization of hair cell extrusion was noted in the rat data (Sedó-Cabezón et al., 2015) frequently, while its observation in the mouse was not as abundant. Hair cell extrusion is unique to sub-chronic ototoxic exposures, while hair cell apoptosis and necrosis is typically observed in acute ototoxic models (Seoane et al., 2001a; Op de Beeck et al., 2011). The different mechanisms in hair cell death demonstrate that the sub-chronic model is mechanistically different from the acute models.

Mice set for a washout period demonstrated a large capacity for recovery with clearly visible and intact calyceal junctions, demonstrating the capacity for reconstruction after the removal of the ototoxic insult. Additionally, we observed that membrane-to-membrane distances of intact calyceal junctions varied very little between the treatment groups and fell within previously reported distances (Sousa et al., 2009), but dismantled junctions were much more present in mice treated with IDPN for 8 weeks indicating much larger membrane-to-membrane distances. Washout mice recovered in calyceal junction abundance as well as intact membrane-to-membrane distances to control levels. In the rat data (Sedó-Cabezón et al., 2015), the progression of calyceal junction dismantlement and afferent fragmentation, leading to hair cell extrusion, was not as well detailed. In some mice, we observed afferent fragmentation and calyceal

junctions that were partially intact, and in other mice, they had progressed to afferent detachment and complete absence of the calyceal junction. In the rat, the majority examined was found to have complete loss of the calyceal junctions; only a few rats with the lowest VDRs had partially intact junctions and afferent fragmentation. This process of afferent fragmentation and detachment with the progressive loss of the calyceal junctions can be observed at a more detailed rate within the mouse. This will be useful for future studies that target the proteins and mechanisms involved in this progressive damage.

By combining SEM and TEM results, we can conclude that initial morphological damage is observed in low VDR mice, where initial calyceal junction breakdown occurs. Then, as vestibular dysfunction progresses, there is the complete loss of the calyceal junction and fragmentation followed by retraction of the afferent, along with stereociliary coalescence, observed in the higher VDR mice. The highest VDR mice demonstrate that vestibular dysfunction worsens due to the extended intoxication and eventually causes hair cells to be extruded from the epithelia; an example being the worst-case mouse with the highest VDR (18) with the largest loss in vestibular hair cells compared to any other mouse. This marked progressive damage coincides with the progressive damage observed in rats, although the mouse model demonstrates a more gradual process of the morphological changes and the progression as it occurs. This will be helpful in identifying proteins and mechanisms implicated during the ototoxic insult.

7.2.3 Sub-chronic IDPN effects on proteins involved with the calyceal junction in type I vestibular hair cells and their afferents

The immunofluorescent data obtained for caspr1 and tenascin-c in the cristae described a quantifiable loss of the two proteins during IDPN intoxication. These proteins are two major components of the calyceal junction. Caspr1 is localized in the afferent membrane and has a major role in junction organization (Sousa et al., 2009). Tenascin-c is a cell-adhesion modifying protein located in the extracellular matrix that characterizes the calyceal junction area (Lysakowski et al., 2011). The results of the immunofluorescent study coordinated with the TEM results in that the dismantlement and loss of the calyceal junctions coincided with the loss of caspr1 and tenascin-c. Likewise, these proteins were newly observed in washout animals, just as TEM data demonstrated the reconstruction of calyceal junctions in washout animals. Caspr1 is a key part of the structure and organization of calyceal junctions, so caspr1 loss is expected during junction dismantlement and loss. Meanwhile, tenascin-c is known to have varying functions including its involvement in axonal growth during development and post-lesion, cell migration, forming and maintaining discrete morphological boundaries (Bartsch, 1996; Joester and Faissner, 2001), and promoting sites for neurons for cell-binding, repulsion, and neurite outgrowth (Götz et al., 1996). The loss of tenascin-c may be a contributor to afferent fragmentation, detachment, and retraction, along with the recovery of these junctions once the ototoxic insult is removed. The mechanisms that contribute towards caspr1 and tenascin-c loss are not yet known.

These results are comparable to the immunofluorescent rat data, which also observed the loss and recovery of both caspr1 and tenascin-c in cristae samples (Sedó-Cabezón et al., 2015). However, in the mouse, the quantity of caspr1 did not fully recover to control levels, unlike tenascin-c and the colocalizations of caspr1 and tenascin-c that did fully recover; this may lead to molecular scarring of the vestibular afferents and/or the calyceal junctions between HCIs and their calyx afferents. Despite the fact that the mice had regained vestibular functionality after the washout period, it is not known whether the diminished quantity of caspr1 will have future consequences for those mice.

The qRT-PCR data of tenascin-c gave a clue as to why tenascin-c was observed to disappear during intoxication and its reappearance after the washout period. In the vestibular epithelia, the expression of the tenascin-c gene (*Tnc*) was observed to be downregulated during intoxication, but then made a full recovery after washout. This result was reflected in the immunofluorescent data. The expression of caspr1

and tenascin-c in the vestibular ganglia did not yield any significant results. So, while the vestibular ganglia was not altering mRNA expression of caspr1 or tenascin-c during the exposure, the vestibular sensory epithelia was downregulating Tnc expression; this downregulation may be weakening or devaluing calyceal junction support and structure perhaps due its roles in cell-binding, maintenance in axonal boundaries, and/or repulsion. This may aid in junction dismantlement, afferent fragmentation, detachment, and retraction, and/or as a part of the mechanism leading to hair cell extrusion, which involves cellular adhesion.

In the rat data, Tnc expression was not downregulated in the vestibular epithelium. In fact, the opposite was observed: Tnc expression was shown to be upregulated during sub-chronic exposure in the vestibular ganglia. There may be a few explanations for this: this may be a species-specific occurrence, the rat qRT-PCR data may not be accurate, or the rat vestibular tissue may be at a different stage of damage when compared to the mouse tissue. While the first two explanations may be a possibility, the most likely explanation is the last one. The previous SEM and TEM data demonstrated that the sub-chronic mouse model shows a more gradual progression of the damage occurring in the vestibular epithelia and ganglia when compared to the rat data. We also observed higher VDRs in rats when compared to mice, meaning more vestibular dysfunction for the rats. In this case, we may be observing what occurs to Tnc expression in the rat when the tissue is in a more damaged state; tenascin-c performs numerous roles so its expression may depend on the level of damage occurring as well. Additionally, we had pointed out in the “Results” section that we had observed an upregulation of expression for Tnc in the vestibular ganglion for the mouse, but Tnc expression was observed at approximately 20-fold lower levels in the vestibular ganglion compared to the vestibular epithelium and it resulted in not being statistically significant. In this sense, the changes of Tnc expression may be highly sensitive to the stages of damage each tissue is realizing during the sub-chronic IDPN exposure.

7.2.4 Sub-chronic IDPN effects on active synapses of vestibular hair cells

The number of active synapses, comprised of ribeye from the pre-synaptic cell and the groupings of GluA2 subunits from the post-synaptic cell, was quantified within the three HC-afferent units. Calyx-only units demonstrated a marked decrease in ribeye due to the exposure, which partially recovered after the washout period. The calyces of dimorphic afferents also noted a decline in ribeye, along with a decline in the ribeye and GluA2 colocalizations (the active synapses). Both ribeye and the colocalizations recovered to control levels after the washout period. In HCII units, ribeye, GluA2, and their colocalizations all decreased due to the exposure. The ribeye puncta were partially recovered after washout, and the GluA2 puncta and colocalizations completely recovered. These results demonstrated a general decline in ribeye for all HC-afferent units, which would indicate that fewer vesicles would be released during the receptor potential, leading to a decline in neurotransmitter release into the synaptic cleft. Additionally, colocalizations within the calyces of dimorphic afferent units and HCII units indicate direct loss of active synapses in these units, which would lead to a decline in overall signal transmission. HCII units also lost GluA2 subunits, indicating a decline in ionotropic AMPA receptors, which may be a direct result of lessened signal transmission. It is known that if a post-synaptic neuron is not receiving input from the pre-synaptic cell, the neuron will eliminate receptors from the PSD (Kessels and Malinow, 2009; Hugarir and Nicoll, 2013; Jurado, 2018). These results indicate that sub-chronic IDPN exposure affects the HC-afferent units differently, and may trigger different responses due to the ototoxic insult.

Counts of active synapses using ribeye and GluA2 puncta counts are being used to evaluate cochlear damage, in particular following acoustic overstimulation (Kujawa and Liberman, 2009, 2015, 2019). In the cochlea, reduced counts at the IHC level at prolonged periods after insult can be directly interpreted as afferent degeneration, since each afferent forms a single post-synaptic bouton on only one IHC (Kujawa and Liberman, 2015). In the vestibular epithelium, a different relationship is established for calyceal

endings on HCI and bouton endings on HCII. In the calyces, several synaptic puncta are formed on one single calyx. Our counts are obtained on a per cell basis, and so alterations in the number of puncta indicate altered density of synaptic sites in afferent terminals that remain in place. In HCII, a reduced number of puncta may indicate a loss of synaptic boutons, but this may not directly indicate complete afferent degeneration since the 1:1 afferent to synapse relationship characterizing the cochlear afferent is not present here (Sadeghi et al., 2014).

The qRT-PCR data demonstrated a downregulation of ribeye expression in the vestibular epithelium during the exposure, and it remained in a downregulated state after washout. The loss of ribeye was noted in the immunofluorescent studies, and the downregulation of its gene expression may contribute to this protein loss. The fact that ribeye mRNA expression does not return to control levels after the washout period may also explain why complete ribeye puncta numbers were not recovered in the calyx-only and HCII units. In the vestibular ganglion, GluA2 expression remained at controls levels during the exposure, but then was upregulated after the washout period. This may be a compensatory mechanism for all HC-afferent units, or the upregulation observed may contribute to its protein recovery after washout in the HCII units specifically.

Some of these results are comparable to the rat data; only the calyx-only and calyces of the dimorphic afferent units were analyzed in the rat. Rat data demonstrated a loss of ribeye in both units, with a partial recovery in calyx-only units and a full recovery in the calyces of dimorphic afferents (Sedó-Cabezón et al., 2015). This is equal to the mouse data. However, rat data also demonstrated a loss and recovery of both GluA2 puncta and their colocalizations in calyx-only afferent units, while mouse data only demonstrated a decline in colocalizations in the calyces of the dimorphic afferents. Rat data also demonstrated a downregulation of GluA2 expression in the vestibular ganglia during intoxication that was not observed in the mouse. These differences may be species-specific, dependent on which crista (horizontal vs. superior vs. posterior) was being analyzed, or that the rat vestibular tissue may have been at a different stage of damage when compared to the mouse tissue. As had been observed earlier in the SEM and TEM studies, the progression of ototoxic (reversible) damage in mice appears to be a more gradual breakdown of the calyceal junction and afferent fragmentation when compared to rats. In this sense, we may be observing active synapse loss and/or recovery at different stages for the mouse when compared to the rat.

Taken together, the present data confirms and extends the rat data demonstrating dynamic regulation of active synapse numbers during sub-chronic vestibular toxicity. Overall, the ultrastructural data and immunofluorescence data for adhesion and synaptic proteins from both the rat (Sedó-Cabezón et al., 2015) and present mouse model allows for the proposal of the following schema of cellular and molecular events characterizing sub-chronic vestibular damage and recovery in the HCI-calyx units (fig. 42).

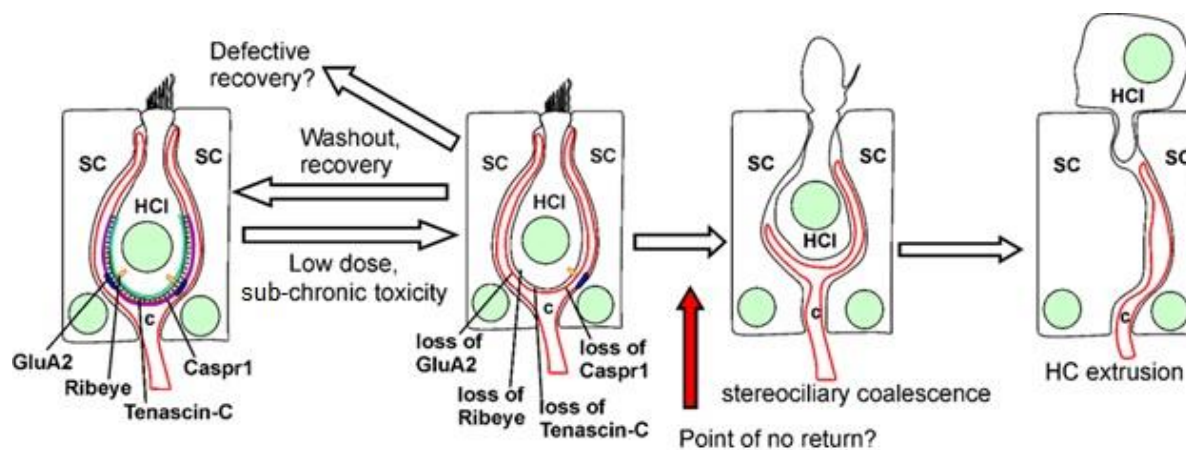


Figure 42: Proposed schema of sub-chronic vestibular damage and recovery in HCI-calyx units. Progressive damage starts with the loss of the calyceal junctions and active synapses with prolonged exposure resulting in calyx afferent fragmentation and retraction. A proposed “point of no return” is suggested and stereociliary coalescence occurs; prolonged exposure eventually leads to hair cell extrusion. SC: supporting cell, c: calyx afferent.

7.2.5 Sub-chronic IDPN effects on scaffolding proteins of the post-synaptic vestibular afferent

Two key scaffolding proteins in the PSD were analyzed in the three HC-afferent units using immunofluorescent studies. The PSD contains hundreds of proteins ranging from scaffolding to signaling proteins and with numerous receptors, organized in close proximity to pre-synaptic active zones for neurotransmitter release. We first analyzed PSD95, located in the PSD of the afferent, and it is an important component in the majority of excitatory glutamatergic synapses; KO mice for PSD95 demonstrate a loss in AMPA receptors and function that is synapse-specific (Béique et al., 2006), while overexpression of PSD95 increases AMPAR-mediated synaptic transmission (Béique and Andrade, 2003). The immunofluorescent study analyzed PSD95 with ribeye, since ribbon synapses are a part of the active zones for neurotransmitter release of the pre-synaptic cell and the receptors of the PSD tend to congregate near release sites in which PSD95 organizes and anchors them (Sheng and Sala, 2001). Calyx-only units declined in ribeye puncta during the exposure, and then completely recovered after the washout period. The loss of ribeye in calyx-only units was observed in the previous immunofluorescent study, although ribeye had only partially recovered after the washout period in that study. The calyces of dimorphic afferent units demonstrated no loss of ribeye puncta, despite the observed loss in the previous immunofluorescent study. However, statistical analyses revealed that both ribeye counts ($p = 0.056$) and colocalization counts ($p = 0.055$) were extremely close to statistical significance in their loss and gain, respectively. In HCII units, there were no alterations in ribeye observed, although ribeye alterations in HCII units had been observed previously. There was an increase in PSD95 puncta and their colocalizations with ribeye during the exposure, and these counts returned to control-like numbers after the washout period. The increase in PSD95 may be a compensatory mechanism to stabilize the structure of the PSD of the afferent(s) and/or to recruit new GluA2 subunits to the PSD, since GluA2 puncta as well as active synapses had been observed to be decreasing in the HCII units during the exposure. PSD95 regulates AMPA receptor localization and stabilization of the PSD during synaptic changes (Béique and Andrade, 2003); if active synapses were being lost, the increase of PSD95 may be triggered to increase the stability of the PSD during this alteration and/or to renew the GluA2 subunits that had been lost.

In the qRT-PCR data, we observed a slight upregulation of the expression of PSD95 in the vestibular ganglia during the exposure, which increased after the washout period. This result indicates that PSD95 expression is upregulated during the ototoxic insult, possibly causing an increase in PSD95 protein levels

in the PSD as observed in the immunofluorescent data of HCII units, and remains upregulated after the washout period as a possible compensatory and/or stabilization mechanism.

In the rat, PSD95 counts declined during exposure for both the calyx-only and the calyces of dimorphic afferent units, with partial or no recovery after washout (Sedó-Cabezón et al., 2015). These alterations were not found in the mouse data. As mentioned before, this may be due to a species-specific difference, dependent on which crista (horizontal vs. superior vs. posterior) was being analyzed, or the rat vestibular tissue may be at a different stage of damage when compared to the mouse tissue.

The second key scaffolding protein analyzed was Homer1. Homer1 is abundant in the PSD and creates a mesh-like structure with Shank, serving as a framework for other PSD proteins, like GKAP and PSD95, as a binding platform (Hayashi et al., 2009). For this reason, Homer1 was also examined with ribeye as a pre-synaptic cell marker. A decrease in ribeye puncta was observed in calyx-only afferent units, which recovered completely after washout, similar to the GluA2 and PSD95 immunostudies. No significant alterations were observed for Homer1 or their colocalizations in calyx-only afferent units. Additionally, no alterations in ribeye, Homer1, or their colocalizations were found in the calyces of dimorphic afferent units or in HCII units. However, qRT-PCR data of the vestibular ganglia demonstrated that Homer1 expression was upregulated during the sub-chronic IDPN exposure. These results demonstrate that the number of Homer1 puncta remain unaltered during the ototoxic insult as seen in the immunofluorescent study for the cristae, and the upregulation of Homer1 expression in the vestibular ganglia does not result in an increase in the number of Homer1 puncta. The upregulation of Homer1 expression may be a compensatory mechanism sustaining Homer1 protein levels during the exposure or they were altered in different areas of the ganglion that were not studied.

These results continue to uphold the hypothesis that IDPN ototoxicity affects the HC-afferent units differently. However, we have observed differences in ribeye puncta counts between the HC-afferent units between the three immunofluorescent studies. This may be due to a change in image analysis techniques or dependent on which crista (horizontal vs. superior vs. posterior) was being examined. The active synapse immunostudy was analyzed using ImageJ by compiling various images of each stack in order to quantify puncta, whereas the PSD95 and Homer1 immunostudies were analyzed using Imaris, a program that projects the entire confocal image stack as a 3D image. By using ImageJ, the possibility of counting a duplicated puncta or missing a puncta entirely is more possible, while Imaris distorts the Z axis in the 3D projection, which makes quantification of individual puncta more difficult. Additionally, identifying cell types (calyx-only, calyces of dimorphic afferents, or HCII) may introduce some discrepancies as well. The ability to define these cell types and their boundaries depend on the robustness of the calretinin-labeling, or lack of it, in order to correctly assign puncta to the cell being analyzed. Lack of robustness or difficulty in defining cell boundaries and/or the quantification of puncta with the different analyzing techniques may have influenced puncta number counts differently for the different HC-afferent unit types. However, a more probable reason as to why ribeye puncta counts were different between immunostudies may come from the comparison of different cristae. The same mice were compared in all three immunostudies, but this results in different cristae being used for each study; cristae were not identified as being horizontal, superior, or posterior prior to the immunostudies either. It should be noted that cristae were randomly selected and remained unidentified for the immunofluorescent puncta studies for the rat data as well (Sedó-Cabezón et al., 2015). It is not known whether all three cristae are affected by the sub-chronic ototoxic insult at the same time and sustain the same amount of damage, or if intoxication and/or damage vary between the three cristae. The cristae are more susceptible to damage compared to the utricle and saccule, but whether one crista is more susceptible to damage compared to the other two is unknown. If a difference exists, we may be observing it in the puncta counts within the mouse data and in comparison to the rat data. If each tissue is affected differently, individual alterations may not be noted.

Additionally, other proteins of interest were analyzed in the qRT-PCR study for the vestibular ganglion, which were GKAP1 (DLGAP1) and Rest (REST). GKAP1 is a known scaffolding protein of the PSD that interacts with PSD95 and Homer1 (Hayashi et al., 2009), while Rest is a silencing transcription factor that has been linked to GluA2 subunit gene downregulation during ischemia (Noh et al., 2012). Neither of these proteins demonstrated significant alterations in mRNA expression. This demonstrates that not all scaffolding proteins are being affected by the ototoxic insult, at least on an expression level, following the alterations that occur to the PSD during afferent fragmentation and retraction and junction dismantlement. Additionally, a known silencing transcription factor for the GluA2 subunit was excluded in being a factor relating to GluA2 expression change and protein loss.

7.2.6 Possible mechanisms affected within vestibular sensory epithelia and ganglia by sub-chronic IDPN exposure

The RNAseq study of the vestibular ganglion led to numerous genes and molecular mechanisms being affected by the sub-chronic IDPN exposure. 54% of differentially expressed genes were downregulated, with the most highly significant genes being downregulated. In the KEGG pathway analysis, the “synaptic vesicle cycle” pathway emerged as one of the highly significant mechanisms being implicated during progressive ototoxicity. Twelve of the thirteen differentially expressed genes were downregulated and the thirteenth gene was upregulated. All the downregulated genes aided in neurotransmitter release (SYT1, STXBP1, SLC17a6, UNC13A; Swanson et al., 1998; Fernández-Chacón et al., 2001; Shigeri et al., 2004; Böhme et al., 2016), calcium sensing (SYT1; Fernández-Chacón et al., 2001), vesicle structure (ATP6V1B2, CLTC, ATP6V1A, AP2B1, SLC17a6, AP2A1, ATP6V0A1; Gallusser and Kirchhausen, 1993; Ruscetti et al., 1994; Finbow and Harrison, 1997; Smith et al., 2003; Shigeri et al., 2004; Yuan et al., 2014), and/or vesicle linkage for the exocytic process (STXBP1, STX1B, VAMP2, UNC13A; Betz et al., 1997; Swanson et al., 1998; Schoch et al., 2001; Böhme et al., 2016), while the upregulated gene (UNC13B) contributed towards vesicle linkage to the plasma membrane for the exocytic process (Böhme et al., 2016). This gene in particular promoted a distant linkage of the vesicle to the plasma membrane, while its isomer (UNC13A), which was downregulated, promoted a closer linkage (Böhme et al., 2016); the differentially expressed genes of this pathway all point towards a hindrance towards the synaptic vesicle cycle.

Likewise, the “endocytosis” pathway also emerged as a highly significant mechanism being affected by the ototoxic insult. There was a mixture of differentially expressed genes being downregulated or upregulated for this pathway. The downregulated genes (KIF5A, ASAP2, CLTC, LDLRAP1, EPS15, AP2B1, TFRC, AP2A1, DNAJC6, PDCD6IP, SH3GL2, F2R) aided in the process of neurotransmitter, molecular, or vesicular transport and/or the formation of vesicles (Gallusser and Kirchhausen, 1993; Ruscetti et al., 1994; Giachino et al., 1997; Chen et al., 1998; Vito et al., 1999; Scheele et al., 2001; He et al., 2002; Aisen, 2004; Hirokawa et al., 2010; Seuter et al., 2014; Tsai et al., 2019), while upregulated genes aided in vesicle trafficking at the plasma membrane (RAB11FIP2, RAB5A, EHD2; Hales et al., 2002; Guilherme et al., 2004; Edler et al., 2017; Segawa et al., 2019), activating various signaling cascades (FGFR2, H2-K1, H2-D1, GRK2, AGAP3; Janeway et al., 2001; Raveh et al., 2010; Oku and Haganir, 2013; Tiong et al., 2013; Mayor et al., 2018), vesicle formation (PRKCI, RAB5A; Tisdale, 2002; Segawa et al., 2019), cell locomotion (ARPC1B, RAB5A; Gournier et al., 2001; Segawa et al., 2019), and/or returning molecules and/or neurotransmitters present in the cytosol to the endoplasmic reticulum (ER) or Golgi apparatus (PRKCI, ARF3, EHD2; Kanoh et al., 1997; Tisdale, 2002; Park et al., 2004). This strengthened the hypothesis that sub-chronic IDPN exposure causes a depression in the vestibular ganglion neurons due to the suspension of synaptic vesicle release of neurotransmitters and vesicle formation; this leads to less signal transmission between the ganglion neurons and their post-synaptic partners in the CNS.

The second RNAseq study of the vestibular epithelium also demonstrated that the majority of the differentially expressed genes identified, along with the most highly significant, were downregulated due to the sub-chronic IDPN exposure. The “cell-cell adhesion via plasma-membrane adhesion molecules” pathway had emerged as highly significant with 46 differentially expressed genes being downregulated, and the remaining 6 genes being upregulated. The majority of the downregulated genes were cadherin or protocadherin proteins, which are calcium-dependent cell-cell adhesion glycoproteins or proteins, integrated into neuronal synapse connections (Obata et al., 1995; Fernández-Monreal et al., 2009; Schalm et al., 2010). The significance of this pathway leads to the hypothesis that the sensory hair cells are losing cell-cell adhesion with its corresponding afferent, as observed in the TEM images and immunofluorescent study of calyceal junctions (tenascin-c). This loss of adhesion would contribute to junction breakdown, afferent retraction from the hair cell, and eventual hair cell extrusion. Therefore, the sequence of events occurring in sub-chronic ototoxicity, described in the schema of fig. 42, would be directed, at least in part, by changes in gene expression in the vestibular epithelium cells.

A follow-up qRT-PCR study was completed to validate the downregulation of key synaptic, receptor, transport, and signaling proteins in vestibular sensory epithelia and ganglia after IDPN exposure as seen in the RNAseq studies. A downregulation of all genes studied (SLC17a6, SLC2a4, Camk1G, NGFR, KCNQ5, Chrna6, Nptx2) in the vestibular ganglia were observed, which may attribute towards the depression of the vestibular afferents and decreased signal transduction. Some of these genes, namely SLC17a6, Camk1G, and Nptx2, have been identified to be sensitive to changes in neuronal activity (Chin and Means, 2000; Moechars et al., 2006; Pelkey et al., 2015; Farhy-Tselnick et al., 2017; Lee et al., 2017), supporting the conclusion that the vestibular ganglion neurons are firing a decreased frequency of action potentials. In the vestibular epithelia, the single gene tested, BDNF, was also observed to be downregulated as seen in the RNAseq study. BDNF is an important neurotrophic signaling factor in the brain and vestibular system (Ruan et al., 1999; Binder and Scharfman, 2004; Caldeira et al., 2007), and its depression may trigger, at least in part, the observed changes in gene expression in the vestibular ganglion during ototoxicity.

We also compared the previous qRT-PCR data with the RNAseq studies; in the vestibular ganglia, no alterations in expression were found for PSD95, caspr1, or tenascin-c and Homer1 was upregulated due to the sub-chronic exposure. The results of the RNAseq studies matched what had been analyzed in the previous qRT-PCR studies. However, GluA2 expression was downregulated in the RNAseq study of the vestibular ganglia due to the sub-chronic exposure, which had not been noted in the previous qRT-PCR study (but this was observed in rats). In the vestibular epithelia, RNAseq results demonstrated that both tenascin-c and ribeye expression remained unaltered, which does not match previous qRT-PCR data. One reason for these differences may be that the RNAseq technique is more precise in determining expression changes compared to qRT-PCR techniques. We noticed a smaller variability among replicates in the RNAseq data compared to the qRT-PCR data. The other reason may be that the RNAseq studies used mice with high VDRs, while the mice used for the previous qRT-PCR studies were a mixture of low to high VDR mice. We had noted previously with the rat data that perhaps the tissue is very sensitive to the different stages of damage, so if a more affected system is compared with a less damaged system, there may be differences in the mRNA expression and protein levels.

After completion of these two, initial RNAseq mouse studies and confirmatory qRT-PCR studies, two working hypotheses were created. In the vestibular epithelia, hair cells are depressing signal transmission and losing adhesion with their corresponding afferents during sub-chronic IDPN exposure. The calyceal junctions dismantle and become lost, and the afferents fragment and retract. Simultaneously, the vestibular ganglion neurons are receiving reduced synaptic and neurotrophic input from the HCs. This results in depressed activity of these neurons due to the ototoxic insult. In consequence, the synaptic vesicle cycle is downregulated in the neurons, along with various other mechanisms; the facilitation of the

signal becomes substantially hindered, and less signal transduction is occurring. This leads to fewer signals being sent to the CNS and the processing centers of vestibular information, and so a deficiency is created in the mice. However, afferent fragmentation and retraction and calyceal junction dismantlement are reversible, so the “point of no return” for hair cell extrusion and loss are not achieved yet; initial alterations do not lead to permanent loss, and can still be recovered if the exposure time is discontinued. Further studies need to be completed to understand whether these mechanisms continue to contribute towards stereociliary coalescence and/or hair cell extrusion and loss.

7.3 The Auditory Model

7.3.1 *Sub-chronic IDPN effects on a second sub-strain of mouse*

Once the sub-chronic IDPN exposure mouse model was established in our laboratory, we extended our research of sub-chronic ototoxicity of the vestibular system to the auditory system. In these experiments, a different sub-strain of mice, 129S2/SvPasCrl, was utilized because of the availability of this strain in the laboratory (in Groningen) where the hearing studies were carried out. The toxicity of IDPN is strain-dependent (Boadas-Vaello et al., 2017), so there was a risk that the sub-chronic IDPN model established in the 129S1 sub-strain during the previous part of the Thesis would not be replicated in the 129S2 sub-strain. Nevertheless, these sub-strains have a close lineage (Simpson et al., 1997) and we hoped the 129S2 mice would respond similarly to IDPN toxicity. We planned for an identical IDPN administration (30 mM IDPN in the drinking water of male 129S2 mice) with an exposure duration of 8 weeks. Up until 6 weeks of the exposure, we observed the characteristic alterations of body weight. Control mice continuously gained weight, while treated mice initially decreased in weight, but never reached a 20% loss that would have required euthanasia. We also observed an increase in vestibular dysfunction as the exposure progressed, a trend also noted for the 129S1 mice. However, vestibular dysfunction was found to be more robust in the 129S2 sub-strain compared to the 129S1 sub-strain. After 4 weeks of IDPN exposure, 129S2 mice had an average VDR of 5.3 ± 0.4 , while 129S1 mice had an average VDR of 3.5 ± 0.3 . After 6 weeks of exposure, 129S2 mice had an average VDR of 13.5 ± 1.2 , whereas 129S1 mice had an average VDR of 6 ± 0.5 . The average VDR of the 129S2 mice had doubled in value compared to the 129S1 mice at the 6 week time point. This lends to the conclusion that 129S2 mice were more robustly affected by the IDPN intoxication with a more accelerated response compared to the 129S1 mice. Nonetheless, it is important to distinguish that the average VDR of 129S2 mice at week 4 and the average VDR of 129S1 mice at week 5 (4.2 ± 0.3) both fall within the “low VDR” category (3 to 6) utilized in the previous 129S1 data. With this in mind, data obtained for 129S2 mice at the 4 week time point are comparable to the low VDR data obtained for 129S1 mice; and data obtained for the 129S2 mice at the 6 week time point correspond more closely with a much higher VDR when compared to the 129S1 mice at their 8 week time point. Ultimately, the IDPN exposure model functions as a robust model for the 129S2 sub-strain and is comparable to the previous mouse data of this Thesis and the previous rat model (Sedó-Cabezón et al., 2015).

7.3.2 *Sub-chronic IDPN effects on mouse hearing*

ABRs of the mice were measured at weeks 0 and 4 in order to gauge whether the 129S2 mice were experiencing hearing loss during the initially planned 8 week IDPN exposure. ABRs were consistent at week 0 for all mice, although it should be noted that healthy mice were determined to be deaf at 32 kHz, a characteristic defining this particular sub-strain of mice and where hearing impairment is found for numerous 129 mouse strains (Zheng et al., 1999). After 4 weeks of exposure, we observed that the treated mice had become completely deaf at 24 kHz, and a large deficit was observed at 16 and 8 kHz compared to control mice. At this time, we determined that an 8 week exposure in order to achieve total hearing loss for studying auditory ototoxicity was unnecessary; the rate of loss observed after only 4 weeks of

exposure warranted concluding the exposure after 6 weeks instead of 8 weeks. At 6 weeks, the remaining treated mice recorded ABRs demonstrating complete deafness at 32, 24, 16, and 8 kHz, while controls at the week 0, 2, 4, and 6 time points remained unchanged (with continued deafness at 32 kHz for control mice). The ABRs of this sub-chronic exposure demonstrated that the cochlea is indeed affected by the IDPN intoxication, hearing loss can be tracked throughout the exposure, and profound hearing loss, like vestibular dysfunction, are robust in this sub-strain and model.

Next, a second exposure was completed in order to examine the recoverability of hearing for intoxicated mice. Mice were exposed for 2 weeks and then given a washout period of either 2 or 4 weeks. Intoxication for 2 weeks indicated that mice were deaf at 24 kHz with smaller hearing deficits at 16 and 8 kHz. Selected treated mice underwent washout periods and their ABRs determined that those selected for a 2 week recovery exhibited a small amount for recovery, with partial recoveries for the click stimuli and at 8 kHz. Those mice that underwent a 4 week recovery demonstrated greater recovery with a complete recovery for the click stimuli and at 8 and 16 kHz. A partial recovery was recorded at 24 kHz. These results indicate that longer IDPN exposure causes deeper and more profound hearing loss, although only 2 weeks of exposure was sufficient to cause hearing loss. Hearing loss after a washout period following 2 weeks of IDPN exposure was partially reversible, with hearing loss recovering somewhat after a washout period of two weeks and even more after a washout period of 4 weeks. Hearing recovery is noted to take longer after ototoxic insult than from noise-induced injury (Ciuman, 2010). Any capacity for further or full recovery after 4 or 6 weeks of IDPN exposure has yet to be examined.

The amplitudes and latencies of the Wave I peak for the sub-chronic exposure and the recovery model were analyzed for the click stimuli and at 8 and 16 kHz. No alterations were observed for the click stimuli. For the sub-chronic exposure, Wave I peak amplitude size decreased for mice treated with IDPN for 2 weeks at 8 and 16 kHz, with no changes in latency; Wave I peak amplitude size for mice treated with IDPN for 4 weeks demonstrated a continued reduction in size at 8 kHz with no latency changes, but at 16 kHz, the peak amplitude recovered to a control-like size and a longer latency was recorded for it. The longer latency recorded for the Wave I peak at 16 kHz for mice treated with IDPN for 4 weeks may have recovered the peak amplitude to a control-like size.

For the recovery model, we did not observe any changes in Wave I peak amplitude size at 8 kHz, and decreases of mean latency values in the treated mice did not reach statistically significant differences with control and recovery mean values. At 16 kHz, we observed a decrease in Wave I peak amplitude size after 2 weeks of IDPN exposure that did not recover, despite a washout period of 4 weeks. The latency data did not demonstrate any alterations; therefore, latency alterations only occur after a prolonged exposure to IDPN and the recovery of peak amplitude size with a longer latency time is not a compensatory mechanism utilized by the system.

These results indicate that initial (2 week) sub-chronic IDPN exposure causes amplitude sizes of the Wave I peak evoked at 8 and 16 kHz to decrease. Continued exposure (4 week IDPN) results in a continued decreased state of peak amplitude size in the lower frequency and a prolongation of the latency in the higher frequency. By lengthening the latency of the Wave I peak, as observed in the 16 kHz data, amplitude size was recovered, but this is not a compensatory mechanism utilized by the system. The recovery model demonstrated that no alterations in latency were observed for washout animals with affected amplitude sizes. The lengthening of the latency for the Wave I peak is dependent on the duration of the sub-chronic IDPN exposure; this coincidentally leads to the result that the longer latency may have recovered the Wave I peak amplitude size. The hypothesis that latency may recover amplitude size during ototoxic insult has not been observed before; previous studies for tinnitus or hearing loss due to moderate noise exposure or aging have demonstrated simultaneous reductions for various Wave peak amplitudes and the lengthening of latencies for mice (Mehraei et al., 2016), nonhuman primates (Ng et al.,

2015), and humans (Konrad-Martin et al., 2012; Konadath and Manjula, 2016; Mehraei et al., 2016). The implications for changes in Wave peak amplitude and latency are not well studied; in general, amplitude size is linked to the synchrony of the neurons firing together and if this synchrony increases, the latency of these peaks also decrease, increasing signal transmission and narrowing the wave, which increases the amplitude (Pratt, 2011). In this sense, amplitude and latency are linked. The prolongation of the latency may be a result of delayed synchronous firing. The IDPN intoxication may be delaying signal firing due to suppressed signal transmission and/or a loss of afferent contacts with the IHCs; however, the resulting signal that is transmitted is with control-like robustness, as seen in the recovered amplitude size. The extended latency allowed for the depressed signal or the reduced contacts to finally build up enough of an electrochemical gradient to cause a receptor potential that transmitted a signal with control-like strength. After the exposure, the latency returns to a control-like velocity, but the decrease in amplitude is a scar in the system that persists, perhaps due to afferent contact loss, which is similar to “hidden hearing loss” observed during noise-induced hearing loss (Liberman, 2017) despite hearing recovery. The observed absolute threshold shifts recorded during the exposure may be influenced by the decrease in amplitude size and the increased latency; it may be due to a delayed or weakened signal coming from the hair cell transmitting to the spiral ganglion afferent or a reduction in afferent contacts to the IHCs thus reducing the signal.

7.3.3 Sub-chronic IDPN effects on inner and outer hair cell morphology

The number of IHCs remained unchanging throughout the exposure, regardless of IDPN exposure. In all cochlear sections, all IHC nuclei were observed in their regular placement (base of the cell), in a single row, which characterizes control cochlea. On the contrary, mice exposed to IDPN demonstrated a loss of OHCs that varied as a function of the time of exposure and the frequency zone. Ten IHCs and their corresponding thirty OHCs were chosen to be analyzed for each frequency and for each treatment group. Control mice and mice treated with IDPN for 2 weeks demonstrated no OHC loss. Mice treated with IDPN for 4 weeks demonstrated a loss of OHCs at 24 and 32 kHz, but not at 8 or 16 kHz. Mice treated with IDPN for 6 weeks demonstrated a small loss of OHCs at 8 kHz, more than half of the OHCs were lost at 16 kHz, more than three-quarters of the OHCs were lost at 24 kHz, and there was a complete loss of OHCs at 32 kHz. This result demonstrates that this IDPN exposure, at least up until 6 weeks of intoxication, does not result in any IHC loss. However, OHC loss occurs. This OHC effect is tonotopic and time-dependent. The highest frequencies demonstrated a loss first, and the longer the IDPN exposure, the more OHCs were lost. A similar result has been recorded in rats using SEM observations; sub-chronic administration of IDPN resulted in OHC loss in a basal to apical pattern in the organ of Corti (Seoane and Llorens, 2005), demonstrating the tonotopic effect observed in these data and for the “classic” pattern of ototoxicity in the cochlea (Forge and Schacht, 2000; Heydt et al., 2004; Op de Beeck et al., 2011). No loss of IHC was observed either.

The observed tonotopy in OHC loss is in agreement with the recorded loss of auditory function. These data demonstrate that sub-chronic IDPN ototoxicity progresses from higher to lower frequencies as known to occur with other ototoxic compounds, such as cisplatin and the aminoglycoside antibiotics (Forge and Schacht, 2000; Heydt et al., 2004; Op de Beeck et al., 2011). This loss of OHCs contributes towards the reduction of absolute thresholds for the different frequencies since OHCs contribute in amplifying sound vibrations within the cochlea to strengthen the signal. The observed time-dependency indicates that the cochlear toxicity of sub-chronic IDPN will provide a good model to study the cellular and molecular events involved in progressive auditory toxicity.

7.3.4 Sub-chronic IDPN does not directly affect caspr1

Simultaneous immunofluorescent studies on caspr1 in the vestibular utricular hair cells and the cochlear inner hair cells were completed in order to determine whether caspr1 was affected by sub-chronic IDPN exposure in both the vestibular and auditory systems. The caspr1 immunostudy of the utricle demonstrated that the total number of vestibular hair cells remained equal to control numbers after 6 weeks of IDPN intoxication; however, what is observable is the loss of caspr1 in the epithelium. This indicates a loss of calyceal junctions, which was observed in the previous rat data (Sedó-Cabezón et al., 2015) and confirmed by the previous TEM and immunofluorescent studies for the cristae of this Thesis, and now have been observed in the utricle.

In the cochlea, caspr1 is located in the first heminode of type I afferents, which make contact with the IHCs, and has a cylindrical appearance. Caspr1 lengths were measured at each frequency and resulted in no changes throughout the IDPN exposure. Despite the fact that no alterations were occurring to caspr1 in the cochlea, we are given a very important insight from this result: caspr1 is not directly affected by the sub-chronic IDPN ototoxicity. Caspr1 is a key protein implicated in upholding the structure of paranodal sections of the neuronal axon (Rios et al., 2000; Zou et al., 2017) and the calyceal junctions between vestibular HCIs and their calyx afferents (Sousa et al., 2009); these structures are crucial for saltatory conduction of action potentials and neurotransmission, respectively. The fact that it is affected in the vestibule but not the cochlea implies that a mechanism that controls the calyceal structure and/or its maintenance is what is being targeted by the sub-chronic ototoxicity. The mechanisms response to this toxicity is what causes caspr1 to disappear during calyceal junction dismantlement and breakdown.

Besides its ototoxic effects, IDPN is well known to cause proximal neurofilamentous axonopathy, associated to impairment in the axonal transport of cytoskeletal proteins (Griffin et al., 1978). Therefore, it is possible that the loss of caspr1 in the calyceal junction area was not secondary to the ototoxic effect of IDPN, but secondary to an impairment of its transport from the cell body of the ganglion neuron to the afferent terminal, as suggested previously (Seoane et al., 2003). However, more recent unreported data from our laboratory implies that paranodal caspr1 remains unaffected in the vestibular afferents during IDPN intoxication, suggesting that the loss of caspr1 in the calyceal junction is associated with ototoxicity, not to the axonal transport effect. Labeling paranodal caspr1 in the vestibular afferents can be inconsistent and unclear, so this observed result is difficult to replicate. However, the auditory afferents have provided a more convenient placement of paranodal caspr1 for quantification, providing more conclusive evidence in support of the ototoxic hypothesis. Ongoing studies in our laboratory (unpublished results by Alberto Maroto) have further demonstrated that caspr1 loss and vestibular calyceal junction dismantlement appear in other models of chronic ototoxicity by using compounds that do not cause alterations in neurofilament transport as well.

7.3.5 Sub-chronic IDPN effects on the active synapses of cochlear inner hair cells

Simultaneous immunofluorescent studies of the synapses in the vestibular utricular hair cells and the cochlear inner hair cells were completed in order to determine whether active synapses were being affected by sub-chronic IDPN exposure in both the vestibular and auditory systems. In the utricle, we observed a decrease in ribeye puncta, GluA2 puncta, and their colocalizations after 6 weeks of IDPN exposure. These results indicate that the overall number of active synapses is decreasing in the utricles of IDPN exposed mice and this is comparable to the active synapse loss seen in the cristae, recorded in previous studies for this Thesis and in the rat data (Sedó-Cabezón et al., 2015).

In the IHCs of the cochlea, we observed no loss of ribeye puncta, GluA2 puncta, or their colocalizations at 8 kHz. At 16 kHz, we observed a loss of active synapses for mice treated with IDPN for 6 weeks. At

24 kHz, we observed a loss of active synapses for mice treated with IDPN for 4 weeks, and a greater loss of active synapses for mice treated with IDPN for 6 weeks. At 32 kHz, we observed a large loss of active synapses equal for mice treated with IDPN for 4 and 6 weeks. There was no active synapse loss recorded at any frequency studied for mice treated with IDPN for 2 weeks. These results indicate a loss of active synapses in a tonotopic pattern, similar to OHC loss. The higher frequencies lost their active synapses more readily compared to lower frequencies, and a longer IDPN exposure resulted in more frequencies being affected. This indicates that sub-chronic ototoxicity affects the active synapses of higher frequencies in the organs of Corti first, and depending on the exposure time, may affect lower frequencies. These losses of active synapses contribute towards the signal transmission reduction and the reduction of absolute thresholds observed in the ABR measurements. The impact of ototoxic phenomena on cochlear afferents has received little attention compared to the studies on HC damage and loss. Nevertheless, some reports exist on the loss of IHC synapses following aminoglycoside exposure by injecting mice with daily doses of gentamicin, which resulted in recorded hearing loss with ribbon synapse loss (Liu et al., 2015; Li et al., 2016) or afferent dendritic and efferent axonal loss (Ruan et al., 2014).

The loss of OHCs is noted in all four examined frequencies of the cochlea, including the lowest one tested, 8 kHz, while active synapse loss is not observed until 16 kHz. Additionally, mice treated with IDPN for 6 weeks demonstrated a complete loss of OHCs at 32 kHz, while a third of the active synapses of the IHCs remained at this frequency. The data are demonstrating that apart from the highest frequencies being affected first and a longer IDPN exposure resulting in the lower frequencies being affected, the OHCs are being affected by the sub-chronic IDPN exposure before there are changes in the active synapses of IHCs. This follows similar observations of OHCs being more sensitive to aminoglycoside ototoxicity (Govaerts et al., 1990; Hashino et al., 1997; Forge and Schacht, 2000). However, undetermined mechanisms and/or proteins are also being affected since the absolute threshold data are demonstrating hearing loss, including complete hearing loss at 24 kHz, of mice treated with IDPN for 2 weeks, despite no OHC loss and no active synapse loss in the IHCs. This may include a loss of HC function not reflected in morphological changes, or the loss or malfunction of the efferent contacts, which can cause problems with the fine regulation of hearing perception and the signal to noise ratio (Ciuman, 2010). With this in mind, more studies need to be completed in order to determine what mechanisms are being affected in the cochlea causing hearing loss besides OHC and active synapse loss.

7.4 Sub-chronic IDPN Effect Similarities and Differences between the Vestibular and Auditory Systems

The vestibular and auditory systems share similarities and differences pertaining to the results of the sub-chronic IDPN ototoxic exposure. In general, the progression of sub-chronic ototoxicity in the auditory system appears to occur more rapidly than in the vestibular system. After only 4 weeks of IDPN exposure, mice were recorded to be deaf at 24 kHz, with large losses in OHC and active synapse numbers, and enormous hearing deficits at 16 and 8 kHz. For the vestibular epithelia, 4 weeks of intoxication demonstrates low VDR scores (3 to 6) for the 129S2 sub-strain, similar to the low VDR scores of the 129S1 sub-strain at 5 weeks of intoxication. Vestibular results for the 129S1 sub-strain with low VDRs indicated no vestibular HC loss as seen in the SEM data and minimal calyceal junction loss and afferent fragmentation from the TEM data. Therefore, mice with low VDRs, regardless of sub-strain, can be interpreted as having the same vestibular results with that rating. This means that the observed result of the auditory sensory epithelia being affected more rapidly than the vestibular sensory epithelia can be made despite different sub-strains being compared.

We also observed that OHCs were much more sensitive to IDPN toxicity than IHCs and vestibular hair cells, as described for the aminoglycoside antibiotics (Govaerts et al., 1990; Hashino et al., 1997; Forge and Schacht, 2000). Their loss was observed as early as 4 weeks of intoxication at higher frequencies,

whereas no IHC loss had been noted throughout the exposure, and vestibular hair cell loss was not observed until 8 weeks of intoxication. Both systems demonstrated a capacity for recovery from the ototoxic insult, although recovery in the cochlea was slower (Ciuman, 2010) and was tested for mice treated with IDPN for 2 weeks only. Whether more thorough damage accumulated after 4 or 6 weeks of IDPN exposure can be recovered has yet to be examined. Additionally, OHCs were not lost after 2 weeks of IDPN exposure, so a possible hypothesis is as long as the cochlear hair cells remain intact, the capacity for complete recovery is possible.

Another difference between the two systems is the role of *caspr1*. In the cochlea, *caspr1* plays a role in paranodal section morphology and structure, necessary for saltatory conduction of myelinated neurons (Rios et al., 2000; Zou et al., 2017). In the vestibular epithelia, it is also a key component of the calyceal junctions, the junctions created between HCIs and their calyx afferents (Sousa et al., 2009), creating an intimate environment for signal transduction. We observed the disappearance of *caspr1* after calyceal junction dismantlement and breakdown, along with its recovery with the reconstruction of the junctions after washout. However, *caspr1* remained unaffected in the first heminode of type I afferents in the cochlea. This indicates that *caspr1* is not directly targeted by the sub-chronic ototoxicity, but rather, an upstream mechanism that dictates *caspr1* localization in vestibular afferents during ototoxicity. We also know this upstream mechanism is not affected due to a failure in axonal transport caused by IDPN toxicity, as previously considered (Seoane et al., 2003), but by the sub-chronic ototoxicity which is reinforced by previously unreported data and ongoing studies within our laboratory. The fact that there were no observable alterations in *caspr1* mRNA expression in the vestibular ganglia also contributes towards this conclusion.

One important similarity is the loss of active synapses. In the vestibular epithelia, we observed the loss of active synapses in particular HC-afferent units of the cristae and an overall loss of synapses in the utricle. In the cochlea, we observed a loss of active synapses that began at the highest frequencies and extended towards the lower frequencies, depending on the duration of the exposure. This lends to the hypothesis that signal transduction is being hindered between the hair cells and afferents in both systems and that similar mechanisms are being triggered during sub-chronic intoxication. The depression of signal transmission to the CNS due to a loss of active synapses of cochlear and vestibular hair cells contribute to the overt hearing loss and vestibular dysfunction recorded in intoxicated mice.

Overall, we recorded the various stages of reversible damage accrued in the vestibular system of the mouse comparable to the reversible damage observed in rats during sub-chronic IDPN ototoxicity, along with the first recorded alterations in the auditory system during the same type of exposure. The vestibular epithelia and ganglia undergo a progression of damage beginning with afferent fragmentation and calyceal junction dismantlement and progresses towards complete calyceal junction loss and afferent detachment and retraction. Continued intoxication causes the stereociliary bundles to coalesce and the mechanisms for hair cell extrusion are initiated. Hair cells are extruded out of the epithelium and the tissue becomes permanently damaged. Meanwhile, numerous proteins are being downregulated in the epithelia and ganglia, resulting in numerous mechanisms being affected. These mechanisms include the loss of *caspr1* in the calyceal junctions, the loss of active synapses, and cell-cell adhesion of the vestibular epithelia, and a hindrance to vesicle exocytosis and endocytosis in the vestibular ganglion neurons. The progression of damage results in the interruption of signal transmission between vestibular hair cells and their afferents towards the CNS causing overt dysfunction. The majority of this initial damage, up until stereociliary coalescence, is reversible allowing for behavioral recovery, but with molecular scarring that may or may not have future impacts on the tissue.

The cochlea demonstrates a tonotopical progression of damage that is dependent on the duration of the intoxication; higher frequencies are affected first and continued exposure leads to a more profound

hearing loss that will affect the lower frequencies. The OHCs are lost first, followed by active synapse loss for the IHCs and their afferents. Perhaps for this reason, this is why we observed hearing loss at such an accelerated rate; the loss of the OHCs, which amplify sound vibrations, and the loss of active synapses in the IHCs all contribute towards a very weakened signal to the CNS. The loss of active synapses demonstrates a similar mechanism being affected in both systems during the ototoxicity. However, other factors are being implicated since hearing loss was observed for mice treated with IDPN for 2 weeks, but no loss of OHCs or active synapses were recorded. For this same reason perhaps we were able to record a recovery in the hearing of these treated mice since no OHC loss had been accrued. Whether active synapse loss can be recovered in IHCs and/or an observable recovery in hearing for mice treated with IDPN for 4 or 6 weeks is not yet known, since recovery studies have not been completed for mice exposed for these durations. Additional studies to identify new targets being affected during ototoxicity are also necessary and could be performed in the future.

The results and findings of this Thesis have characterized reversible damage obtained in the vestibular system of the mouse during sub-chronic IDPN ototoxicity. It has also begun the characterization of the damage accrued in the cochlea of the mouse during sub-chronic IDPN ototoxicity, although it has yet to be determined whether those altered factors may be reversible or not. The sub-chronic mouse model will be useful for future studies that wish to identify more mechanisms and proteins being altered during the exposure and the possibility of reversing the damage that occurs in order to decipher techniques to protect sensorial hair cells and afferents of the inner ear.

8. Conclusions

1. The administration of 30 mM 3,3'-iminodipropionitrile (IDPN) in the drinking water for 8 weeks is a functional sub-chronic ototoxic exposure model for male 129S1/SvImJ mice to cause progressive damage in the vestibular sensory epithelia and ganglia that can be recovered with an adequate washout period.
2. Ultrastructural results reveal a similar progress of vestibular damage in mice that has been recorded in rats. The calyceal junctions begin to degrade as afferent fragmentation and retraction occurs after 5 weeks of sub-chronic IDPN intoxication. The junctions disappear completely after 8 weeks of intoxication, along with stereociliary coalescence and hair cell extrusion and loss, depending on the severity of vestibular dysfunction. The afferent and junction damage is mostly recoverable with the restoration of vestibular function after the washout period.
3. Key components of the calyceal junction, caspr1 and tenascin-c, are lost during the progressive damage contributing towards the loss of the calyceal junctions. This has been observed in the cristae and utricle. Caspr1 and tenascin-c show extensive recovery with the reconstruction of the calyceal junctions after the washout period. Caspr1 loss is not driven by reduced gene expression, whereas changes in gene expression may underlie, at least in part, the observed changes in tenascin-c.
4. Active synapse loss is observed in the cristae, but the extent of the effect and its recovery during washout differed among the different hair-cell afferent units. Ribeye mRNA expression in the vestibular epithelia demonstrates a downregulation of the gene that remains after washout, perhaps contributing to only a partial recovery observed in some units. GluA2 puncta reduction attained significance in HCII units only, but GluA2 expression in the vestibular ganglia is upregulated after the washout period, perhaps as a compensatory or restoration mechanism. Active synapse loss is also observed in the utricle.
5. An increase in PSD95 is noted in HCII units only, the only HC-afferent unit to experience GluA2 loss. The expression of PSD95 is upregulated in washout mice, suggesting a compensatory mechanism in order to stabilize the alterations occurring in the PSD and/or contribute towards GluA2 loss and recovery. Homer1 protein levels were not affected by the sub-chronic exposure, although expression levels were upregulated in the vestibular ganglia. Whether this upregulation is a compensatory mechanism or alters the number of Homer1 proteins has yet to be seen.
6. Mechanisms revealed in the RNAseq studies indicate an overall depression of neuronal activity in the vestibular ganglia and a loss of cell-cell adhesion for the vestibular epithelia. The observed changes are in agreement with the vestibular dysfunction noted in mouse behavior and the afferent fragmentation and retraction and calyceal junction dismantlement.
7. The administration of 30 mM 3,3'-iminodipropionitrile (IDPN) in the drinking water for 6 weeks is a functional sub-chronic ototoxic exposure model for male 129S2/SvPasCrl mice to cause progressive hearing loss and damage in the cochlear sensory epithelia.
8. The sub-chronic IDPN exposure causes profound hearing loss that occurs in a tonotopic manner starting at the higher frequencies and affects the lower frequencies depending on the duration of the intoxication.
9. OHC loss is observed in a tonotopic pattern, and occurs before active synapse loss within the IHCs. No IHC loss is recorded in this model. The capacity for hearing loss recovery has been partially explored at the functional level only. Mechanisms that contribute towards hearing loss and recovery express a need for future studies on the subject.
10. There are some differences and similarities between the two sensory systems during sub-chronic IDPN exposure that call for further study. Overall, the loss of active synapses from both systems contributes towards inner ear ototoxicity implying that similar mechanisms are being affected, and causes a form of signal depression that result in overt vestibular and hearing alterations in mice.

9. Bibliography

A

Ahmed RM, Hannigan IP, MacDougall HG, Chan RC, Halmagyi GM. (2012) Gentamicin ototoxicity: a 23-year selected case series of 103 patients. *Med J Aust.* 196(11):701-704.

Aisen P. (2004) Transferrin receptor 1. *Int J Biochem Cell Biol.* 36(11):2137-2143.

Andrianov GN, Puyal J, Raymond J, Venteo S, Demêmes D, Ryzhova IV. (2005) Immunocytochemical and pharmacological characterization of metabotropic glutamate receptors of the vestibular end organs in the frog. *Hear Res.* 204(1-2):200-209.

Aran JM, Erre JP, Da Costa DL, Debbarh I, Dulon D. (1999) Acute and chronic effects of aminoglycosides on cochlear hair cells. *Ann N Y Acad Sci.* 884:60–68.

Ashmore J. (2008) Cochlear outer hair cell motility. *Physiological Reviews.* 88(1):173-210.

B

Balbuena E; Llorens J. (2001) Behavioral disturbances and sensory pathology following allylnitrile exposure in rats. *Brain Res.* 904:298-306.

Balbuena E; Llorens J. (2003) Comparison of cis- and trans-crotononitrile effects in the rat reveals specificity in the neurotoxic properties of nitrile isomers. *Toxicol Appl Pharmacol.* 187(2):89-100.

Bartsch U. (1996) The extracellular matrix molecule tenascin-c: expression in vivo and functional characterization in vitro. *Prog Neurobiol.* 49(2):145-168.

Béique JC, Andrade R. (2003) PSD-95 regulates synaptic transmission and plasticity in rat cerebral cortex. *J Physiol.* 546(Pt 3):859-867.

Béique JC, Lin DT, Kang MG, Aizawa H, Takamiya K, Huganir RL. (2006) Synapse-specific regulation of AMPA receptor function by PSD-95. *Proc Natl Acad Sci USA.* 103(51):19535-19540.

Beutner D, Voets T, Neher E, Moser T. (2001) Calcium dependence of exocytosis and endocytosis at the cochlear inner hair cell afferent synapse. *Neuron.* 29(3):681-690.

Betz A, Okamoto M, Benseler F, Brose N. (1997) Direct interaction of the rat unc-13 homologue Munc13-1 with the N terminus of syntaxin. *J Biol Chem.* 272(4):2520-2526.

Binder DK, Scharfman HE. (2004) Brain-derived neurotrophic factor. *Growth Factors.* 22(3):123-131.

Bitner-Glindzicz M, Rahman S. (2007) Ototoxicity caused by aminoglycosides. *BMJ.* 335(7624):784-785.

Blackwell DL, Lucas JW, Clarke TC. (2014) Summary health statistics for U.S. adults: National Health Interview Survey, 2012. *National Center for Health Statistics. Vital Health Stat.* 10(260).

Boadas-Vaello P, Jover E, Díez-Padrisa N, Bayona JM, Llorens J. (2007) Differential role of CYP2E1-mediated metabolism in the lethal and vestibulotoxic effects of cis-crotononitrile in the mouse. *Toxicol Appl Pharmacol.* 225(3):310-317.

Boadas-Vaello P, Jover E, Saldaña-Ruiz S, Soler-Martín C, Chabbert C, Bayona JM, Llorens J. (2009) Allylnitrile metabolism by CYP2E1 and other CYPs leads to distinct lethal and vestibulotoxic effects in the mouse. *Toxicol Sci.* 107(2):461-472.

- Boadas-Vaello P, Riera J, Llorens J. (2005) Postural control and the vestibulospinal system. In: Bronstein AM (ed) Oxford textbook of vertigo and imbalance. *Oxford University Press, Oxford*. pp 35-48.
- Boadas-Vaello P, Sedó-Cabezón L, Verdú E, Llorens J. (2017) Strain and sex differences in the vestibular and systemic toxicity of 3,3'-iminodipropionitrile in mice. *Toxicol Sci.* 156(1):109-122.
- Böhme MA, Beis C, Reddy-Alla S, Reynolds E, Mampell MM, Grasskamp AT, Lützkendorf J, Bergeron DD, Driller JH, Babikir H, Göttfert F, Robinson IM, O'Kane CJ, Hell SW, Wahl MC, Stelzl U, Loll B, Walter AM, Sigrist SJ. (2016) Active zone scaffolds differentially accumulate Unc13 isoforms to tune Ca(2+) channel-vesicle coupling. *Nat Neurosci.* 19(10):1311-1320.
- Bok J, Zenczak C, Hwang CH, Wu DK. (2013) Auditory ganglion source of Sonic hedgehog regulates timing of cell cycle exit and differentiation of mammalian cochlear hair cells. *Proc Natl Acad Sci USA.* 110(34):13869-13874.
- Bosher SK, Warren RL. (1968) Observations on the electrochemistry of the cochlear endolymph of the rat: a quantitative study of its electrical potential and ionic composition as determined by means of flame spectrophotometry. *Royal Society.* 171(1023):227-247.
- Braude, J P, Vijayakumar, S, Baumgarner, K, Laurine, R, Jones, TA, Jones, S M, Pyott, S. (2015) Deletion of *Shank1* has minimal effects on the molecular composition and function of glutamatergic afferent postsynapses in the mouse inner ear. *Hear Res.* 321:52-64.
- Brugeaud A, Travo C, Demêmes D, Lenoir M, Llorens J, Puel J-L, Chabbert C. (2007) Control of hair cell excitability by vestibular primary sensory neurons. *J Neurosci.* 27(13):3503–3511.
- Burkard R. (2006) Calibration of acoustic transients. *Brain Res.* 1091(1):27-31.

C

- Caldeira MV, Melo CV, Pereira DB, Carvalho R, Correia SS, Backos DS, Carvalho AL, Esteban JA, Duarte CB. (2007) Brain-derived neurotrophic factor regulates the expression and synaptic delivery of alpha-amino-3-hydroxy-5-methyl-4-isoxazole propionic acid receptor subunits in hippocampal neurons. *J Biol Chem.* 282(17):12619-12628.
- Campo P, Morata TC, Hong OS. (2013) Chemical exposure and hearing loss. *Dis Mon.* 59(4):119-138.
- Chen H, Fre S, Slepnev VI, Capua MR, Takei K, Butler MH, Di Fiore PP, De Camilli P. (1998) Epsin is an EH-domain-binding protein implicated in clathrin-mediated endocytosis. *Nature.* 394(6695):793-797.
- Chin D, Means AR. (2000) Calmodulin: a prototypical calcium sensor. *Trends Cell Biol.* 10(8):322-328.
- Chiquet-Ehrismann R. (2004) Tenascins. *Int J Biochem Cell Biol.* 36(6):986-990.
- Chittka L, Brockmann A. (2005) Perception space- The final frontier. *PLoS Biol.* 3(4):e137.
- Ciuman, RR. (2010) The efferent system or olivocochlear function bundle – fine regulator and protector of hearing perception. *Int J Biomed Sci.* 6(4):276-288.

D

- Dalet A, Bonsacquet J, Gaboyard-Niay S, Calin-Jageman I, Chidavaenzi RL, Venteo S, Desmadryl G, Goldberg JM, Lysakowski A, Chabbert C. (2012) Glutamate transporters EAAT4 and EAAT5 are expressed in vestibular hair cells and calyx endings. *PLoS ONE.* 7(9): e46261.

Dechesne C, Mbiene JP, Sans A. (1986) Postnatal development of vestibular receptor surfaces in the rat. *Acta Otolaryngologica*. **101**(1-2):11-18.

Desai SS, Zeh C, Lysakowski A. (2005a) Comparative morphology of rodent vestibular periphery. I. Saccular and Utricular Maculae. *J Neurophysiol*. **93**: 251-266.

Desai SS, Ali H, Lysakowski A. (2005b) Comparative morphology of rodent vestibular periphery. II. Cristae Ampullares. *J Neurophysiol*. **93**:267-280.

Deulofeu M, Carreres-Pons M, Greguske E, Prades S, Sedó-Cabezón L, Domenech-Vadillo E, Boadas-Vaello P, Llorens J. (2014) Vestibular dysfunction and afferent detachment and reattachment in a mouse model of chronic ototoxicity. *Acta Physiologica*. 212:92 Abstract

Dulon D, Hiel H, Aurousseau C, Erre JP, Aran JM. (1993) Pharmacokinetics of gentamicin in the sensory hair cells of the organ of Corti: rapid uptake and long term persistence. *C R Acad Sci III*. **316**(7):682–687.

E

Eckrich T, Varakina K, Johnson SL, Franz C, Singer W, Kuhn S, Knipper M, Holley MC, Marcotti W. (2012) Development and function of the voltage-gated sodium current in immature mammalian cochlear inner hair cells. *PLoS ONE*. **7**(9): e45732.

Edler E, Schulze E, Stein M. (2017) Membrane localization and dynamics of geranylgeranylated Rab5 hypervariable region. *Biochem Biophys Acta Biomembr*. **1859**(8):1335-1349.

Ehret G, Frankenreiter M. (1977) Quantitative analysis of cochlear structures in the house mouse in relation to mechanisms of acoustical information processing. *J Comp Physiol*. **122**(1):65-85.

F

Farhy-Tselnicker I, van Casteren ACM, Lee A, Chang VT, Aricescu AR, Allen NJ. (2017) Astrocyte-secreted glypican 4 regulates release of neuronal pentraxin 1 from axons to induce functional synapse formation. *Neuron*. **96**(2):428-445.

Fernández-Chacón R, Königstorfer A, Gerber SH, Garcia J, Matos MF, Stevens CF, Brose N, Rizo J, Rosenmund C, Südhof TC. (2001) Synaptotagmin I functions as a calcium regulator of release probability. *Nature*. **410**(6824):41-49.

Fernández-Monreal M, Kang S, Phillips GR. (2009) Gamma-protocadherin hemophilic interaction and intracellular trafficking is controlled by the cytoplasmic domain in neurons. *Mol Cell Neurosci*. **40**(3):344-353.

Finbow ME, Harrison MA. (1997) The vacuolar H⁺-ATPase: a universal proton pump of eukaryotes. *Biochem J*. **324**(Pt 3):697-712.

Forge A, Schacht J. (2000) Aminoglycoside antibiotics. *Audiol Neurootol*. **5**(1):3–22.

Fritsch B, Straka H. (2014) Evolution of vertebrate mechanosensory hair cells and inner ears: toward identifying stimuli that select mutation driven altered morphologies. *J Comp Physiol A Neuroethol Sens Neural Behav Physiol*. **200**(1):5-18.

Fritsch B, Jahan I, Pan N, Kersigo J, Duncan J, Kopeccky B. (2011) Dissecting the molecular basis of organ of Corti development: where are we now? *Hear Res*. **276**(1-2):16-26.

G

Gaboyard-Niay S, Travo C, Saleur A, Broussy A, Brugeaud A, Chabbert C. (2016) Correlation between afferent rearrangements and behavioral deficits after local excitotoxic insult in the mammalian vestibule: a rat model of vertigo symptoms. *Dis Model Mech.* 9(10):1181-1192.

Gagnaire F, Marignac B, Ban M, Langlais C. (2001) The ototoxic effects induced in rats by treatment for 12 weeks with 2-butenenitrile, 3-butenenitrile and cis-2-pentenenitrile. *Pharmacol Toxicol.* 88(3):126-134.

Gallusser A, Kirchhausen T. (1993) The beta 1 and beta 2 subunits of the AP complexes are the clathrin coat assembly components. *EMBO J.* 12(13):5237-5244.

Giachino C, Lantelme E, Lanzetti L, Saccone S, Bella Valle G, Migone N. (1997) A novel SH3-containing human gene family preferentially expressed in the central nervous system. *Genomics.* 41(3):427-434.

Goodyear RJ, Gale JE, Ranatunga KM, Kros CJ, Richardson GP. (2008) Aminoglycoside-induced phosphatidylserine externalization in sensory hair cells is regionally restricted, rapid, and reversible. *J Neurosci.* 28(40):9939-9952.

Götz B, Scholze A, Clement A, Joester A, Schütte K, Wigger F, Frank R, Spiess E, Ekblom P, Faissner A. (1996) Tenascin-c contains distinct adhesive, anti-adhesive, and neurite outgrowth promoting sites for neurons. *J Cell Biol.* 132(4):681.

Gournier H, Goley ED, Niederstrasser H, Trinh T, Welch MD. (2001) Reconstitution of human Arp2/3 complex reveals critical roles of individual subunits in complex structure and activity. *Mol Cell.* 8(5):1041-1052.

Govaerts PJ, Claes J, Van De Heyning PH, Jorens PG, Marquet J, De Broe ME. (1990) Aminoglycoside-induced ototoxicity. *Toxicol Lett.* 52:227-251.

Gray, Lincoln. (1997-present) Chapter 10: Vestibular System: structure and function. *Neuroscience Online, McGovern Medical School at UTHealth, Department of Neurobiology and Anatomy*. Retrieved from <https://nba.uth.tmc.edu/neuroscience/s2/chapter10.html>

Gray, Lincoln. (1997-present) Chapter 11: Vestibular System: Pathways and Reflexes. *Neuroscience Online, McGovern Medical School at UTHealth, Department of Neurobiology and Anatomy*. Retrieved from <https://nba.uth.tmc.edu/neuroscience/m/s2/chapter11.html>

Griffin JW, Hoffman PN, Clark AW, Carroll PT, Price DL. (1978) Slow axonal transport of neurofilament proteins: impairment of beta,beta'-iminodipropionitrile administration. *Science.* 202(4368):633-635.

Guilherme A, Soriano NA, Bose S, Holik J, Bose A, Pomerleau DP, Furcinitti P, Leszyk J, Corvera S, Czech MP. (2004) EHD2 and the novel EH domain binding protein EHBP1 couple endocytosis to the actin cytoskeleton. *J Biol Chem.* 279(11):10593-10605.

H

Hales CM, Vaerman JP, Goldenring JR. (2002) Rab 11 family interacting protein 2 associates with Myosin Vb and regulates plasma membrane recycling. *J Biol Chem.* 277(52):50415-50421.

Hashino E, Shero M, Salvi R. (1997) Lysosomal targeting and accumulation of aminoglycoside in sensory hair cells. *Brain Res.* 777:75-85.

Hayashi MK, Tang C, Verpelli C, Narayanan R, Stearns MH, Xu RM, Li H, Sala C, Hayashi Y. (2009) The postsynaptic density proteins Homer and Shank form a polymeric network structure. *Cell*. 137(1):159-171.

He G, Gupta S, Yi M, Michaely P, Hobbs HH, Cohen JC. (2002) ARH is a modular adaptor protein that interacts with the LDL receptor, clathrin, and AP-2. *J Biol Chem*. 277(46):44044-44049.

Hearing Loss Association of America, accessed 4 April 2019, <<https://www.hearingloss.org/hearing-help/hearing-loss-basics/>>

Heydt JL, Cunningham LL, Rubel EW, Coltrera MD. (2004) Round window gentamicin application: an inner ear hair cell damage protocol for the mouse. *Hear Res*. 192(1-2):65-74.

Hirokawa N, Niwa S, Tanaka Y. (2010) Molecular motors in neurons: transport mechanisms and roles in brain function, development, and disease. *Neuron*. 68(4):610-638.

Holt JC, Lysakowski A, Goldberg JM. (2010) Chapter 6: The efferent vestibular system. In: Auditory and Vestibular Efferents. *Springer Science+Business Media, New York*. pp 136-142.

Huganir RL, Nicoll RA. (2013) AMPARs and synaptic plasticity: The last 25 years. *Neuron*. 80(3):704-717.

J

Janeway CA Jr, Travers P, Walport M, Shlomchik MJ. (2001) Chapter 5. Antigen presentation to T lymphocytes: The major histocompatibility complex and its functions. In: Immunobiology: The immune system in health and disease, 5th edition. *New York: Garland Science*.
<https://www.ncbi.nlm.nih.gov/books/NBK27156/>

Joester A, Faissner A. (2001) The structure and function of tenascins in the nervous system. *Matrix Biol*. 20(1):13-22.

Jones PL, Jones FS. (2000) Tenascin-c in development and disease: gene regulation and cell function. *Matrix Biol*. 19(7):581-596.

Jurado S. (2018) AMPA receptor trafficking in natural and pathological aging. *Front Mol Neurosci*. 10: 446.

K

Kanoh H, Williger BT, Exton JH. (1997) Arfaptin 1, a putative cytosolic target protein of ADP-ribosylation factor, is recruited to Golgi membranes. *J Biol Chem*. 272(9):5421-5429.

Kessels HW, Malinow R. (2009) Synaptic AMPA receptor plasticity and behavior. *Neuron*. 61(3):340-350.

Konadath S, Manjula P. (2016) Auditory brainstem response and late latency response in individuals with tinnitus having normal hearing. *Intractable Rare Dis Res*. 5(4):262-268.

Konrad-Martin D, Dille MF, McMillan G, Griest S, McDermott D, Fausti SA, Austin DF. (2012) Age-related changes in the auditory brainstem response. *J Am Acad Audiol*. 23(1):18-75.

Krey JF, Wilmarth PA, David LL, Barr-Gillespie PG. (2017) Chapter 18 – Analysis of the proteome of hair-cell stereocilia by mass spectrometry. *Proteomics of Biology, Part A, Methods of Enzymology*. 585:329-354.

Kujawa SG, Liberman CM. (2019) Translating animal models to human therapeutics in noise-induced and age-related hearing loss. *Hear Res*. 377:44-52.

Kujawa SG, Liberman CM. (2015) Synaptopathy in the noise-exposed and aging cochlea: Primary neural degeneration in acquired sensorineural hearing loss. *Hear Res.* 330(Pt B):191-199.

Kujawa SG, Liberman CM. (2009) Adding insult to injury: cochlear nerve degeneration after “temporary” noise-induced hearing loss. *J Neurosci.* 29(45):14077-14085.

L

Lee SJ, Wei M, Zhang C, Maxeiner S, Pak C, Calado Botelho S, Trotter J, Sterky FH, Südhof TC. (2017) Presynaptic neuronal pentraxin receptor organizes excitatory and inhibitory synapses. *J Neurosci.* 37(5):1062-1080.

Li L, Nevill G, Forge A. (1995) Two modes of hair cell loss from the vestibular sensory epithelia of the guinea pig inner ear. *J Comp Neurol.* 355(3):405-417.

Li S, Hang L, Ma Y. (2016) FGF22 protects hearing function from gentamycin ototoxicity by maintaining ribbon synapse number. *Hear Res.* 332:39-45.

Liberman LD, Wang H, Liberman MC. (2011) Opposing gradients of ribbon size and AMPA receptor expression underlie sensitivity differences among cochlear-nerve/hair-cell synapses. *J Neurosci.* 31(3):801-808.

Liberman MC. (2017) Noise-induced and age-related hearing loss: new perspectives and potential therapies [version 1; referees: 4 approved]. *F1000Research.* 6(F1000 Faculty Rev): 927.

Lim DJ. (1986) Functional structure of the organ of Corti: a review. *Hear Res.* 22:117-146.

Liu K, Chen D, Guo W, Yu N, Wang X, Ji F, Hou Z, Yang WY, Yang S. (2015) Spontaneous and partial repair of ribbon synapse in cochlear inner hair cells after ototoxic withdrawal. *Mol Neurobiol.* 52(3):1680-1689.

Llorens J, Callejo A, Greguske EA, Maroto AF, Cutillas B, Martins-Lopes V. (2018) Physiological assessment of vestibular function and toxicity in humans and animals. *NeuroToxicology.* 66:204-212.

Llorens J, Demêmes D. (1994) Hair cell degeneration resulting from 3,3'-iminodipropionitrile toxicity in the rat vestibular epithelia. *Hear Res.* 76(1-2):78-86.

Llorens J, Demêmes D, Sans A. (1993) The behavioral syndrome caused by 3,3'-iminodipropionitrile and related nitriles in the rat is associated with degeneration of the vestibular sensory hair cells. *Toxicol Appl Pharmacol.* 123(2):199-210.

Llorens J, Rodríguez-Farré E. (1997) Comparison of behavioral, vestibular, and axonal effects of subchronic IDPN in the rat. *Neurotoxicol Teratol.* 19(2):117-127.

Lysakowski, A, Gaboyard-Niay, S, Calin-Jageman, I, Chatlani, S, Price, S D, Eatock, R A. (2011) Molecular microdomains in a sensory terminal, the vestibular calyx ending. *J Neurosci.* 31(27):10101-10114.

M

Malgrange B, Thiry M, Van De Water TR, Nguyen L, Moonen G, Lefebvre PP. (2002) Epithelial supporting cells can differentiate into outer hair cells and Deiters' cells in the cultured organ of Corti. *Cell Mol Life Sci.* 59(10):1744-1757.

- Mann ZF, Thiede BR, Chang W, Shin JB, May-Simera HL, Lovett M, Corwin JT, Kelley MW. (2014) A gradient of BMP7 specifies the tonotopic axis in the developing inner ear. *Nat Commun.* 5:3839.
- Mayer ML. (2005) Glutamate receptor ion channels. *Curr Opin Neurobiol.* 15(3):282-288.
- Mayor F Jr, Cruces-Sande M, Arcones AC, Vila-Bedmar R, Briones AM, Salaices M, Murga C. (2018) G protein-coupled receptor kinase 2 (GRK2) as an integrative signaling node in the regulation of cardiovascular function and metabolic homeostasis. *Cell Signal.* 41:25-32.
- Mehraei G, Hickox AE, Bharadwaj HM, Goldberg H, Verhulst S, Liberman MC, Shinn-Cunningham BG. (2016) Auditory brainstem response latency in noise as a marker of cochlear synaptopathy. *J Neurosci.* 36(13):3755-3764.
- Meyer D, Bonhoeffer T, Scheuss V. (2014) Balance and stability of synaptic structures during synaptic plasticity. *Neuron.* 82(2):430-443.
- Mingeot-Leclercq MP, Glupczynski Y, Tulkens PM. (1999) Aminoglycosides: activity and resistance. *Antimicrob Agents Chemother.* 43(4):727-737.
- Moechars D, Weston MC, Leo S, Callaerts-Vegh Z, Goris I, Daneels G, Buist A, Cik M, van der Spek P, Kass S, Meert T, D'Hooge R, Rosenmund C, Hampson RM. (2006) Vesicular glutamate transporter VGLUT2 expression levels control quantal size and neuropathic pain. *J Neurosci.* 26(46):12055-12066.
- Morrill S, He DZZ. (2017) Apoptosis in inner ear sensory hair cells. *J Otol.* 12(4):151-164.
- Müller M, von Hünenbein K, Hoidis S, Smolders JW. (2005) A physiological place-frequency map of the cochlea in the CBA/J mouse. *Hear Res.* 202(1-2):63-73.
- Murillo-Cuesta S, García-Alcántara F, Vacas E, Sistiaga JA, Camarero G, Varela-Nieto I, Rivera T. (2009) Direct drug application to the round window: a comparative study of ototoxicity in rats. *Otolaryngol Head Neck Surg.* 141(5):584-590.
- Murillo-Cuesta S, Contreras J, Cediél R, Varela-Nieto I. (2010) Comparison of different aminoglycoside antibiotic treatments to refine ototoxicity studies in adult mice. *Lab Anim.* 44(2):124-131.
- N**
- National Council on Aging, accessed 4 April 2019, < <https://www.ncoa.org/news/resources-for-reporters/get-the-facts/falls-prevention-facts/> >
- Neiberg M, Graham V, Mosconi T. (2018) Chapter 6: The brainstem, cranial nerves, and visual pathways. In: *Neuroscience for Rehabilitation. USA: McGraw-Hill Education.*
- Ng CW, Navarro X, Engle JR, Recanzone GH. (2015) Age-related changes of auditory brainstem responses in nonhuman primates. *J Neurophysiol.* 114(1):455-467.
- Niedzielski AS, Wenthold RJ. (1995) Expression of AMPA, kainite, and NMDA receptor subunits in cochlear and vestibular ganglia. *J Neurosci.* 15(3):2338-2353.
- Noh KM, Hwang JY, Follenzi A, Athanasiadou R, Miyawaki T, Grealley JM, Bennett MV, Zukin RS. (2012) Repressor element-1 silencing transcription factor (REST)-dependent epigenetic remodeling is critical to ischemia-induced neuronal death. *Proc Natl Acad Sci USA.* 109(16):E962-971.

O

Obata S, Sago H, Mori N, Rochelle JM, Seldin MF, Davidson M, St John T, Taketani S, Suzuki ST. (1995) Protocadherin Pcdh2 shows properties similar to, but distinct from, those of classical cadherins. *J Cell Sci.* 108(Pt 12):3765-3773.

Oesterle EC, Campbell S, Taylor RR, Forge A, Hume CR. (2008) Sox2 and JAGGED1 in normal and drug-damaged adult mouse inner ear. *J Assoc Res Otolaryngol.* 9(1):65-89.

Oku Y, Hujanir RL. (2013) AGAP3 and Arf6 regulate trafficking of AMPA receptors and synaptic plasticity. *J Neurosci.* 33(31):12586-12598.

Op de Beeck K, Schacht J, Van Camp G. (2011) Apoptosis in acquired and genetic hearing impairment: the programmed death of the hair cell. *Hear Res.* 281(1-2):18-27.

P

Park SY, Ha BG, Choi GH, Ryu J, Kim B, Jung CY, Lee W. (2004) EHD2 interacts with the insulin-responsive glucose transporter (GLUT4) in rat adipocytes and may participate in insulin-induced GLUT4 recruitment. *Biochemistry.* 43(23):7552-7562.

Parsons TD, Sterling P. (2003) Synaptic ribbon. Conveyor belt or safety belt? *Neuron.* 37(3):379-382.

Pelkey KA, Barksdale E, Craig MT, Yuan X, Sukumaran M, Vargish GA, Mitchell RM, Wyeth MS, Petralia RS, Chittajallu R, Karlsson RM, Cameron HA, Murata Y, Colonnese MT, Worley PF, McBain CJ. (2015) Pentraxins coordinate excitatory synapse maturation and circuit integration of parvalbumin interneurons. *Neuron.* 85(6):1257-1272.

Pratt H. (2011) Part Two: Commonly studied ERP components; Sensory ERP components. In: The Oxford Handbook of Event-Related Potential Components. *New York, NY: Oxford University Press, Inc.* pp. 89-95.

Puel JL, Saffiedine S, Gervais d'Aldin C, Eybalin M, Pujol R. (1995) Synaptic regeneration and functional recovery after excitotoxic injury in the guinea pig cochlea. *C R Acad Sci III.* 318(1):67-75

Purves D, Augustine GJ, Fitzpatrick D, Hall WC, LaMantia AS, McNamara JO, Williams SM. (2004a) Chapter 12: The Auditory System. Hair cells and the mechano-electrical transduction of sound waves. In: *Neuroscience*, 3rd edition. *Sunderland (MA): Sinauer Associates.* pp 294-300.

Purves D, Augustine GJ, Fitzpatrick D, Hall WC, LaMantia AS, McNamara JO, Williams SM. (2004b) Chapter 12: The Auditory System. Two kinds of hair cells in the cochlea. In: *Neuroscience*, 3rd edition. *Sunderland (MA): Sinauer Associates.* pp 300-301.

Purves D, Augustine GJ, Fitzpatrick D, Hall WC, LaMantia AS, McNamara JO, Williams SM. (2004c) Chapter 12: The Auditory System. How information from the cochlea reaches targets in the brainstem. In: *Neuroscience*, 3rd edition. *Sunderland (MA): Sinauer Associates.* pp 303-313.

R

Raveh A, Cooper A, Guy-David L, Reuveny E. (2010) Nonenzymatic rapid control of GIRK channel function by a G protein-coupled receptor kinase. *Cell.* 143(5):750-760.

Raymond J, Demêmes D, Nieoullon A. (1988) Neurotransmitters in vestibular pathways. *Prog Brain Res.* 76:29-43.

Reijntjes DOJ, Schubert NMA, Pietrus-Rajman A, van Dijk P, Pyott SJ. (2018) Changes in spontaneous movement in response to silent gaps are not robust enough to indicate the perception of tinnitus in mice. *PLoS ONE*. 13(8): e0202882.

Rios JC, Melendez-Vasquez CV, Einheber S, Lustig M, Grumet M, Hemperly J, Peles E, Salzer JL. (2000) Contacting-associated protein (Caspr) and contactin form a complex that is targeted to the paranodal junctions during myelination. *J Neurosci*. 20(22):8354-8364.

Ruan Q, Ao H, He J, Chen Z, Yu Z, Zhang R, Wang J, Yin S. (2014) Topographic and quantitative evaluation of gentamicin-induced damage to peripheral innervation of mouse cochleae. *Neurotoxicology*. 40:86-96.

Ruan RS, Leong SK, Mark I, Yeoh KH. (1999) Effects of BDNF and NT-3 on hair cell survival in guinea pig cochlea damaged by kanamycin treatment. *Neuroreport*. 10(10):2067-2071.

Ruscetti T, Cardelli JA, Niswonger ML, Halloran TJ. (1994) Clathrin heavy chain functions in sorting and secretion of lysosomal enzymes in *Dictyostelium discoideum*. *J Cell Biol*. 126(2):343-352.

Rzadzinska AK, Schneider ME, Davies C, Riordan GP, Kachar B. (2004) An actin molecular treadmill and myosins maintain stereocilia functional architecture and self-renewal. *J Cell Biol*. 164(6):887-897.

S

Sadeghi SG, Pyott SJ, Yu Z, Glowatzki E. (2014) Glutamatergic signaling at the vestibular hair cell calyx synapse. *J Neurosci*. 34(44):14536-14550.

Saldaña-Ruíz S, Hernández-Mir G, Sedó-Cabezón L, Cutillas B, Llorens J. (2012) Vestibular toxicity of *cis*-2-pentenitrile in the rat. *Toxicol Lett*. 211(3):281-288.

Saldaña-Ruíz S, Boadas-Vaello P, Sedó-Cabezón L, Llorens J. (2013) Reduced systemic toxicity and preserved vestibular toxicity following co-treatment with nitriles and CYP2E1 inhibitors: a mouse model for hair cell loss. *J Assoc Res Otolaryngol*. 14(5):661-671.

Santos-Sacchi J, Song L, Zheng J, Nuttall AL. (2006) Control of mammalian cochlear amplification by chloride anions. *J Neurosci*. 26(15):3992-3998.

Schalm SS, Ballif BA, Buchanan SM, Philips GR, Maniatis T. (2010) Phosphorylation of protocadherin proteins by the receptor tyrosine kinase Ret. *Proc Natl Acad Sci USA*. 107(31):13894-13899.

Scheele U, Kalthoff C, Ungewickell E. (2001) Multiple interactions of auxilin 1 with clathrin and the AP-2 adaptor complex. *J Biol Chem*. 276(39):36131-36138.

Schindelin J, Arganda-Carreras I, Frise E, Kaynig V, Longair M, Pietzsch T, Preibisch S, Rueden C, Saalfeld S, Schmid B, Tinevez JY, White DJ, Hartenstein V, Eliceiri K, Tomancak P, Cardona A. (2012) Fiji: an open-source platform for biological-image analysis. *Nat Methods*. 9(7):676-682.

Schneider CA, Resband WS, Eliceiri KW. (2012) NIH Image to ImageJ: 25 years of image analysis. *Nat Methods*. 9(7):671-675.

Schoch S, Deák F, Königstorfer A, Mozhayeva M, Sara Y, Südhof TC, Kavalali ET. (2001) SNARE function analysed in synaptobrevin/VAMP knockout mice. *Science*. 294(5544):1117-1122.

- Schuth O, McLean WJ, Eatock, RA, Pyott SJ. (2014) Distribution of Na,K-ATPase α subunits in rat vestibular sensory epithelia. *JARO*. 15(5):739-754.
- Sedó-Cabezón L, Boadas-Vaello P, Soler-Martín C, Llorens J. (2014) Vestibular damage in chronic ototoxicity: A mini-review. *Neurotoxicology*. 43:21-27.
- Sedó-Cabezón L, Jedynak P, Boadas-Vaello P, Llorens J. (2015) Transient alterations of the vestibular calyceal junction and in response to chronic ototoxic insult in rats. *Dis Model Mech*. 8(10):1323-1327.
- Segawa K, Tamura N, Mima J. (2019) Homotypic and heterotypic trans-assembly of human Rab-family small GTPases in reconstituted membrane tethering. *J Biol Chem*. doi: 10.1074/jbc.RA119.007947
- Seoane A, Demêmes D, Llorens J. (2001a) Relationship between insult intensity and mode of hair cell loss in the vestibular system of rats exposed to 3,3'-iminodipropionitrile. *J Comp Neurol*. 439(4):385-399.
- Seoane A, Demêmes D, Llorens J. (2001b) Pathology of the rat vestibular sensory epithelia during subchronic 3,3'-iminodipropionitrile exposure: hair cells may not be the primary target of toxicity. *Acta Neuropathol*. 102(4):339-348.
- Seoane A, Demêmes D, Llorens J. (2003) Distal effects in a model of proximal axonopathy: 3,3'-iminodipropionitrile causes specific loss of neurofilaments in rat vestibular afferent endings. *Acta Neuropathol*. 106(5):458-470.
- Seoane A, Llorens J. (2005) Extruding auditory hair cells in rats exposed to subchronic 3,3'-iminodipropionitrile. *Environ Toxicol Pharmacol*. 19:571-574.
- Seuter S, Ryyänen J, Carlberg C. (2014) The ASAP2 gene is a primary target of 1,25-dihydroxyvitamin D3 in human monocytes and macrophages. *J Steroid Biochem Mol Biol*. 144(Pt A):12-18.
- Sheng M, Sala C. (2001) PDZ domains and the organization of supramolecular complexes. *Annu Rev Neurosci*. 24:1-29.
- Shi X, Gillespie PG, Nuttall AL. (2005) Na⁺ influx triggers bleb formation on inner hair cells. *Am J Physiol Cell Physiol*. 288(6):C1332-C1341.
- Shigeri Y, Seal RP, Shimamoto K. (2004) Molecular pharmacology of glutamate transporters, EAATs and VGLUTs. *Brain Res Brain Res Rev*. 45(3):250-265.
- Simpson EM, Linder CC, Sargent EE, Davisson MT, Mobraaten LE, Sharp JJ. (1997) Genetic variation among 129 substrains and its importance for targeted mutagenesis in mice. *Nat Genet*. 16(1):19-27.
- Smith AN, Lovering RC, Futai M, Takeda J, Brown D, Karet FE. (2003) Revised nomenclature for mammalian vacuolar-type H⁺-ATPase subunit genes. *Molecular Cell*. 12(4):801-803.
- Smith PF, Darlington CL. (2013) Personality changes in patients with vestibular dysfunction. *Front Hum Neurosci*. 7:678.
- Soler-Martín C, Díez-Padrisa N, Boadas-Vaello P, Llorens J. (2007) Behavioral disturbances and hair cell loss in the inner ear following nitrile exposure in mice, guinea pigs, and frogs. *Toxicol Sci*. 96(1):123-132.
- Sousa AD, Andrade LR, Salles FT, Pillai AM, Buttermore ED, Bhat MA, Kachar B. (2009) The septate junction protein caspr is required for structural support and retention of KCNQ4 at calyceal synapses of vestibular hair cells. *J Neurosci*. 29(10):3103-3108.

Stelzer G, Rosen R, Plaschkes I, Zimmerman S, Twik M, Fishilevich S, Iny Stein T, Nudel R, Lieder I, Mazor Y, Kaplan S, Dahary D, Warshawsky D, Guan-Golan Y, Kohn A, Rappaport N, Safran M, and Lancet D. (2016) The GeneCards Suite: From Gene Data Mining to Disease Genome Sequence Analysis. *Current Protocols in Bioinformatics*. 54:1.30.1-1.30.33

Swanson DA, Steel JM, Valle D. (1998) Identification and characterization of the human ortholog of rat STXBP1, a protein implicated in vesicle trafficking and neurotransmitter release. *Genomics*. 48(3):373-376.

T

Tateya T, Imayoshi I, Tateya I, Hamaguchi K, Torii H, Ito J, Kageyama R. (2013) Hedgehog signaling regulates prosensory cell properties during the basal-to-apical wave of hair cell differentiation in the mammalian cochlea. *Development*. 140:3848-3857.

Taylor RR, Nevill G, Forge A. (2008) Rapid hair cell loss: a mouse model for cochlear lesions. *J. Assoc Res Otolaryngol*. 9(1):44-64.

Thalmann I, Thallinger G, Comegys TH, Thalmann R. (1986) Collagen- the predominant protein of the tectorial membrane. *ORL*. 48(2):107-115.

Tiong KH, Mah LY, Leong CO. (2013) Functional roles of fibroblast growth factor receptors (FGFRs) signaling in human cancers. *Apoptosis*. 18(12):1447-1468.

Tisdale EJ. (2002) Glyceraldehyde-3-phosphate dehydrogenase is phosphorylated by protein kinase Ciota/lambda and plays a role in microtubule dynamics in the early secretory pathway. *J Biol Chem*. 277(5):3334-3341.

Tran Ba Huy P, Meulemans A, Wassef M, Manuel C, Sterkers O, Amiel C. (1983) Gentamicin persistence in rat endolymph and perilymph after a two-day constant infusion. *Antimicrob Agents Chemother*. 23:344-346.

Tsai CC, Kuo FT, Lee SB, Chang YT, Fu HW. (2019) Endocytosis-dependent lysosomal degradation of Src induced by protease-activated receptor 1. *FEBS Lett*. 593(5):504-517.

Tsuprun V, Santi P. (2002) Structure of outer hair cell stereocilia side and attachment links in the chinchilla cochlea. *J Histochem Cytochem*. 50(4):493-502.

U

Uthaiyah RC, Hudspeth AJ. (2010) Molecular anatomy of the hair cell's ribbon synapse. *J Neurosci*. 30(37):12387-12399.

V

Virtual Medical Centre (2018, May 27) Ototoxicity. Retrieved from <https://www.myvmc.com/diseases/ototoxicity/>

Vito P, Pellegrini L, Guet C, D'Adamio L. (1999) Cloning of AIP1, a novel protein that associates with the apoptosis-linked gene ALG-2 in a Ca²⁺-dependent reaction. *J Biol Chem*. 274(3):1533-1540.

W

Weisz CJC, Glowatzki E, Fuchs PA. (2014) Excitability of type II cochlear afferents. *J Neurosci*. 34(6):2365-2373.

Wright A, Vissel B. (2012) The essential role of AMPA receptor GluA2 subunit RNA editing in the normal and diseased brain. *Front Mol Neurosci.* **5**:34.

X

Xiao B, Tu JC, Petralia RS, Yuan JP, Doan A, Breder CD, Ruggiero A, Lanahan AA, Wenthold RJ, Worley PF. (1998) Homer regulates the association of group 1 metabotropic glutamate receptors with multivalent complexes of homer-related, synaptic proteins. *Neuron.* **21**(4):707-716.

Y

Yuan Y, Zhang J, Chang Q, Zeng J, Xin F, Wang J, Zhu Q, Wu J, Lu J, Guo W, Yan X, Jiang H, Zhou B, Li Q, Gao X, Yuan H, Yang S, Han D, Mao Z, Chen P, Lin X, Dai P. (2014) De novo mutation in ATP6V1B2 impairs lysosome acidification and causes dominant deafness-onychodystrophy syndrome. *Cell Res.* **24**(11):1370-1373.

Z

Zheng J, Shen W, He DZ, Long KB, Madison LD, Dallos P. (2000) Prestin is the motor protein of cochlear outer hair cells. *Nature.* **405**(6783):149-155.

Zheng QY, Johnson KR, Erway LC. (1999) Assessment of hearing in 80 inbred strains of mice by ABR threshold analyses. *Hear Res.* **130**(1-2):94-107.

Zou Y, Zhang WF, Liu HY, Li X, Zhang X, Ma XF, Sun Y, Jiang SY, Ma QH, Xu DE. (2017) Structure and function of the contactin-associated protein family in myelinated axons and their relationship with nerve diseases. *Neural Regen Res.* **12**(9):1551-1558.

